A Coordination-Based Model for Transition Metal Alloy Nanoparticles

Electronic Supplementary Information

Luke T. Roling[1#] Tej S. Choksi[1#], and Frank Abild-Pedersen[2*]

[1]SUNCAT Center for Interface Science and Catalysis, Department of Chemical Engineering, Stanford University, Stanford, CA 94305, USA

[2]SUNCAT Center for Interface Science and Catalysis, SLAC National Accelerator Laboratory, 2575 Sand Hill Road, Menlo Park, California 94025, USA

[#] These authors contributed equally to this work.
[*]Corresponding Author
E-mail: abild@slac.stanford.edu

Supplementary Discussion

1. Calculation of Metal Adsorption Energies from monometallic α_i^Z parameters

We here provide a brief example of how adsorption energies are calculated using the α_i^Z parameters considered in this study. We first consider the case in which the parameters from the monometallic analysis published in our previous work were directly used to predict adsorption energies. We will use Figure 1 of the main text as an illustration for these examples, considering Pt as the surface metal B (grey) and Pd as the heterospecies A (blue).

We first consider the adsorption of a single Pd atom on a (111) slab of pure Pt. The Pd atom changes coordination from 0 to 3, so we need to use the corresponding parameter α_{1-3}^{Pd} from the Pd-Pd section of Table 1 (-1.832 eV). Three surface Pt metal atoms change coordination from 9 to 10, so we also need to consider the parameter α_{10}^{Pt} from the Pt-Pt section of Table 1 (-0.111 eV). The adsorption energy of the Pd atom is calculated as the difference in total energies

between the starting state (clean slab + metal in the gas phase) and the final state (adsorbed metal) and is therefore simply the sum of these parameters representing coordination changes:

$\Delta E_{ads} = \alpha_{1-3}^{Pd} + 3\alpha_{10}^{Pt} = -1.832 + 3 * (-0.111) = -2.165\ eV$

In the second adsorption shown in Figure 1, we consider the adsorption of a Pt atom adjacent to the Pd atom added in the first step. This Pt atom changes coordination from 0 to 5 (due to the periodic boundary conditions), so we need to use the monometallic parameters α_{1-3}^{Pt} (-3.414 eV), α_{4}^{Pt} (-0.228 eV), and α_{5}^{Pt} (-0.206 eV). The surface Pd atom changes coordination from 3 to 5, so we need α_{4}^{Pd} (-0.237 eV) and α_{5}^{Pd} (-0.096 eV). Finally, two surface Pt atoms change coordination from 10 to 11 (α_{11}^{Pt} = -0.088 eV) and one from 9 to 10 (α_{10}^{Pt} = -0.111 eV). The adsorption energy of the Pt atom is therefore:

$\Delta E_{ads} = \left(\alpha_{1-3}^{Pt} + \alpha_{4}^{Pt} + \alpha_{5}^{Pt}\right) + \left(\alpha_{4}^{Pd} + \alpha_{5}^{Pd}\right) + \alpha_{10}^{Pt} + 2\alpha_{11}^{Pt} = -4.468\ eV$

Calculation of Metal Adsorption Energies from Re-Optimized Bimetallic α_i^Z Parameters

The calculation of bimetallic adsorption energies using the bimetallic parameters proceeds in a similar way to those described in the previous subsection, though the parameter selection proceeds more carefully. We illustrate the same example as before for Pd-Pt adsorption, using Figure 1 as an illustrative example. Since we are interested in a bimetallic Pd-Pt system, we must only use parameters from Table 1 corresponding to these two metals.

The coordination number changes corresponding to all adsorptions are the same as described in the previous section: the first Pd atom adsorbs to the slab in a 3-fold coordinated position, and three Pt atoms shift from 9-fold to 10-fold coordination. To account for these changes in coordination, we select the rows α_i^Z corresponding to the particular atom whose energy is calculated, and the column corresponding to the particular bimetallic system under

consideration. To account for the Pd atom's change in coordination, we select the α_{1-3}^{Pd} row from the top right of Table 1, and choose the value from the Pt column (-2.049 eV). To account for the changes in the three Pt atom coordination, we select the α_{10}^{Pt} row from the right side of Table 1, and choose the value from the Pd column (-0.166 eV). The adsorption energy of the Pd atom is predicted as the sum of these quantities:

$$\Delta E_{ads} = \alpha_{1-3}^{Pd} + 3\alpha_{10}^{Pt} = -2.049 + 3 * (-0.166) = -2.547\ eV$$

We also consider the subsequent adsorption of Pt into a 5-fold coordinated position. This Pt atom changes coordination from 0 to 5, so we need to choose the parameters α_{1-3}^{Pt} (-3.146 eV), α_{4}^{Pt} (-0.317 eV), and α_{5}^{Pt} (-0.190 eV) from the Pd column of the corresponding rows. The surface Pd atom changes coordination from 3 to 5, so we need α_{4}^{Pd} (-0.170 eV) and α_{5}^{Pd} (-0.103 eV) from the Pt column of the corresponding rows. Finally, two surface Pt atoms change coordination from 10 to 11 (α_{11}^{Pt} = -0.111 eV) and one from 9 to 10 (α_{10}^{Pt} = -0.166 eV), with both values taken from the Pd column of the α_{i}^{Pt} rows of Table 1. The adsorption energy of the Pt atom is:

$$\Delta E_{ads} = \left(\alpha_{1-3}^{Pt} + \alpha_{4}^{Pt} + \alpha_{5}^{Pt}\right) + \left(\alpha_{4}^{Pd} + \alpha_{5}^{Pd}\right) + \alpha_{10}^{Pt} + 2\alpha_{11}^{Pt} = -4.314\ eV$$

For comparison of these monometallic-only and bimetallic predictions, the explicit DFT-calculated adsorption energies of the (first) Pd and (second) Pt atoms are -2.63 eV and -4.31 eV.

2. Reducing the Size of the Bimetallic Training Set

We originally considered 140 adsorption energies when determining the α_{i}^{Z} parameters for a given bimetallic A-B system. We briefly attempted to see how the error in describing these 140 adsorption energies changes when reducing the number of calculations used in training the α_{i}^{Z} parameters, which would in principle reduce the number of DFT calculations required to

describe a new system. We chose the subset of seven bimetallic pairings for which no adsorption geometries were discarded on the basis of reconstruction: Ag-Au, Ag-Pd, Au-Pd, Au-Pt, Pd-Pt, Ir-Rh, Pt-Rh. The MAE for all 7 x 140 adsorption energies considered in this analysis is 0.061 eV when all 140 adsorption energies are considered in the parameterization for each bimetallic system. We performed a non-exhaustive analysis in which geometries were removed sequentially from the original set of 140 geometries; the removed geometry was selected to have the least impact on the MAE when using the optimized parameters to describe the larger dataset. (This is similar in concept to, though not exactly, a "leave-one-out" analysis.) Using this methodology, we found that the MAE for all 7 x 140 adsorption energies increased from 0.061 eV (when all adsorption geometries were considered) to 0.072 eV (110 geometries), 0.080 eV (84 geometries), and 0.100 (70 geometries). This analysis shows there is likely a high level of redundancy in the 140 considered DFT adsorption energies, and not all would need to be obtained to reliably describe the behavior of a new bimetallic system. We emphasize that this analysis is a non-exhaustive sampling of geometric subsets, and that establishing a true Pareto-optimality curve for MAE and number of considered configurations would require a great deal more optimization. In particular, we considered here only a set of 140 sequential adsorption energies of metals A and/or B on host slabs of pure A or B. A better sampling of adsorption energies might be realized by using different unit cells (e.g. the 3x3 surface unit cell discussed elsewhere in the main text) or alloy surface slabs with mixed compositions of A/B.

3. Fixed-Shell/Variable-Core Calculations on Additional Bimetallic Systems

As a control system we calculate fluctuations in energy as a function of local composition, at different overall bulk compositions for bulk Pt/Pd alloys. (3x3x3) unit cells are used with lattice constants determined through Vegard's law. These results are presented in

Figure S1. In comparison with our coordination-based model which predicts no changes in energy for shuffling atoms at given bulk composition, DFT calculations reveal variations of 0.017 eV per 27 atom shuffles. This validates our approach and also confirms that larger fluctuations observed in 147 atom nanoparticles are because of charge redistribution in the 1st sublayer.

We performed additional calculations with a fixed shell and variable core, to determine how the internal arrangements of atoms affect the DFT-calculated energies in systems less miscible than pure Pt and Pd. The next set of fixed-shell/variable-core calculations was performed on a Cu-Au system. This case represents an important limitation of our model, as the bimetallic Cu-Au system exhibits well-known, highly stable 3:1, 1:1, and 1:3 ordered alloy phases. Additionally, the large size disparity between Au and Cu atoms (~12%) creates severe strain when Au-Au and Cu-Cu pairs are found with interatomic distances far from their equilibrium monometallic bond distances. As a result, the DFT-calculated energies exhibit a wide degree of variance (Figure S2) that cannot be accounted for even with the second-layer atom corrections. The difference between Au and Cu subsurface corrections is just 0.05 eV, which is small compared to the energetic penalties of having Au and Cu atoms in close proximity. The average deviation from the mean is 0.20 eV in the case of the fixed Au shell, and an even larger 0.29 eV with the fixed Cu shell (which is a case with substantially higher correction). As a result, we do not observe any substantial improvement when explicitly including different subsurface corrections for the Au-Cu system. This represents one of the most extreme cases of our model failure, as it simply will not capture the strong preference for internal order observed in real systems.

We also evaluated the Cu-Rh system. These elements have somewhat similar sizes (similar to the Pt-Pd system), though different electronic properties from belonging to different groups of the periodic table. These elements also demonstrated a relatively poor fit when parameterizing the bond-associated energies, so we anticipated that we may observe deviations from ideal behavior in which internal swapping would be isoenergetic. The results of these calculations are shown in Figure S3. As anticipated, a fairly large spread is seen (though not as extreme as in the Au-Pt case): the average deviation from the mean is 0.18 eV in the Rh shell case, and 0.23 eV with the fixed Cu shell. These deviations are again substantially large that second-layer corrections, as implemented for the Pt-Pd scheme, have a relatively small effect (< 0.05 eV).

The last case we considered was a Au-Pt system. These atoms have relatively similar sizes (<5% difference in radii) and are both 5d metals, so we anticipated that there should be a possibility for more interchangability within the nanoparticle core. The results are shown in Figure S4. Interestingly, the case with the fixed Pt shell has relatively low degrees of scatter yet the fixed Au shell shows substantially more scatter. Further studies are clearly needed to understand the nature of how the shell composition affects the internal exchange of atoms. Notably, however, in this case the separate treatment of Au and Pt subsurface corrections is highly beneficial to understanding internal swapping: the average deviation is reduced from 0.36 eV to 0.22 eV in the Au shell case, and from 0.17 eV to 0.10 eV in the Pt shell case. Further studies of these internal effects, although less important for understanding the surface effects relevant for heterogeneous catalysis, can help understand how the details of atomic structuring are affected by catalyst composition.

Core-Shell Swapping Calculations on Au-Cu

We performed the same core-shell shuffling calculations as done for the Pt-Pd bimetallic systems shown in Figure 4 of the main text at intermediate energy ranges on the Au-Cu bimetallic system. As discussed above for the fixed-shell/variable core calculations, we expect this system to exhibit large model errors due to the known preference for ordered Au-Cu structures. In this system, we found that the model was qualitatively accurate in predicting the relative stabilities of nanoparticles, since these differences are driven by the segregation of Au and Cu between the surface and subsurface (Figure S5). The scatter around the best-fit line is notably much larger than in the Pt-Pd system, which arises due to the highly unstable nature of Au-Cu particles that have been shuffled randomly and is consistent with the results described in the previous section for the fixed-shell case. However, the relative ordering of particles (despite the scatter) suggests that the model is accurately representing segregation phenomena even in this non-ideal system. This accurate representation of surface atom preferences, even for bimetallic systems deviating from fcc stacking, is the most important feature of our model, as these atoms are the most relevant from a catalytic perspective.

4. Comparisons of our coordination-based model with other approaches

We compare predictions from our approach to other models reported in the literature. Specifically, we focus on comparisons with effective medium theory (EMT)[1], the bond centric model (BCM)[2], Bayesian linear regressions[3,4] and cluster expansions[5]. For this purpose, we build on the analysis presented in Figures 4 and 5 of the main text and utilize 147 atom Pt/Pd random nanoalloys as a probe system. Using both Pd-Pt and Pt-Pd core-shell geometries as an initial guess, we generate two sets of 18 random alloy structures. Relative energies of each structure are referenced to the energy of the structure denoted as “mix-1”. Cohesive energies are also computed and referenced to gas phase Pd and Pt. Tables S14, S15, and S16 list relative energies

obtained from Pd-Pt core shell strucures using DFT, α_i^Z parameters and EMT. The parity plot in Figure S7 clearly indicates that α_i^Z parameters more accurately determine relative energies in comparison to EMT. Furthermore, the slope of the best fit line for our model (1.16) is closer to the parity line than the best fit line for EMT (1.63). Similar trends are obtained for random alloys starting from a Pt-Pd core-shell structure (Figure S8, Tables S17, S18, and S19). Overall, in comparison to our model, EMT consistently predicts more negative cohesive energies (Table S16 and S19). This is not surprising because EMT was originally conceived to describe bulk solids and does not accurately predict energies of low coordinated surface atoms.

Next, we compare our model predictions to those obtained using the recently proposed Bond Centric Model (BCM)[2]. Within this framework, cohesive energies of nanoparticles are determined as a function of both coordination numbers of individual atoms and weight factors that depend on the considered binary combination. Predictions using the BCM model are obtained using the code posted by Yan et al.[2] at https://github.com/mpourmpakis/bc_model. We first compare cohesive energies of 147 atom cuboctahedral monometallic nanoparticles using DFT, α_i^Z parameters, EMT and the bond centric model in Table S20. While α_i^Z parameters yield monometallic cohesive energies with a MAE of 0.09 eV, predictions using BCM display far greater deviations from DFT calculations. Likewise, cohesive energies with EMT are also significantly more negative than DFT determined values, as also noted in Tables S16 and S19. Parity plots comparing cohesive energies of PtPd bimetallic nanoparticles obtained using both α_i^Z parameters and BCM are illustrated in Figures S9, S10 with further details provided in Tables S21, S22. In comparison to α_i^Z parameters, BCM derived cohesive energies are further away from the parity line and are more negative than DFT derived cohesive energies by 0.50 to 0.80 eV.

Moreover, BCM displays an opposite trend to DFT and α_i^Z parameters as a function of the local composition as seen in Figure S9. Within the BCM framework, energy fluctuations due to variations in local compositions are also far more aggressive than observed using either DFT or α_i^Z parameters, as indicated in slopes of best fit lines in Figures S9 and S10. This increased sensitivity may occur in the BCM because composition dependence is controlled by only two parameters fitted from energies of gas phase dimers, and gas phase dimers do not adequately represent low coordinated surface atoms. Deviations in cohesive energy between BCM and DFT are exaggerated in Figures S9 and S10 because unlike Yan et al.[2] who benchmark BCM to DFT calculations using the PBE functional and localized basis sets, we use plane wave DFT with the RPBE functional which is known to better describe surface properties and generally speaking weakens adsorption and surface energies in comparison with PBE. Yan et al. state that while the BCM works well for alloys of Au, Cu, Ag and Zr, it is not universally applicable and may yield incorrect predictions for bimetallic systems when trends in dimer dissociation energies do not match trends in bulk monometallic cohesive energies. In conclusion for PtPd alloys, the BCM predicts far stronger cohesive energies in general, and displays an aggressive dependence of cohesive energies as a function of composition as compared to our approach using α_i^Z parameters.

Bayesian linear regression[3,4] and cluster expansions[5] parameterize energies of bimetallic nanoparticles in terms of weight factors and effective cluster interactions. We compare the number of parameters, computational cost for parameter fitting, and accuracy on the training set (cohesive energies of alloys) in Table S23 and Figure S11. Bayesian linear regression uses 800 parameters to describe binary interactions requiring a training set of 1106 DFT calculations on surface slabs and nanoparticle structures. Although the MAE for cohesive energies is remarkably low, fitting this large a parameter set for every binary alloy combination is cumbersome and

computationally expensive. Similarly, cluster expansion techniques also possess a high computational cost as they are fitted to 107 DFT derived energies on 145-147 atom nanoparticles. As an order of magnitude estimate, 107 145-147 atom nanoparticle calculations cost ~ 165,000 core hours (24 hours for 64 cores with Quantum ESPRESSO) while 70 DFT calculations on surfaces cost ~ 11,200 core hours (10 hours for 16 cores with Quantum ESPRESSO), making our approach ~15 times computationally cheaper in comparison. Furthermore, unlike our approach wherein α_i^Z parameters determined on simple slab models are tested on nanoparticle structures, Teeriniemi et al. test effective cluster interactions on a structurally similar training set which perhaps contributes to the lower MAE. In constrast to both cluster expansion and Bayesian linear regression, α_i^Z parameters predict atomic energies at a site-by-site resolution, and these atomic energies are in turn, correlated to catalytic properties like binding energies of adsorbates.[6] Finally, with either cluster expansions or Bayesian linear regression, the physical understanding in the magnitude of fitted parameters remains elusive. In contrast, our method exploits the "near sightedness" in alloys wherein perturbations in morphology or chemical composition decay rapidly beyond the first coordination shell[7]. By exploiting this phenomenon, we describe generic changes in structure and composition more efficiently using a considerably smaller parameter set (10 α_i^Z parameters per metal), without significantly compromising on accuracy. The physical meaning melded within the α_i^Z parameters is discussed in the main text.

We compare MAEs in cohesive energies of bimetallic alloys obtained using α_i^Z parameters, EMT, bond centric model, Bayesian linear regression, and cluster expansions in Figure S11. As discussed earlier, in comparison to α_i^Z parameters, EMT and the bond centric

model show larger errors; overestimate cohesive energies and display greater errors in describing variations in local composition. While Bayesian linear regressions and cluster expansions yield lower errors, they are computationally expensive as evidenced from Table S23, and physical insights within fitted parameters remains elusive. In contrast, our approach uses fewer parameters that are rapidly determined from simple surface calculations and predict cohesive energies of 147 atom nanoparticles within 0.15 eV. This error will significantly decrease for larger nanoparticles as the system represents extended surfaces more closely, and quantum/finite size effects begin to diminish.[8,9] Our coordination-based model is an acceptable compromise between accuracy and model complexity.

5. Model Validation across Nanoalloys having Different Morphologies, Compositions, and Sizes

Following a brief discussion of the accuracy of our model in predicting metal atom adsorption energies on corners, edges, and terrace sites, we rigorously evaluate the transferability of our model to nanoparticles comprising different morphologies, sizes, and overall compositions. We predict both cohesive energies (represents the overall stability) and energetic changes of single atom swaps (elementary steps during dynamic processes).

We investigate the fidelity of our model across atoms having different coordination environments by calculating adsorption energies of Pt and Pd surface atoms with coordination numbers of 5, 7, 8, and 9 on 147 cuboctahedral (CUB) nanoparticles. Coordination numbers of 5 and 7 represent corners and edges, while 8-fold and 9-fold atoms compose (100) and (111) terraces. Considered compositions of PtPd nanoparticles range from Pt-rich to Pd-rich, and include $Pt_{10}Pd_{137}$, $Pt_{27}Pd_{120}$, $Pt_{40}Pd_{107}$, $Pt_{55}Pd_{92}$, $Pt_{65}Pd_{82}$, $Pt_{82}Pd_{65}$, $Pt_{92}Pd_{65}$, $Pt_{107}Pd_{40}$, $Pt_{120}Pd_{27}$, $Pt_{137}Pd_{10}$. Model-predicted and DFT derived adsorption energies are compared in Figure S12

with adsorption energies listed in Table S24. Our model is most accurate for low coordinated corner sites (CN: 5) yielding a MAE of 0.09 eV. The low error is because surface tension induced compressive strain is minimal at these low coordinated corner sites.[10] In contrast, nine-fold coordinated (111) terrace atoms reveal the greatest error (0.71 eV) because of excessive in-plane compressive strain. Our geometry independent model is unable to capture this result, consistent with our previous findings for monometallic systems.[11] These deviations show a systematic trend, with best-fit lines having slopes close to unity and an offset representing the extent of the strain induced deviations. Nevertheless, this error can be substantially reduced by calibrating the model using best-fit lines as illustrated in Figure S12. This calibration requires a limited number of additional calculations but retains the simplicity of our coordination-based model. All Pt and Pd atoms having a given coordination number (7 or 9), regardless of their local chemical compositions (Pt/Pd ratios) lie on the best-fit calibrations.

Next, we verify model transferability across composition space. In Figure S13, we compare model-predicted and DFT-derived cohesive energies (indicative of their bulk stabilities) for 147 CUB nanoparticles as the Pt/Pd composition varies from Pt_0Pd_{147}, $Pt_{10}Pd_{137}$, $Pt_{27}Pd_{120}$, $Pt_{40}Pd_{107}$, $Pt_{55}Pd_{92}$, $Pt_{65}Pd_{82}$, $Pt_{82}Pd_{65}$, $Pt_{92}Pd_{65}$, $Pt_{107}Pd_{40}$, $Pt_{120}Pd_{27}$, $Pt_{137}Pd_{10}$, and $Pt_{147}Pd_0$. Pt and Pd atoms are distributed randomly through the structure. Cohesive energies are listed in Table S25. The best fit line has a slope of 1,01 and an offset of 0.17 eV, indicating that our model overestimates cohesive energies of all nanoparticles by a constant extent, irrespective of their overall composition. This deviation of 0.17 eV from the parity line is caused by finite size effects prevalent in 147 atom nanoparticles (1.6 nm), which disappear with increasing nanoparticle size. On the other hand, our model is highly accurate in determining relative energies of PtPd nanoparticles having different compositions (differences of cohesive energies),

as while evaluating relative energies, the constant offset of 0.17 eV for both initial and final states is cancelled out. Cohesive energies referenced to monometallic Pd nanoparticles are compared in Table S25 and reveal a MAE of just 0.005 eV. This indicates that our model can successfully predict relative energies with site-specific resolution as the alloy composition is varied, making it directly applicable to dynamic processes like segregation and sintering. We emphasize the importance of accurately modeling *relative* energies, as this is sufficient for our intended catalytic applications (e.g. sintering, atomic/molecular adsorption); agreement with absolute quantities such as cohesive energies are less relevant for our applications.

We verify the transferability of our coordination-based model to nanoparticles having different morphologies, especially those that deviate from an ideal FCC stacking. In addition to our extensive analysis of cuboctahedral (CUB) nanoparticles (Figures 3-5 of the main text), we include octahedral (OCT), decahedral (DEC), and icosahedral (ICO) morphologies. We note that DEC and ICO structures contain distorted metal-metal bond distances near edges (1.7% and 5.1% distortions respectively), thereby presenting an excellent test case for evaluating the transferability of our model beyond idealized FCC structures. Figure S14 depicts a parity plot for adsorption energies of metal atoms (Pt and Pd) in monometallic OCT, DEC, and ICO nanoparticles. Considered sites include metal atoms having coordination ranging from 4 to 9, along with bulk atoms in the second and third layers. Adsorption energies of metal atoms computed using both DFT and our model are listed in Table S26. Despite deviations from an ideal FCC stacking, MAE's of 0.15 to 0.23 eV are noted, which are consistent with our study on CUB nanoparticles.[11]

Next, we validate our model across bimetallic PtPd nanoparticles having wide ranging sizes, morphologies, and compositions. We compute cohesive energies of nanoparticles

(indicative of their bulk stability), and energetic changes for single atom movements (ΔE_{swap}) that steer dynamic restructuring processes. Considered nanoparticles include CUB, ICO, DEC, and OCT morphologies having compositions ranging from Pt-rich to Pd-rich. All atoms are randomly distributed within the nanoparticle. Finite size effects are evaluated by comparing MAEs for ΔE_{swap} between 147 atom and truncated 309 (half-309) CUB nanoparticles. Atoms in the bottom-most layer of the half-309 nanoparticles are fixed to their bulk positions. Representative examples of these nanoparticles are illustrated in Figure S15. Figure S16(a) shows a parity plot comprising 64 PtPd nanoparticles whose energies are listed in Table S27. The best fit line has a slope of 1.01 and an offset of 0.19 eV. All nanoalloys, irrespective of their size, shape, and overall composition, lie on the best fit line. This deviation of 0.19 eV is as a result of finite size effects as explained in the preceeding paragraphs. This error can be entirely eliminated by calibrating our slab-derived model using best-fit lines obtained from a limited subset of nanoparticle calculations as illustrated in Figure S13 and Figure S16(a). In contrast to cohesive energies, our model yields significantly higher accuracies in determining $\Delta E_{swap.}$ DFT and model predictions for 42 different Pt and Pd swaps (ΔE_{swap}) are listed in Table S13 and Table S28 with a parity plot shown in Figure S16(b). Our model predicts ΔE_{swap} with a MAE of 0.05 eV across all morphologies, compositions, and sizes. We observe a slightly lower MAE of 0.02 eV for the larger half-309 nanoparticles in comparison to 0.05 eV for 147 atom systems. This is because the expanded terraces of the half-309 nanoparticles have reduced finite size effects, and our slab-derived α_i^Z parameters become significantly more accurate. In the limit of infinitely large terraces on periodic slabs, we obtain a MAE of 0.03 eV as shown for Pt_3Pd and Pd_3Pt alloys in Figure 2 (main text). These results are consistent with earlier, more exhaustive studies of finite size effects on Pt and Au nanoparticles.[8–10]

The excellent agreement between DFT and our model predictions as illustrated in Figures S12, S13, and S16 implies that the non-linear exponent (w = 1.93) for the second layer correction obtained using 147 atom CUB nanoparticles is largely independent of local morphologies or compositions. Thus w = 1.93 is directly transferable to PtPd structures having different sizes, morphologies, and compositions. These results imply that through the introduction of one additional parameter (w = 1.93), our model can accurately describe electronic interactions between second layer Pt and Pd atoms.

Our coordination-based model which is fitted using a limited number of simple slabs, is robust enough to predict cohesive energies, adsorption energies of metal atoms, and most crucially, energetic changes for single atom movements (ΔE_{swap}) with the latter being vitally important in simulating dynamic processes on bimetallic nanoparticles. By calibrating finite-size effects using best-fit lines (Figures S13 and S16), we further enhance the accuracy of our model towards predicting total energies of small nanoparticles upto 1.6 nm in size.

6. Supplementary Figures

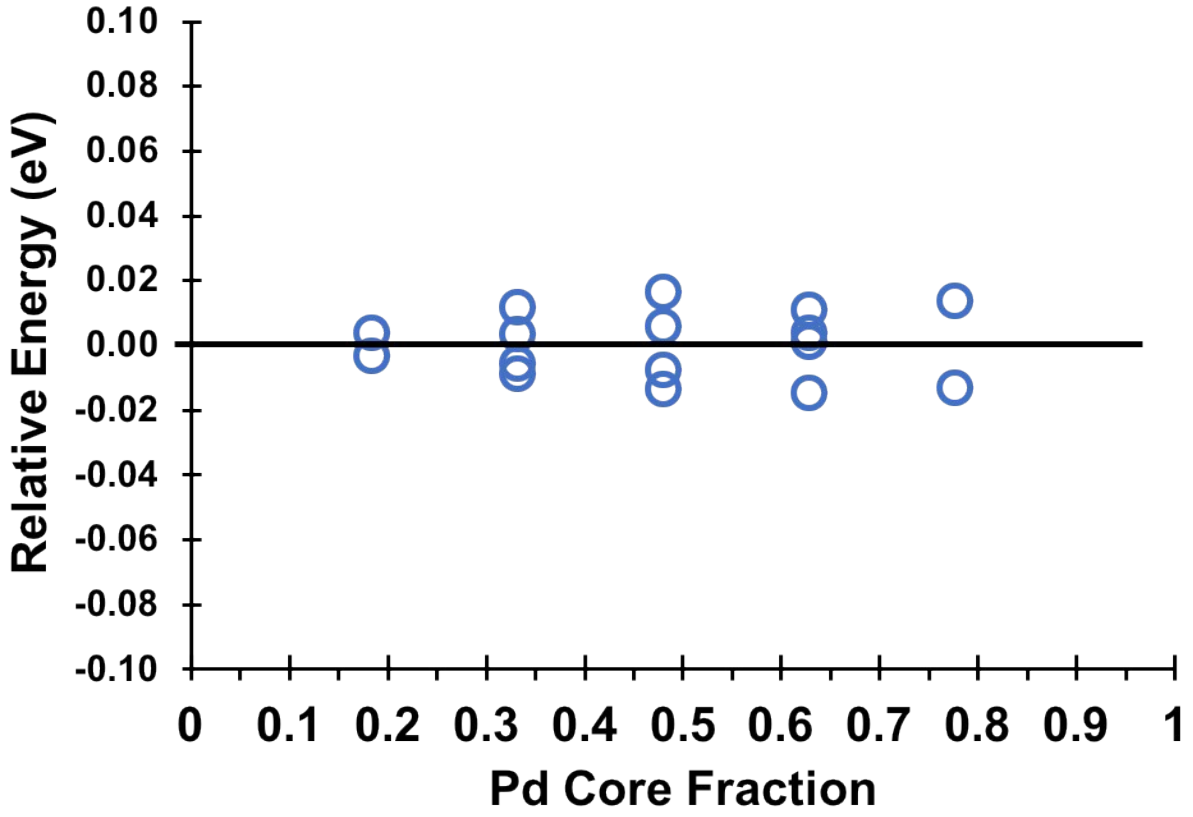

Figure S1: Shuffled Pt-Pd bulk calculations at various bulk compositons. Energies of randomly varied structures at different compositions are reported. Plotted are the relative energies (per 27 atom shuffle) around the mean energy for each composition. To facilitate comparison, the mean energy for each Pt/Pd fraction is realigned to 0.

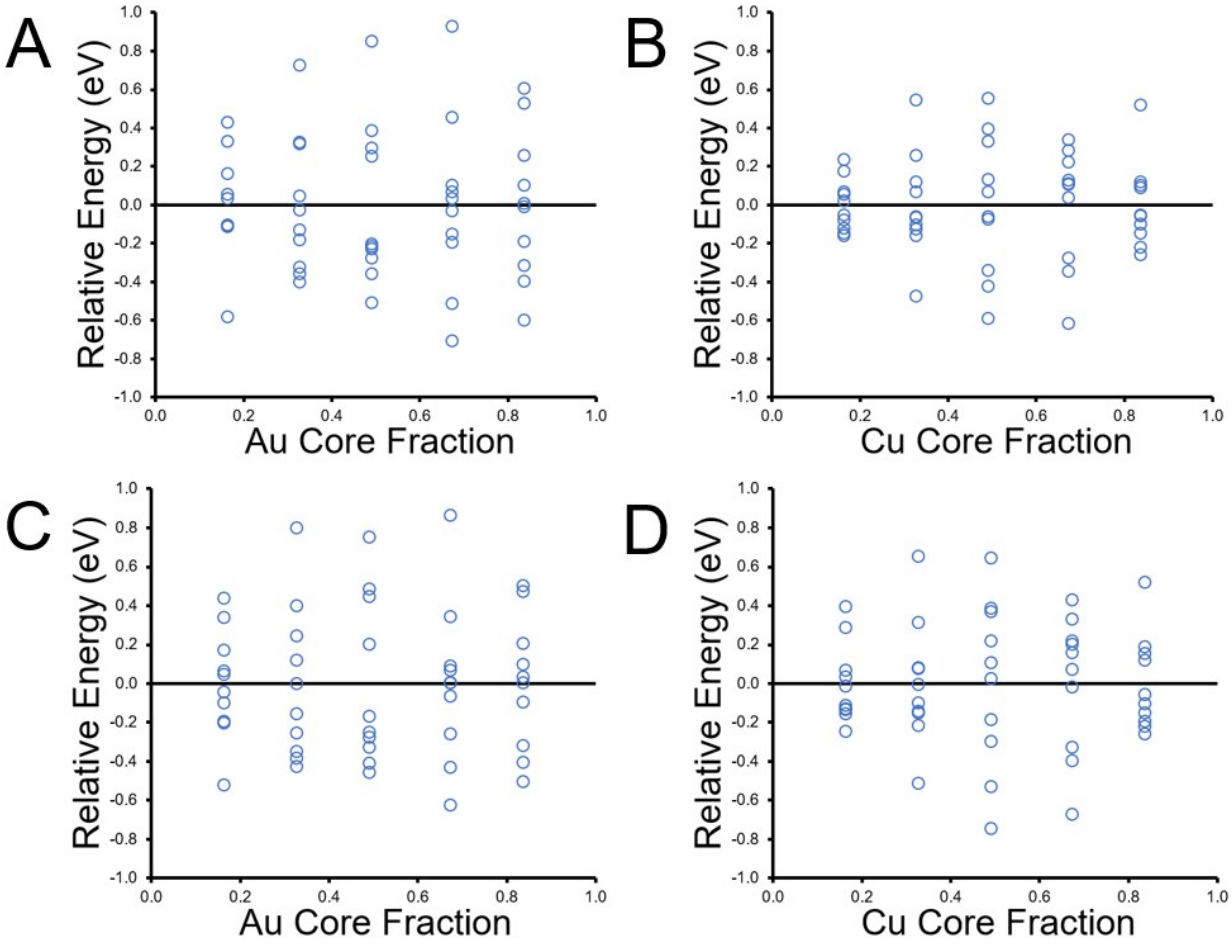

Figure S2: Fixed shell, variable core calculations for the Au-Cu system. Schematic is shown in Figure 3A of the main text. The 92-atom shell is fixed at its optimized nanoparticle coordinates, while the 55-atom core structure is randomly shuffled, and its composition varied. Plotted are the relative energies (per 55 atom shuffle) around the mean energy for each composition for (B) fixed Cu shell; (C) fixed Au shell; (D) fixed Cu shell, Au and Cu subsurface energies corrected separately, (E) fixed Au shell, Au and Cu subsurface energies corrected separately. To facilitate comparison, the mean energy for each Au/Cu core fraction is realigned to 0.

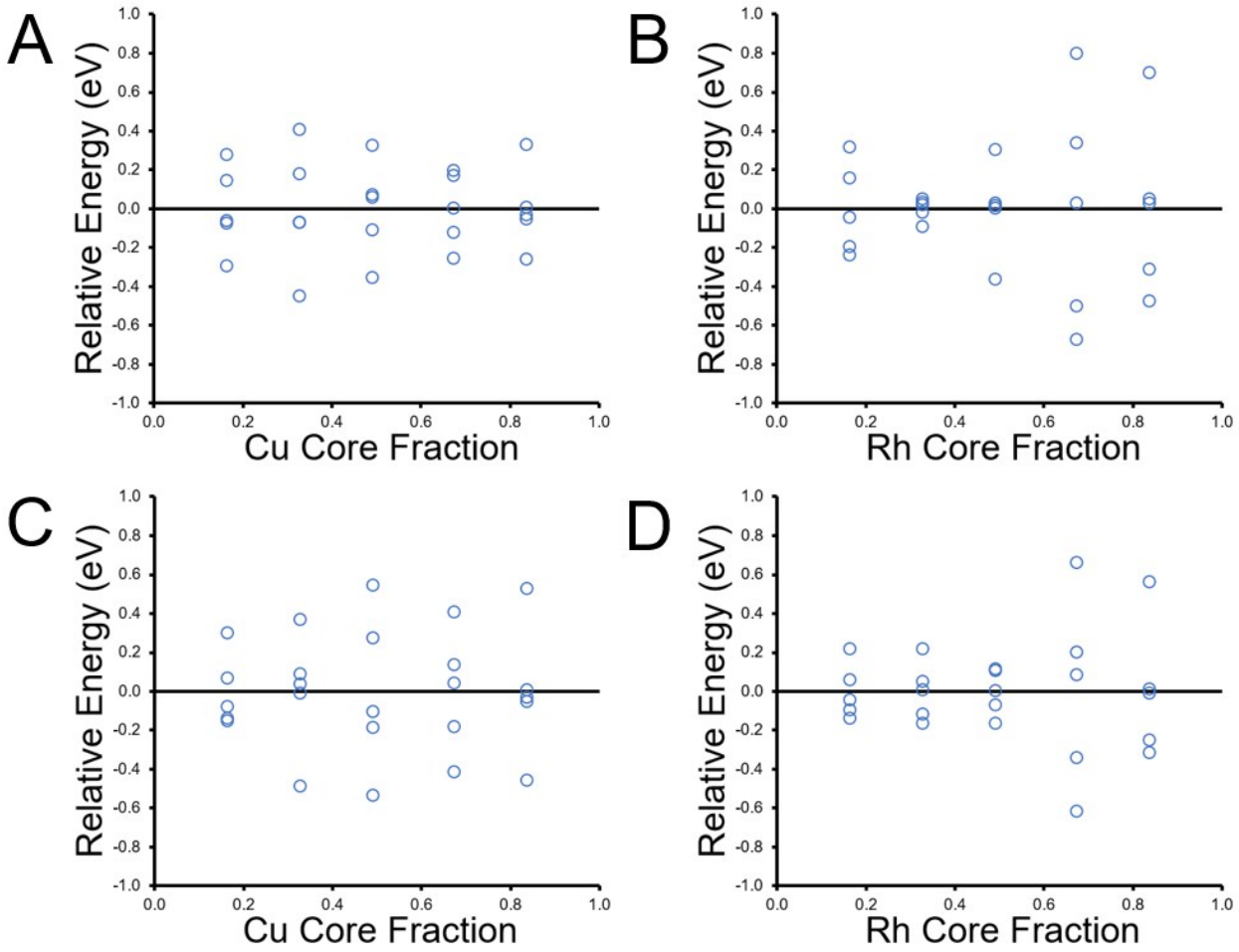

Figure S3: Fixed shell, variable core calculations for the Cu-Rh system. Schematic is shown in Figure 3A of the main text. The 92-atom shell is fixed at its optimized nanoparticle coordinates, while the 55-atom core structure is randomly shuffled, and its composition varied. Plotted are the relative energies (per 55 atom shuffle) around the mean energy for each composition for (B) fixed Rh shell; (C) fixed Cu shell; (D) fixed Rh shell, Cu and Rh subsurface energies corrected separately, (E) fixed Cu shell, Cu and Rh subsurface energies corrected separately. To facilitate comparison, the mean energy for each Cu/Rh core fraction is realigned to 0.

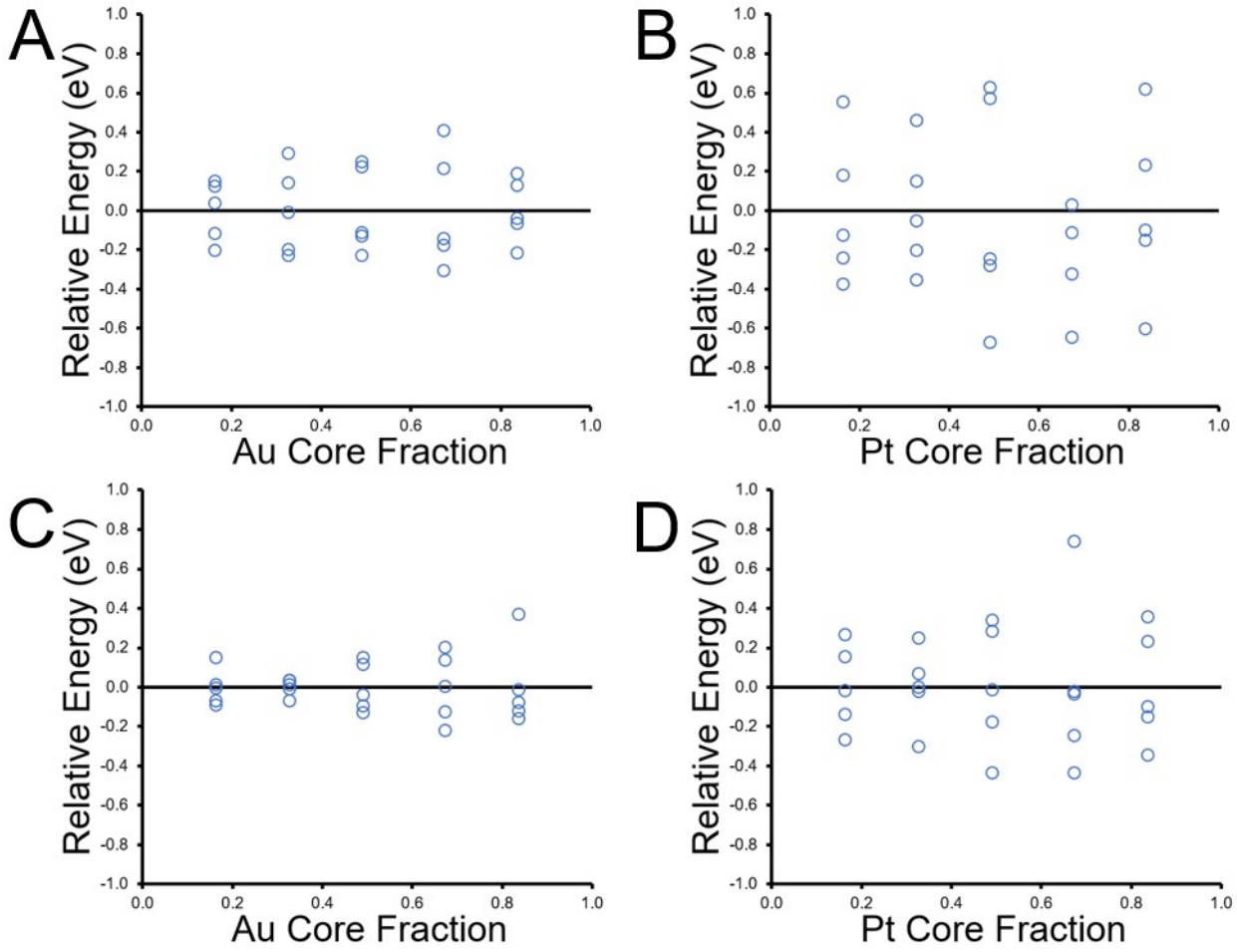

Figure S4: Fixed shell, variable core calculations for the Au-Pt system. Schematic is shown in Figure 3A of the main text. The 92-atom shell is fixed at its optimized nanoparticle coordinates, while the 55-atom core structure is randomly shuffled, and its composition varied. Plotted are the relative energies (per 55 atom shuffle) around the mean energy for each composition for (B) fixed Pt shell; (C) fixed Au shell; (D) fixed Pt shell, Au and Pt subsurface energies corrected separately, (E) fixed Au shell, Au and Pt subsurface energies corrected separately. To facilitate comparison, the mean energy for each Au/Pt core fraction is realigned to 0.

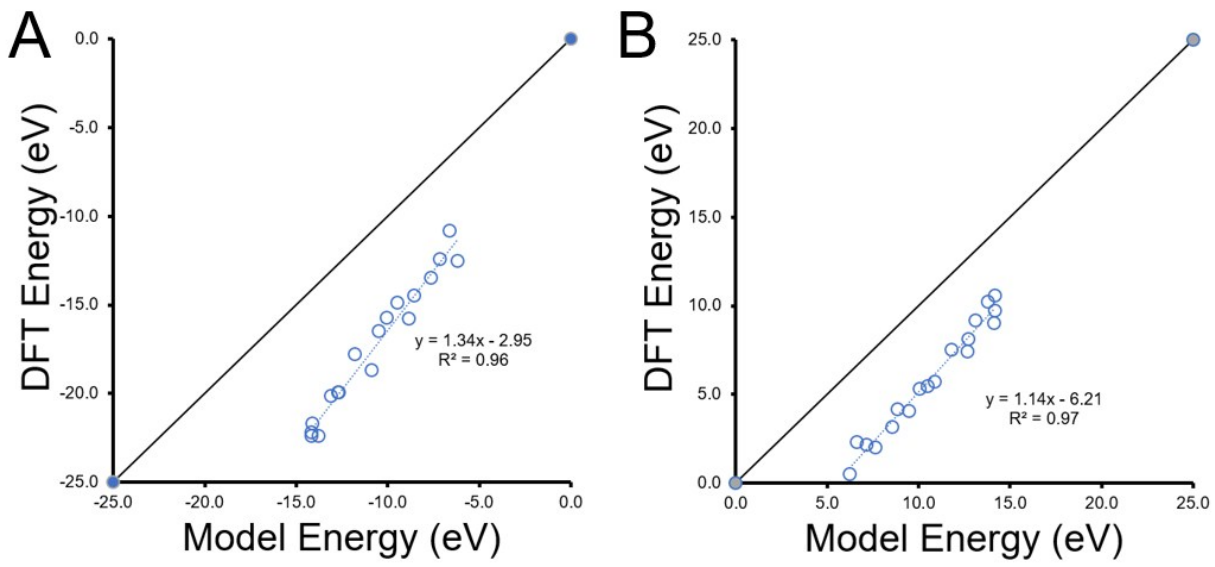

Figure S5: Comparison of model-predicted and DFT-calculated energies relative to core-shell structures using (A) Au-Cu core-shell reference, $w = 1$ correction to subsurface energies; (B) Cu-Au core-shell reference, $w = 1$ correction to subsurface energies.

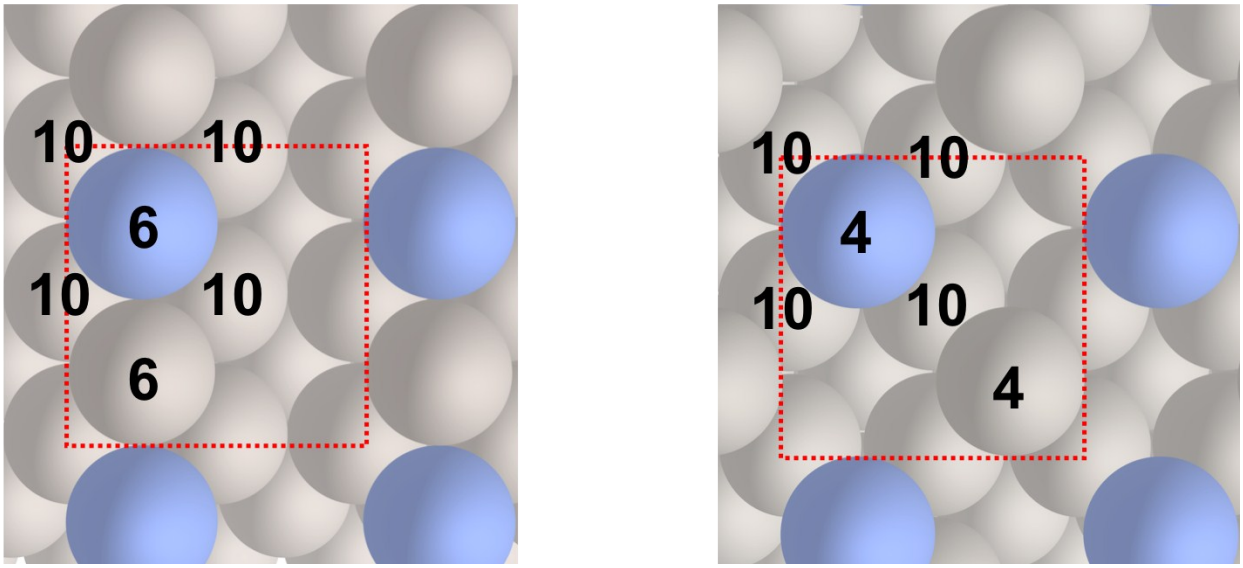

Figure S6: Configurations of surface atoms on a 2x2 fcc (100) surface such that they lie (left) adjacent to each other (denoted as A), or (right) along the surface diagonal (denoted as D). The unit cell of the surface modeled is indicated (red dashed line). The coordination number of surface atoms is shown. Metal A is shown in blue, and metal B in grey.

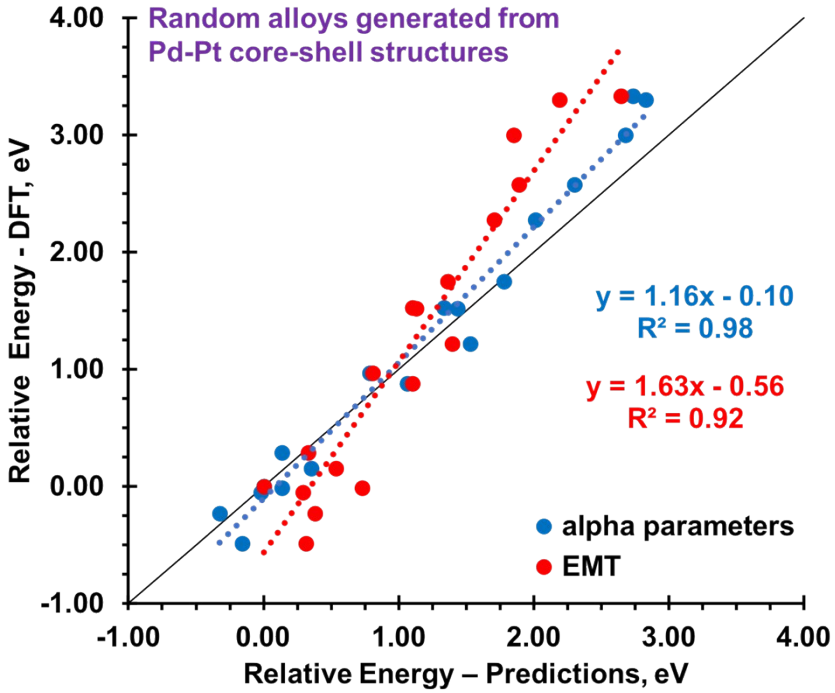

Figure S7: Parity plot between DFT energies and model predictions (α_i^Z parameters and EMT) for random alloys generated from 147 atom Pd-Pt core shell nanoparticles. Predictions using α_i^Z parameters are closer to the parity line. Relative energies are listed in Table S14 and S15.

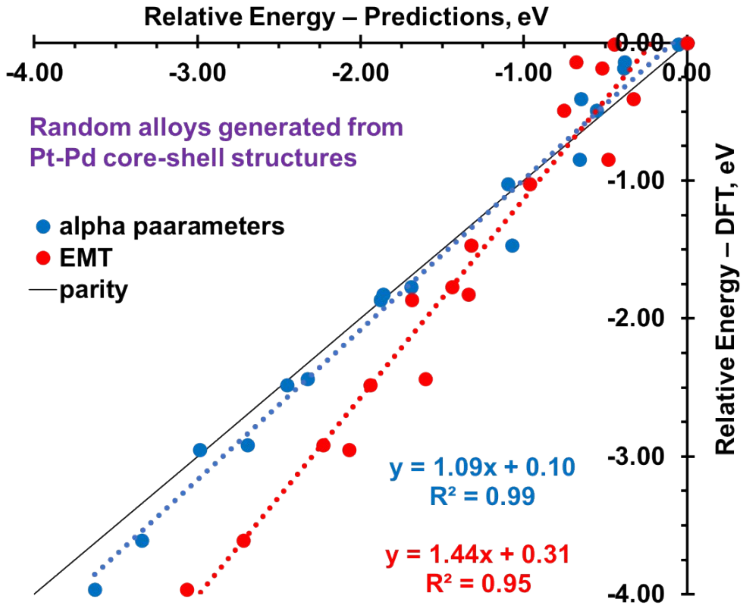

Figure S8: Parity plot between DFT energies and model predictions (α_i^Z parameters and EMT) for random alloys generated from 147 atom Pt-Pd core shell nanoparticles. Predictions using α_i^Z parameters are closer to the parity line. Relative energies are listed in Table S17 and S18.

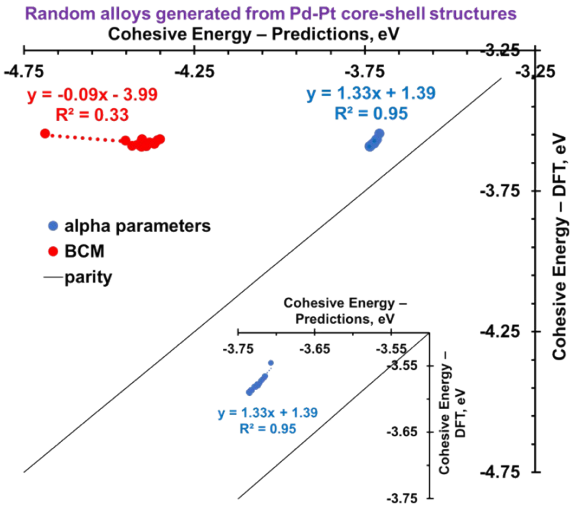

Figure S9: Parity plot between DFT energies and model predictions (α_i^Z parameters and BCM) for cohesive energies of random alloys generated from 147 atom Pd-Pt core shell nanoparticles. Predictions using α_i^Z parameters are closer to the parity line. The inset shows a zoomed in version of the parity plot obtained using α_i^Zparameters Cohesive energies are listed in Table S21.

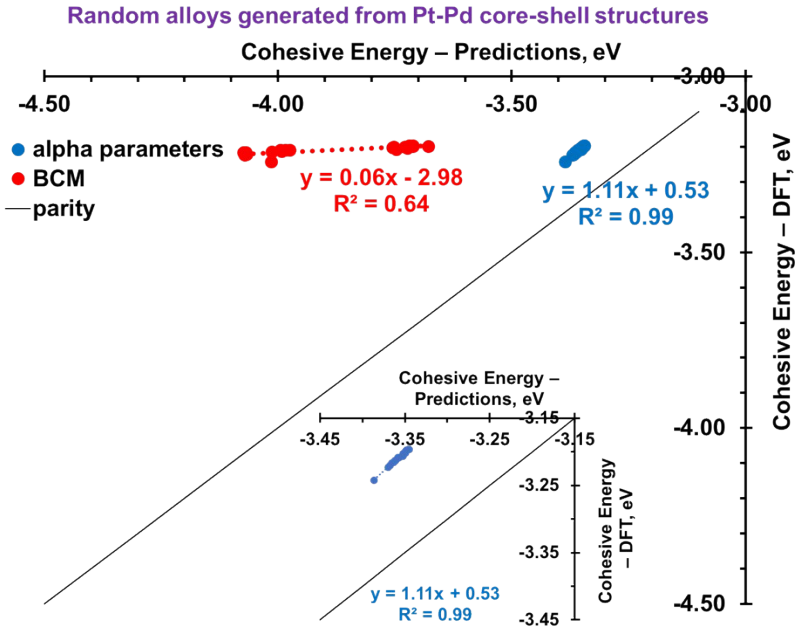

Figure S10: Parity plot between DFT energies and model predictions (α_i^Z parameters and BCM) for cohesive energies of random alloys generated from 147 atom Pt-Pd core shell nanoparticles.

Predictions using α_i^Z parameters are closer to the parity line. The inset shows a zoomed in version of the parity plot obtained using α_i^Z parameters Cohesive energies are listed in Table S22.

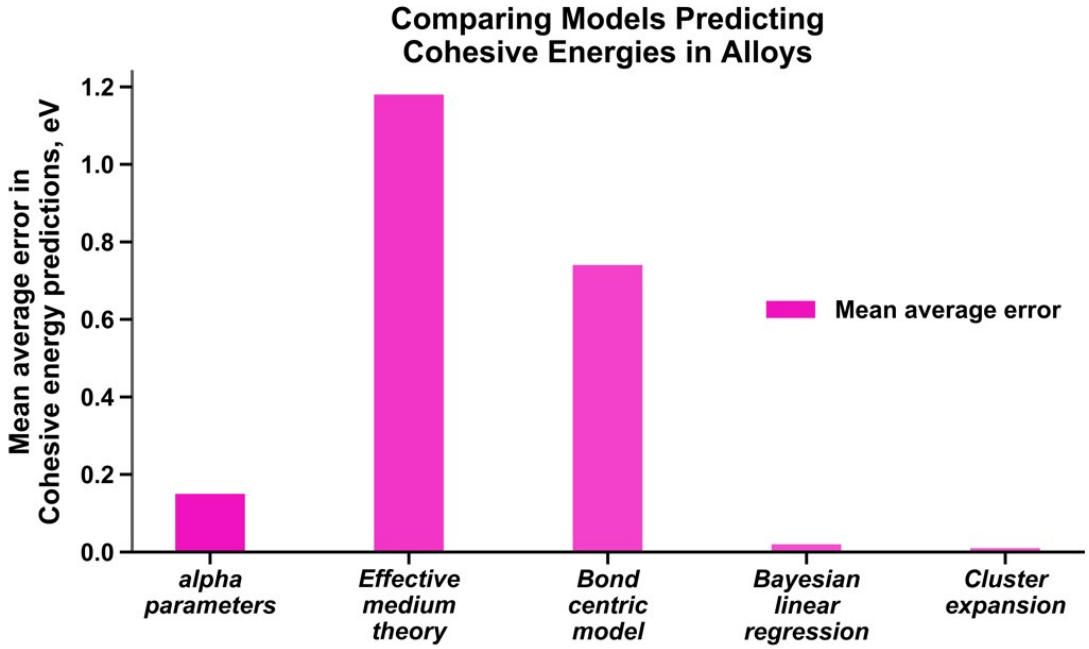

Figure S11: Comparison between MAE's in cohesive energy for nanoparticles predicted using different approaches. A more detailed analysis is presented in Table S23.

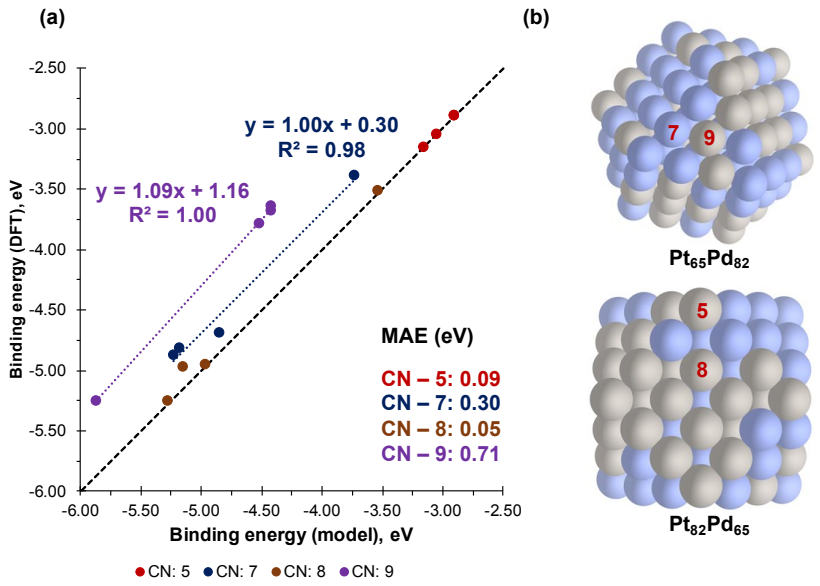

Figure S12: Comparing model predicted and DFT derived adsorption energies for metal atoms (Pt and Pd) in 147 atom CUB nanoparticles. Data points for 5, 7, 8, and 9 coordinated atoms are shown in red, blue, brown, and purple. Considered overall nanoparticle compositions include

$Pt_{10}Pd_{137}$, $Pt_{27}Pd_{120}$, $Pt_{40}Pd_{107}$, $Pt_{55}Pd_{92}$, $Pt_{65}Pd_{82}$, $Pt_{82}Pd_{65}$, $Pt_{92}Pd_{65}$, $Pt_{107}Pd_{40}$, $Pt_{120}Pd_{27}$, and $Pt_{137}Pd_{10}$. Pt and Pd atoms are shown in grey and blue respectively.

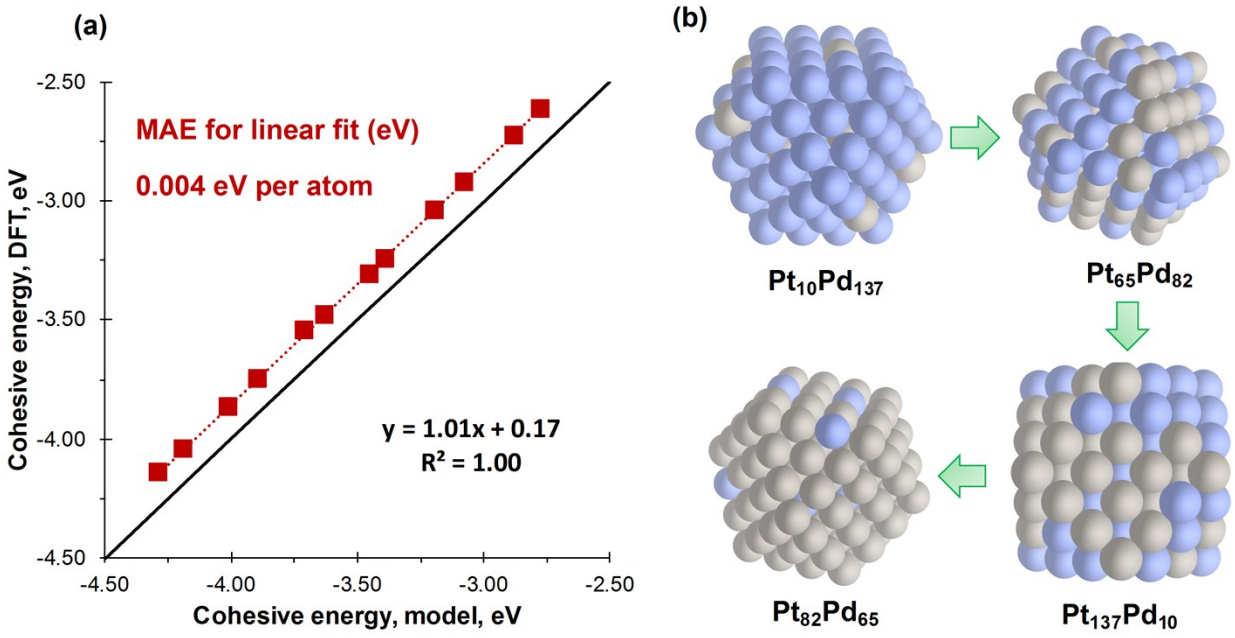

Figure S13: Comparing model predicted and DFT derived cohesive energies for 147 CUB nanoparticles having composition varying from pure Pt to pure Pd. Considered overall nanoparticle compositions include Pt_0Pd_{147}, $Pt_{10}Pd_{137}$, $Pt_{27}Pd_{120}$, $Pt_{40}Pd_{107}$, $Pt_{55}Pd_{92}$, $Pt_{65}Pd_{82}$, $Pt_{82}Pd_{65}$, $Pt_{92}Pd_{65}$, $Pt_{107}Pd_{40}$, $Pt_{120}Pd_{27}$, $Pt_{137}Pd_{10}$, and $Pt_{147}Pd_0$. Pt and Pd atoms are shown in grey and blue respectively.

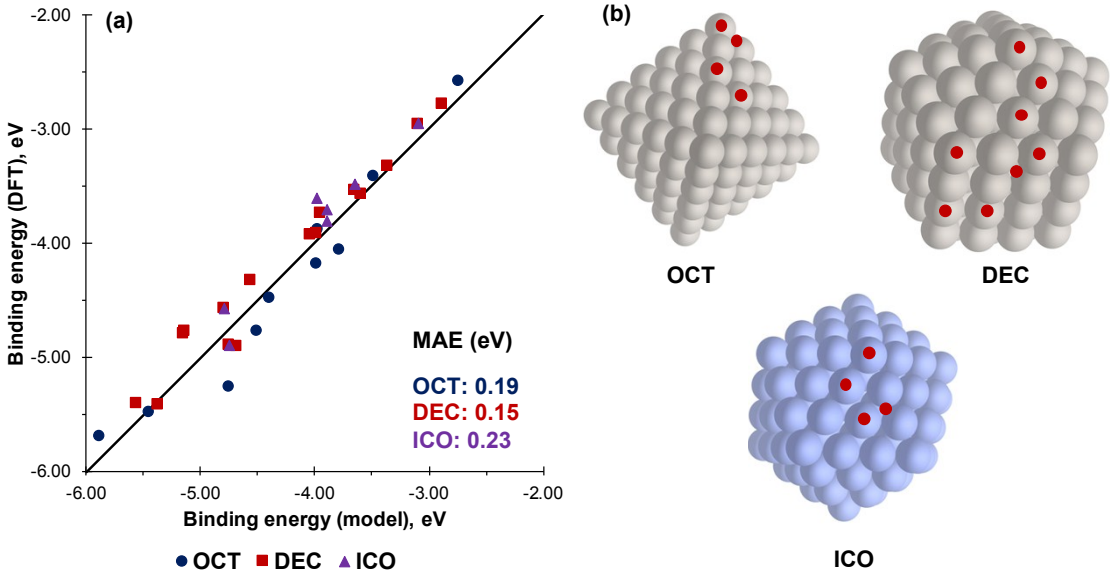

Figure S14: (a) Comparing model predicted and DFT derived metal adsorption energies across different morphologies of Pt and Pd nanoparticles. OCT, DEC, and ICO are shown in blue, red,

and purple. Adsorption energies of metal atoms are calculated for atoms having coordination numbers ranging from 4-9, and bulk atoms located in the 2nd and 3rd layers. **(b)** OCT, DEC, and ICO nanoparticles with red dots representing coordination numbers of considered metal atoms.

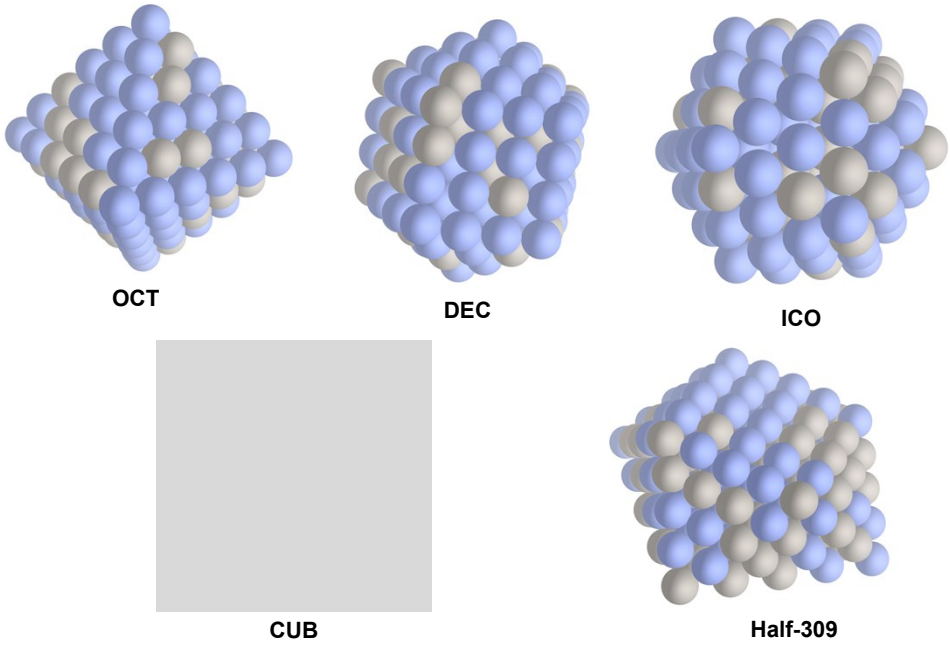

Figure S15: Representative structures of OCT, DEC, ICO, CUB, and CUB-truncated 309 (half-309) nanoparticles. Pt and Pd atoms are shown in grey and blue respectively.

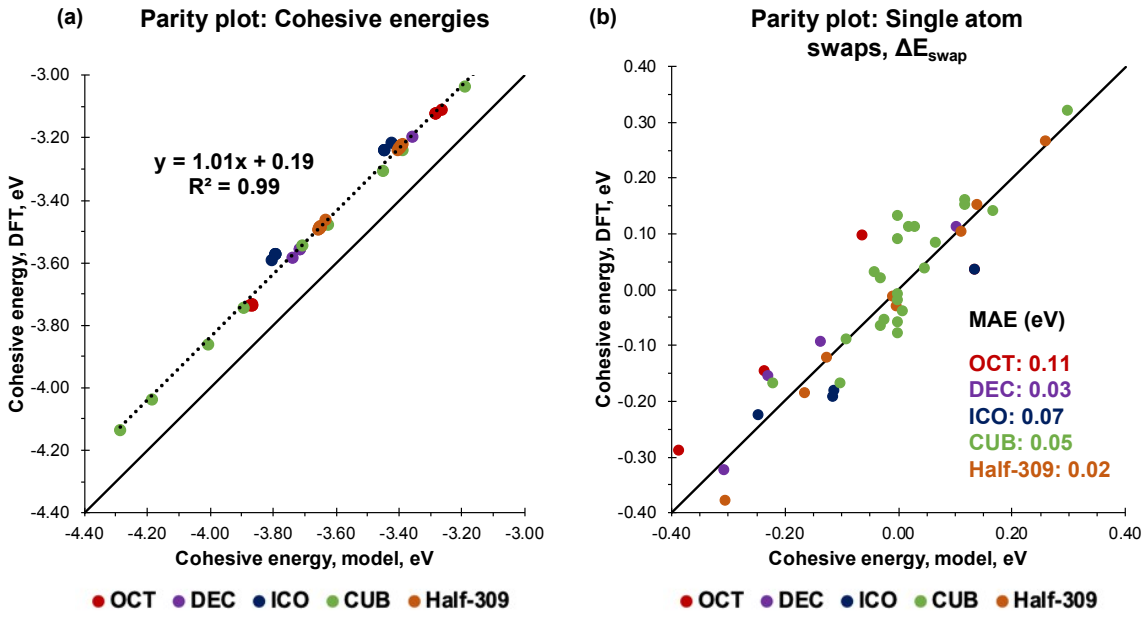

Figure S16: (a) Comparing model predicted and DFT derived cohesive energies for PtPd nanoparticles having wide ranging compositions and different morphologies. **(b)** Comparing

energetic changes of single atom movements (ΔE_{swap}) computed using our model and DFT. These swaps represent atom-by-atom movements that drive sintering and other dynamic restructuring processes in alloys. Across all morphologies/compositions, our model predicts enthalpy changes within 0.05 eV.

7. Supplementary Tables

Table S1: DFT-calculated adsorption energies for monometallic systems, 2x2 fcc(111) surfaces.

Metal	Adsorption Configuration	Reference Configuration	Adsorption Energy (eV)
Ag	1 Adatom	Clean	-1.50
Ag	2 Adatoms	1 Adatom	-1.92
Ag	3 Adatoms	2 Adatoms	-2.18
Ag	4 Adatoms	3 Adatoms	-2.38
Au	1 Adatom	Clean	-1.94
Au	2 Adatoms	1 Adatom	-2.39
Au	3 Adatoms	2 Adatoms	-2.69
Au	4 Adatoms	3 Adatoms	-2.84
Cu	1 Adatom	Clean	-2.26
Cu	2 Adatoms	1 Adatom	-2.85
Cu	3 Adatoms	2 Adatoms	-3.30
Cu	4 Adatoms	3 Adatoms	-3.65
Ir	1 Adatom	Clean	-4.80
Ir	2 Adatoms	1 Adatom	-6.33
Ir	3 Adatoms	2 Adatoms	-7.21
Ir	4 Adatoms	3 Adatoms	-8.23
Pd	1 Adatom	Clean	-2.25
Pd	2 Adatoms	1 Adatom	-2.90
Pd	3 Adatoms	2 Adatoms	-3.47
Pd	4 Adatoms	3 Adatoms	-3.92
Pt	1 Adatom	Clean	-3.74
Pt	2 Adatoms	1 Adatom	-4.56
Pt	3 Adatoms	2 Adatoms	-5.16
Pt	4 Adatoms	3 Adatoms	-5.67
Rh	1 Adatom	Clean	-3.75
Rh	2 Adatoms	1 Adatom	-4.87
Rh	3 Adatoms	2 Adatoms	-5.61
Rh	4 Adatoms	3 Adatoms	-6.37

Table S2: DFT-calculated adsorption energies for monometallic systems, 2x2 fcc (100) surfaces. The (A) and (D) configurations of atoms refer to arrangements in which two atoms are adjacent (A) or along the surface diagonal (D) (see Figure S6 for an illustration).

Metal	Adsorption Configuration	Reference Configuration	Adsorption Energy (eV)
Ag	1 Adatom	Clean	-1.67
Ag	2 Adatoms (D)	1 Adatom	-1.72
Ag	2 Adatoms (A)	1 Adatom	-2.06
Ag	3 Adatoms	2 Adatoms (A)	-2.03
Ag	3 Adatoms	2 Adatoms (D)	-2.38
Ag	4 Adatoms	3 Adatoms	-2.27
Au	1 Adatom	Clean	-2.29
Au	2 Adatoms (D)	1 Adatom	-2.11
Au	2 Adatoms (A)	1 Adatom	-2.57
Au	3 Adatoms	2 Adatoms (A)	-2.40
Au	3 Adatoms	2 Adatoms (D)	-2.86
Au	4 Adatoms	3 Adatoms	-2.65
Cu	1 Adatom	Clean	-2.48
Cu	2 Adatoms (D)	1 Adatom	-2.64
Cu	2 Adatoms (A)	1 Adatom	-3.12
Cu	3 Adatoms	2 Adatoms (A)	-3.11
Cu	3 Adatoms	2 Adatoms (D)	-3.58
Cu	4 Adatoms	3 Adatoms	-3.42
Ir	1 Adatom	Clean	-5.89
Ir	2 Adatoms (D)	1 Adatom	-5.67
Ir	2 Adatoms (A)	1 Adatom	-6.93
Ir	3 Adatoms	2 Adatoms (A)	-6.54
Ir	3 Adatoms	2 Adatoms (D)	-7.80
Ir	4 Adatoms	3 Adatoms	-7.11
Pd	1 Adatom	Clean	-2.63
Pd	2 Adatoms (D)	1 Adatom	-2.62
Pd	2 Adatoms (A)	1 Adatom	-3.10
Pd	3 Adatoms	2 Adatoms (A)	-3.15
Pd	3 Adatoms	2 Adatoms (D)	-3.62
Pd	4 Adatoms	3 Adatoms	-3.65
Pt	1 Adatom	Clean	-4.50
Pt	2 Adatoms (D)	1 Adatom	-4.08
Pt	2 Adatoms (A)	1 Adatom	-4.83
Pt	3 Adatoms	2 Adatoms (A)	-4.63
Pt	3 Adatoms	2 Adatoms (D)	-5.38
Pt	4 Adatoms	3 Adatoms	-5.13
Rh	1 Adatom	Clean	-4.45
Rh	2 Adatoms (D)	1 Adatom	-4.47
Rh	2 Adatoms (A)	1 Adatom	-5.23
Rh	3 Adatoms	2 Adatoms (A)	-5.19
Rh	3 Adatoms	2 Adatoms (D)	-5.95
Rh	4 Adatoms	3 Adatoms	-5.74

Table S3: DFT-calculated adsorption energies for monometallic systems, 1x3 fcc (211) surfaces.

Metal	Adsorption Configuration	Reference Configuration	Adsorption Energy (eV)
Ag	1 Adatom	Clean	-1.85
Ag	2 Adatoms	1 Adatom	-1.98
Ag	3 Adatoms	2 Adatoms	-2.16
Au	1 Adatom	Clean	-2.33
Au	2 Adatoms	1 Adatom	-2.45
Au	3 Adatoms	2 Adatoms	-2.62
Cu	1 Adatom	Clean	-2.79
Cu	2 Adatoms	1 Adatom	-3.00
Cu	3 Adatoms	2 Adatoms	-3.28
Ir	1 Adatom	Clean	-6.21
Ir	2 Adatoms	1 Adatom	-6.43
Ir	3 Adatoms	2 Adatoms	-7.18
Pd	1 Adatom	Clean	-2.85
Pd	2 Adatoms	1 Adatom	-3.09
Pd	3 Adatoms	2 Adatoms	-3.42
Pt	1 Adatom	Clean	-4.43
Pt	2 Adatoms	1 Adatom	-4.70
Pt	3 Adatoms	2 Adatoms	-5.21
Rh	1 Adatom	Clean	-4.83
Rh	2 Adatoms	1 Adatom	-5.05
Rh	3 Adatoms	2 Adatoms	-5.55

Table S4: DFT-calculated adsorption energies for monometallic systems, 3x3 bulk unit cell.

Metal	Adsorption Energy (eV)
Ag	-2.70
Au	-2.82
Cu	-4.04
Ir	-8.57
Pd	-4.32
Pt	-5.46
Rh	-7.07

Table S5: DFT-calculated adsorption energies for bimetallic systems, 2x2 fcc (111) surfaces. Empty rows correspond to cases of reconstruction.

Surface Orientation	Host Slab	Heteroatom	Top Layer Configuration	Reference Configuration	Adsorption Energy (eV)
(111)	Ag	Au	Au1Ag0	Clean Ag	-2.10
(111)	Ag	Au	Au2Ag0	Au1Ag0	-2.49
(111)	Ag	Au	Au3Ag0	Au2Ag0	-2.76
(111)	Ag	Au	Au4Ag0	Au3Ag0	-2.92
(111)	Ag	Au	Au1Ag1	Au0Ag1	-2.58
(111)	Ag	Au	Au1Ag1	Au1Ag0	-1.98
(111)	Ag	Au	Au1Ag2	Au0Ag2	-2.86
(111)	Ag	Au	Au1Ag2	Au1Ag1	-2.21
(111)	Ag	Au	Au2Ag1	Au1Ag1	-2.79
(111)	Ag	Au	Au2Ag1	Au2Ag0	-2.28
(111)	Ag	Au	Au1Ag3	Au0Ag3	-3.07
(111)	Ag	Au	Au1Ag3	Au1Ag2	-2.39
(111)	Ag	Au	Au2Ag2	Au1Ag2	-3.00
(111)	Ag	Au	Au2Ag2	Au2Ag1	-2.42
(111)	Ag	Au	Au3Ag1	Au2Ag1	-2.95
(111)	Ag	Au	Au3Ag1	Au3Ag0	-2.47
(111)	Ag	Cu	Cu1Ag0	Clean Ag	-1.92
(111)	Ag	Cu	Cu2Ag0	Cu1Ag0	
(111)	Ag	Cu	Cu3Ag0	Cu2Ag0	
(111)	Ag	Cu	Cu4Ag0	Cu3Ag0	
(111)	Ag	Cu	Cu1Ag1	Cu0Ag1	-2.34
(111)	Ag	Cu	Cu1Ag1	Cu1Ag0	-1.93
(111)	Ag	Cu	Cu1Ag2	Cu0Ag2	-2.64
(111)	Ag	Cu	Cu1Ag2	Cu1Ag1	-2.22
(111)	Ag	Cu	Cu2Ag1	Cu1Ag1	-2.66
(111)	Ag	Cu	Cu2Ag1	Cu2Ag0	
(111)	Ag	Cu	Cu1Ag3	Cu0Ag3	-2.91
(111)	Ag	Cu	Cu1Ag3	Cu1Ag2	-2.45
(111)	Ag	Cu	Cu2Ag2	Cu1Ag2	-2.95
(111)	Ag	Cu	Cu2Ag2	Cu2Ag1	-2.51
(111)	Ag	Cu	Cu3Ag1	Cu2Ag1	
(111)	Ag	Cu	Cu3Ag1	Cu3Ag0	
(111)	Ag	Ir	Ir1Ag0	Clean Ag	-2.69
(111)	Ag	Ir	Ir2Ag0	Ir1Ag0	
(111)	Ag	Ir	Ir3Ag0	Ir2Ag0	
(111)	Ag	Ir	Ir4Ag0	Ir3Ag0	
(111)	Ag	Ir	Ir1Ag1	Ir0Ag1	-3.58
(111)	Ag	Ir	Ir1Ag1	Ir1Ag0	-2.39
(111)	Ag	Ir	Ir1Ag2	Ir0Ag2	-4.39
(111)	Ag	Ir	Ir1Ag2	Ir1Ag1	-2.73
(111)	Ag	Ir	Ir2Ag1	Ir1Ag1	
(111)	Ag	Ir	Ir2Ag1	Ir2Ag0	
(111)	Ag	Ir	Ir1Ag3	Ir0Ag3	-5.08
(111)	Ag	Ir	Ir1Ag3	Ir1Ag2	-2.87
(111)	Ag	Ir	Ir2Ag2	Ir1Ag2	
(111)	Ag	Ir	Ir2Ag2	Ir2Ag1	
(111)	Ag	Ir	Ir3Ag1	Ir2Ag1	
(111)	Ag	Ir	Ir3Ag1	Ir3Ag0	

Surface Orientation	Host Slab	Heteroatom	Top Layer Configuration	Reference Configuration	Adsorption Energy (eV)
(111)	Ag	Pd	Pd1Ag0	Clean Ag	-2.03
(111)	Ag	Pd	Pd2Ag0	Pd1Ag0	-2.58
(111)	Ag	Pd	Pd3Ag0	Pd2Ag0	-3.21
(111)	Ag	Pd	Pd4Ag0	Pd3Ag0	-3.79
(111)	Ag	Pd	Pd1Ag1	Pd0Ag1	-2.63
(111)	Ag	Pd	Pd1Ag1	Pd1Ag0	-2.11
(111)	Ag	Pd	Pd1Ag2	Pd0Ag2	-3.13
(111)	Ag	Pd	Pd1Ag2	Pd1Ag1	-2.42
(111)	Ag	Pd	Pd2Ag1	Pd1Ag1	-3.13
(111)	Ag	Pd	Pd2Ag1	Pd2Ag0	-2.65
(111)	Ag	Pd	Pd1Ag3	Pd0Ag3	-3.50
(111)	Ag	Pd	Pd1Ag3	Pd1Ag2	-2.55
(111)	Ag	Pd	Pd2Ag2	Pd1Ag2	-3.53
(111)	Ag	Pd	Pd2Ag2	Pd2Ag1	-2.82
(111)	Ag	Pd	Pd3Ag1	Pd2Ag1	-3.65
(111)	Ag	Pd	Pd3Ag1	Pd3Ag0	-3.09
(111)	Ag	Pt	Pt1Ag0	Clean Ag	-3.05
(111)	Ag	Pt	Pt2Ag0	Pt1Ag0	-3.90
(111)	Ag	Pt	Pt3Ag0	Pt2Ag0	
(111)	Ag	Pt	Pt4Ag0	Pt3Ag0	
(111)	Ag	Pt	Pt1Ag1	Pt0Ag1	-3.81
(111)	Ag	Pt	Pt1Ag1	Pt1Ag0	-2.27
(111)	Ag	Pt	Pt1Ag2	Pt0Ag2	-4.43
(111)	Ag	Pt	Pt1Ag2	Pt1Ag1	-2.54
(111)	Ag	Pt	Pt2Ag1	Pt1Ag1	-4.55
(111)	Ag	Pt	Pt2Ag1	Pt2Ag0	-2.93
(111)	Ag	Pt	Pt1Ag3	Pt0Ag3	-4.88
(111)	Ag	Pt	Pt1Ag3	Pt1Ag2	-2.63
(111)	Ag	Pt	Pt2Ag2	Pt1Ag2	-5.00
(111)	Ag	Pt	Pt2Ag2	Pt2Ag1	-2.99
(111)	Ag	Pt	Pt3Ag1	Pt2Ag1	-5.30
(111)	Ag	Pt	Pt3Ag1	Pt3Ag0	
(111)	Ag	Rh	Rh1Ag0	Clean Ag	-2.39
(111)	Ag	Rh	Rh2Ag0	Rh1Ag0	
(111)	Ag	Rh	Rh3Ag0	Rh2Ag0	
(111)	Ag	Rh	Rh4Ag0	Rh3Ag0	
(111)	Ag	Rh	Rh1Ag1	Rh0Ag1	-3.13
(111)	Ag	Rh	Rh1Ag1	Rh1Ag0	-2.24
(111)	Ag	Rh	Rh1Ag2	Rh0Ag2	-3.81
(111)	Ag	Rh	Rh1Ag2	Rh1Ag1	-2.60
(111)	Ag	Rh	Rh2Ag1	Rh1Ag1	
(111)	Ag	Rh	Rh2Ag1	Rh2Ag0	
(111)	Ag	Rh	Rh1Ag3	Rh0Ag3	-4.40
(111)	Ag	Rh	Rh1Ag3	Rh1Ag2	-2.76
(111)	Ag	Rh	Rh2Ag2	Rh1Ag2	-4.68
(111)	Ag	Rh	Rh2Ag2	Rh2Ag1	
(111)	Ag	Rh	Rh3Ag1	Rh2Ag1	
(111)	Ag	Rh	Rh3Ag1	Rh3Ag0	

Surface Orientation	Host Slab	Heteroatom	Top Layer Configuration	Reference Configuration	Adsorption Energy (eV)
(111)	Au	Ag	Ag1Au0	Clean Au	-1.61
(111)	Au	Ag	Ag2Au0	Ag1Au0	-1.88
(111)	Au	Ag	Ag3Au0	Ag2Au0	-2.15
(111)	Au	Ag	Ag4Au0	Ag3Au0	-2.34
(111)	Au	Ag	Ag1Au1	Ag0Au1	-2.04
(111)	Au	Ag	Ag1Au1	Ag1Au0	-2.37
(111)	Au	Ag	Ag1Au2	Ag0Au2	-2.33
(111)	Au	Ag	Ag1Au2	Ag1Au1	-2.68
(111)	Au	Ag	Ag2Au1	Ag1Au1	-2.22
(111)	Au	Ag	Ag2Au1	Ag2Au0	-2.71
(111)	Au	Ag	Ag1Au3	Ag0Au3	-2.49
(111)	Au	Ag	Ag1Au3	Ag1Au2	-2.85
(111)	Au	Ag	Ag2Au2	Ag1Au2	-2.42
(111)	Au	Ag	Ag2Au2	Ag2Au1	-2.87
(111)	Au	Ag	Ag3Au1	Ag2Au1	-2.37
(111)	Au	Ag	Ag3Au1	Ag3Au0	-2.92
(111)	Au	Cu	Cu1Au0	Clean Au	-2.16
(111)	Au	Cu	Cu2Au0	Cu1Au0	-2.43
(111)	Au	Cu	Cu3Au0	Cu2Au0	
(111)	Au	Cu	Cu4Au0	Cu3Au0	
(111)	Au	Cu	Cu1Au1	Cu0Au1	-2.57
(111)	Au	Cu	Cu1Au1	Cu1Au0	-2.34
(111)	Au	Cu	Cu1Au2	Cu0Au2	-2.88
(111)	Au	Cu	Cu1Au2	Cu1Au1	-2.71
(111)	Au	Cu	Cu2Au1	Cu1Au1	
(111)	Au	Cu	Cu2Au1	Cu2Au0	
(111)	Au	Cu	Cu1Au3	Cu0Au3	-3.12
(111)	Au	Cu	Cu1Au3	Cu1Au2	-2.92
(111)	Au	Cu	Cu2Au2	Cu1Au2	-3.10
(111)	Au	Cu	Cu2Au2	Cu2Au1	
(111)	Au	Cu	Cu3Au1	Cu2Au1	
(111)	Au	Cu	Cu3Au1	Cu3Au0	
(111)	Au	Ir	Ir1Au0	Clean Au	-2.92
(111)	Au	Ir	Ir2Au0	Ir1Au0	
(111)	Au	Ir	Ir3Au0	Ir2Au0	
(111)	Au	Ir	Ir4Au0	Ir3Au0	
(111)	Au	Ir	Ir1Au1	Ir0Au1	-3.77
(111)	Au	Ir	Ir1Au1	Ir1Au0	-2.79
(111)	Au	Ir	Ir1Au2	Ir0Au2	-4.53
(111)	Au	Ir	Ir1Au2	Ir1Au1	-3.15
(111)	Au	Ir	Ir2Au1	Ir1Au1	
(111)	Au	Ir	Ir2Au1	Ir2Au0	
(111)	Au	Ir	Ir1Au3	Ir0Au3	-5.13
(111)	Au	Ir	Ir1Au3	Ir1Au2	-3.28
(111)	Au	Ir	Ir2Au2	Ir1Au2	
(111)	Au	Ir	Ir2Au2	Ir2Au1	
(111)	Au	Ir	Ir3Au1	Ir2Au1	
(111)	Au	Ir	Ir3Au1	Ir3Au0	

Surface Orientation	Host Slab	Heteroatom	Top Layer Configuration	Reference Configuration	Adsorption Energy (eV)
(111)	Au	Pd	Pd1Au0	Clean Au	-2.15
(111)	Au	Pd	Pd2Au0	Pd1Au0	-2.58
(111)	Au	Pd	Pd3Au0	Pd2Au0	-3.12
(111)	Au	Pd	Pd4Au0	Pd3Au0	-3.67
(111)	Au	Pd	Pd1Au1	Pd0Au1	-2.69
(111)	Au	Pd	Pd1Au1	Pd1Au0	-2.48
(111)	Au	Pd	Pd1Au2	Pd0Au2	-3.14
(111)	Au	Pd	Pd1Au2	Pd1Au1	-2.83
(111)	Au	Pd	Pd2Au1	Pd1Au1	-3.10
(111)	Au	Pd	Pd2Au1	Pd2Au0	-3.00
(111)	Au	Pd	Pd1Au3	Pd0Au3	-3.44
(111)	Au	Pd	Pd1Au3	Pd1Au2	-2.99
(111)	Au	Pd	Pd2Au2	Pd1Au2	-3.49
(111)	Au	Pd	Pd2Au2	Pd2Au1	-3.23
(111)	Au	Pd	Pd3Au1	Pd2Au1	-3.59
(111)	Au	Pd	Pd3Au1	Pd3Au0	-3.47
(111)	Au	Pt	Pt1Au0	Clean Au	-3.05
(111)	Au	Pt	Pt2Au0	Pt1Au0	-3.87
(111)	Au	Pt	Pt3Au0	Pt2Au0	-4.72
(111)	Au	Pt	Pt4Au0	Pt3Au0	-5.47
(111)	Au	Pt	Pt1Au1	Pt0Au1	-3.74
(111)	Au	Pt	Pt1Au1	Pt1Au0	-2.62
(111)	Au	Pt	Pt1Au2	Pt0Au2	-4.30
(111)	Au	Pt	Pt1Au2	Pt1Au1	-2.95
(111)	Au	Pt	Pt2Au1	Pt1Au1	-4.45
(111)	Au	Pt	Pt2Au1	Pt2Au0	-3.21
(111)	Au	Pt	Pt1Au3	Pt0Au3	-4.67
(111)	Au	Pt	Pt1Au3	Pt1Au2	-3.07
(111)	Au	Pt	Pt2Au2	Pt1Au2	-4.87
(111)	Au	Pt	Pt2Au2	Pt2Au1	-3.36
(111)	Au	Pt	Pt3Au1	Pt2Au1	-5.18
(111)	Au	Pt	Pt3Au1	Pt3Au0	-3.66
(111)	Au	Rh	Rh1Au0	Clean Au	-2.69
(111)	Au	Rh	Rh2Au0	Rh1Au0	
(111)	Au	Rh	Rh3Au0	Rh2Au0	
(111)	Au	Rh	Rh4Au0	Rh3Au0	
(111)	Au	Rh	Rh1Au1	Rh0Au1	-3.39
(111)	Au	Rh	Rh1Au1	Rh1Au0	-2.64
(111)	Au	Rh	Rh1Au2	Rh0Au2	-4.01
(111)	Au	Rh	Rh1Au2	Rh1Au1	-3.01
(111)	Au	Rh	Rh2Au1	Rh1Au1	
(111)	Au	Rh	Rh2Au1	Rh2Au0	
(111)	Au	Rh	Rh1Au3	Rh0Au3	-4.51
(111)	Au	Rh	Rh1Au3	Rh1Au2	-3.18
(111)	Au	Rh	Rh2Au2	Rh1Au2	-4.82
(111)	Au	Rh	Rh2Au2	Rh2Au1	
(111)	Au	Rh	Rh3Au1	Rh2Au1	
(111)	Au	Rh	Rh3Au1	Rh3Au0	

Surface Orientation	Host Slab	Heteroatom	Top Layer Configuration	Reference Configuration	Adsorption Energy (eV)
(111)	Cu	Ag	Ag1Cu0	Clean Cu	-1.75
(111)	Cu	Ag	Ag2Cu0	Ag1Cu0	
(111)	Cu	Ag	Ag3Cu0	Ag2Cu0	
(111)	Cu	Ag	Ag4Cu0	Ag3Cu0	
(111)	Cu	Ag	Ag1Cu1	Ag0Cu1	-2.18
(111)	Cu	Ag	Ag1Cu1	Ag1Cu0	-2.69
(111)	Cu	Ag	Ag1Cu2	Ag0Cu2	-2.46
(111)	Cu	Ag	Ag1Cu2	Ag1Cu1	-3.12
(111)	Cu	Ag	Ag2Cu1	Ag1Cu1	
(111)	Cu	Ag	Ag2Cu1	Ag2Cu0	
(111)	Cu	Ag	Ag1Cu3	Ag0Cu3	-2.61
(111)	Cu	Ag	Ag1Cu3	Ag1Cu2	-3.45
(111)	Cu	Ag	Ag2Cu2	Ag1Cu2	-2.23
(111)	Cu	Ag	Ag2Cu2	Ag2Cu1	
(111)	Cu	Ag	Ag3Cu1	Ag2Cu1	
(111)	Cu	Ag	Ag3Cu1	Ag3Cu0	
(111)	Cu	Au	Au1Cu0	Clean Cu	-2.41
(111)	Cu	Au	Au2Cu0	Au1Cu0	-2.71
(111)	Cu	Au	Au3Cu0	Au2Cu0	
(111)	Cu	Au	Au4Cu0	Au3Cu0	
(111)	Cu	Au	Au1Cu1	Au0Cu1	-3.02
(111)	Cu	Au	Au1Cu1	Au1Cu0	-2.87
(111)	Cu	Au	Au1Cu2	Au0Cu2	-3.40
(111)	Cu	Au	Au1Cu2	Au1Cu1	-3.22
(111)	Cu	Au	Au2Cu1	Au1Cu1	-2.97
(111)	Cu	Au	Au2Cu1	Au2Cu0	-3.13
(111)	Cu	Au	Au1Cu3	Au0Cu3	-3.58
(111)	Cu	Au	Au1Cu3	Au1Cu2	-3.48
(111)	Cu	Au	Au2Cu2	Au1Cu2	-3.00
(111)	Cu	Au	Au2Cu2	Au2Cu1	-3.26
(111)	Cu	Au	Au3Cu1	Au2Cu1	-2.36
(111)	Cu	Au	Au3Cu1	Au3Cu0	
(111)	Cu	Ir	Ir1Cu0	Clean Cu	-3.67
(111)	Cu	Ir	Ir2Cu0	Ir1Cu0	
(111)	Cu	Ir	Ir3Cu0	Ir2Cu0	
(111)	Cu	Ir	Ir4Cu0	Ir3Cu0	-7.88
(111)	Cu	Ir	Ir1Cu1	Ir0Cu1	
(111)	Cu	Ir	Ir1Cu1	Ir1Cu0	
(111)	Cu	Ir	Ir1Cu2	Ir0Cu2	-5.92
(111)	Cu	Ir	Ir1Cu2	Ir1Cu1	
(111)	Cu	Ir	Ir2Cu1	Ir1Cu1	
(111)	Cu	Ir	Ir2Cu1	Ir2Cu0	
(111)	Cu	Ir	Ir1Cu3	Ir0Cu3	-6.74
(111)	Cu	Ir	Ir1Cu3	Ir1Cu2	-4.12
(111)	Cu	Ir	Ir2Cu2	Ir1Cu2	-7.44
(111)	Cu	Ir	Ir2Cu2	Ir2Cu1	-4.40
(111)	Cu	Ir	Ir3Cu1	Ir2Cu1	-7.65
(111)	Cu	Ir	Ir3Cu1	Ir3Cu0	-4.63

Surface Orientation	Host Slab	Heteroatom	Top Layer Configuration	Reference Configuration	Adsorption Energy (eV)
(111)	Cu	Pd	Pd1Cu0	Clean Cu	-2.51
(111)	Cu	Pd	Pd2Cu0	Pd1Cu0	
(111)	Cu	Pd	Pd3Cu0	Pd2Cu0	
(111)	Cu	Pd	Pd4Cu0	Pd3Cu0	
(111)	Cu	Pd	Pd1Cu1	Pd0Cu1	-3.24
(111)	Cu	Pd	Pd1Cu1	Pd1Cu0	-2.99
(111)	Cu	Pd	Pd1Cu2	Pd0Cu2	-3.82
(111)	Cu	Pd	Pd1Cu2	Pd1Cu1	-3.42
(111)	Cu	Pd	Pd2Cu1	Pd1Cu1	-3.60
(111)	Cu	Pd	Pd2Cu1	Pd2Cu0	
(111)	Cu	Pd	Pd1Cu3	Pd0Cu3	-4.19
(111)	Cu	Pd	Pd1Cu3	Pd1Cu2	-3.67
(111)	Cu	Pd	Pd2Cu2	Pd1Cu2	-3.93
(111)	Cu	Pd	Pd2Cu2	Pd2Cu1	-3.75
(111)	Cu	Pd	Pd3Cu1	Pd2Cu1	-3.76
(111)	Cu	Pd	Pd3Cu1	Pd3Cu0	
(111)	Cu	Pt	Pt1Cu0	Clean Cu	-3.71
(111)	Cu	Pt	Pt2Cu0	Pt1Cu0	
(111)	Cu	Pt	Pt3Cu0	Pt2Cu0	
(111)	Cu	Pt	Pt4Cu0	Pt3Cu0	-5.72
(111)	Cu	Pt	Pt1Cu1	Pt0Cu1	-4.72
(111)	Cu	Pt	Pt1Cu1	Pt1Cu0	-3.27
(111)	Cu	Pt	Pt1Cu2	Pt0Cu2	-5.50
(111)	Cu	Pt	Pt1Cu2	Pt1Cu1	-3.63
(111)	Cu	Pt	Pt2Cu1	Pt1Cu1	-5.45
(111)	Cu	Pt	Pt2Cu1	Pt2Cu0	
(111)	Cu	Pt	Pt1Cu3	Pt0Cu3	-6.01
(111)	Cu	Pt	Pt1Cu3	Pt1Cu2	-3.80
(111)	Cu	Pt	Pt2Cu2	Pt1Cu2	-5.79
(111)	Cu	Pt	Pt2Cu2	Pt2Cu1	-3.97
(111)	Cu	Pt	Pt3Cu1	Pt2Cu1	-5.76
(111)	Cu	Pt	Pt3Cu1	Pt3Cu0	-4.06
(111)	Cu	Rh	Rh1Cu0	Clean Cu	-3.15
(111)	Cu	Rh	Rh2Cu0	Rh1Cu0	
(111)	Cu	Rh	Rh3Cu0	Rh2Cu0	
(111)	Cu	Rh	Rh4Cu0	Rh3Cu0	-6.00
(111)	Cu	Rh	Rh1Cu1	Rh0Cu1	
(111)	Cu	Rh	Rh1Cu1	Rh1Cu0	
(111)	Cu	Rh	Rh1Cu2	Rh0Cu2	-4.93
(111)	Cu	Rh	Rh1Cu2	Rh1Cu1	
(111)	Cu	Rh	Rh2Cu1	Rh1Cu1	
(111)	Cu	Rh	Rh2Cu1	Rh2Cu0	
(111)	Cu	Rh	Rh1Cu3	Rh0Cu3	-5.60
(111)	Cu	Rh	Rh1Cu3	Rh1Cu2	-3.96
(111)	Cu	Rh	Rh2Cu2	Rh1Cu2	-5.80
(111)	Cu	Rh	Rh2Cu2	Rh2Cu1	-4.21
(111)	Cu	Rh	Rh3Cu1	Rh2Cu1	-5.95
(111)	Cu	Rh	Rh3Cu1	Rh3Cu0	-4.29

Surface Orientation	Host Slab	Heteroatom	Top Layer Configuration	Reference Configuration	Adsorption Energy (eV)
(111)	Ir	Ag	Ag1Ir0	Clean Ir	-2.00
(111)	Ir	Ag	Ag2Ir0	Ag1Ir0	-2.09
(111)	Ir	Ag	Ag3Ir0	Ag2Ir0	-2.28
(111)	Ir	Ag	Ag4Ir0	Ag3Ir0	-2.31
(111)	Ir	Ag	Ag1Ir1	Ag0Ir1	-2.47
(111)	Ir	Ag	Ag1Ir1	Ag1Ir0	-5.27
(111)	Ir	Ag	Ag1Ir2	Ag0Ir2	-2.79
(111)	Ir	Ag	Ag1Ir2	Ag1Ir1	-6.65
(111)	Ir	Ag	Ag2Ir1	Ag1Ir1	-2.56
(111)	Ir	Ag	Ag2Ir1	Ag2Ir0	-5.73
(111)	Ir	Ag	Ag1Ir3	Ag0Ir3	
(111)	Ir	Ag	Ag1Ir3	Ag1Ir2	
(111)	Ir	Ag	Ag2Ir2	Ag1Ir2	-2.87
(111)	Ir	Ag	Ag2Ir2	Ag2Ir1	-6.97
(111)	Ir	Ag	Ag3Ir1	Ag2Ir1	-2.60
(111)	Ir	Ag	Ag3Ir1	Ag3Ir0	-6.06
(111)	Ir	Au	Au1Ir0	Clean Ir	-2.44
(111)	Ir	Au	Au2Ir0	Au1Ir0	-2.78
(111)	Ir	Au	Au3Ir0	Au2Ir0	-2.91
(111)	Ir	Au	Au4Ir0	Au3Ir0	-2.73
(111)	Ir	Au	Au1Ir1	Au0Ir1	-3.18
(111)	Ir	Au	Au1Ir1	Au1Ir0	-5.53
(111)	Ir	Au	Au1Ir2	Au0Ir2	-3.52
(111)	Ir	Au	Au1Ir2	Au1Ir1	-6.68
(111)	Ir	Au	Au2Ir1	Au1Ir1	-3.21
(111)	Ir	Au	Au2Ir1	Au2Ir0	-5.97
(111)	Ir	Au	Au1Ir3	Au0Ir3	-3.90
(111)	Ir	Au	Au1Ir3	Au1Ir2	-7.58
(111)	Ir	Au	Au2Ir2	Au1Ir2	-3.49
(111)	Ir	Au	Au2Ir2	Au2Ir1	-6.96
(111)	Ir	Au	Au3Ir1	Au2Ir1	-3.12
(111)	Ir	Au	Au3Ir1	Au3Ir0	-6.18
(111)	Ir	Cu	Cu1Ir0	Clean Ir	-2.74
(111)	Ir	Cu	Cu2Ir0	Cu1Ir0	-3.01
(111)	Ir	Cu	Cu3Ir0	Cu2Ir0	-3.42
(111)	Ir	Cu	Cu4Ir0	Cu3Ir0	-3.80
(111)	Ir	Cu	Cu1Ir1	Cu0Ir1	-3.39
(111)	Ir	Cu	Cu1Ir1	Cu1Ir0	-5.46
(111)	Ir	Cu	Cu1Ir2	Cu0Ir2	-3.90
(111)	Ir	Cu	Cu1Ir2	Cu1Ir1	-6.84
(111)	Ir	Cu	Cu2Ir1	Cu1Ir1	-3.71
(111)	Ir	Cu	Cu2Ir1	Cu2Ir0	-6.15
(111)	Ir	Cu	Cu1Ir3	Cu0Ir3	-4.43
(111)	Ir	Cu	Cu1Ir3	Cu1Ir2	-7.73
(111)	Ir	Cu	Cu2Ir2	Cu1Ir2	-4.22
(111)	Ir	Cu	Cu2Ir2	Cu2Ir1	-7.35
(111)	Ir	Cu	Cu3Ir1	Cu2Ir1	-4.04
(111)	Ir	Cu	Cu3Ir1	Cu3Ir0	-6.77

Surface Orientation	Host Slab	Heteroatom	Top Layer Configuration	Reference Configuration	Adsorption Energy (eV)
(111)	Ir	Pd	Pd1Ir0	Clean Ir	-2.93
(111)	Ir	Pd	Pd2Ir0	Pd1Ir0	-3.30
(111)	Ir	Pd	Pd3Ir0	Pd2Ir0	-3.58
(111)	Ir	Pd	Pd4Ir0	Pd3Ir0	-3.87
(111)	Ir	Pd	Pd1Ir1	Pd0Ir1	-3.72
(111)	Ir	Pd	Pd1Ir1	Pd1Ir0	-5.59
(111)	Ir	Pd	Pd1Ir2	Pd0Ir2	-4.15
(111)	Ir	Pd	Pd1Ir2	Pd1Ir1	-6.76
(111)	Ir	Pd	Pd2Ir1	Pd1Ir1	-3.89
(111)	Ir	Pd	Pd2Ir1	Pd2Ir0	-6.18
(111)	Ir	Pd	Pd1Ir3	Pd0Ir3	-4.72
(111)	Ir	Pd	Pd1Ir3	Pd1Ir2	-7.78
(111)	Ir	Pd	Pd2Ir2	Pd1Ir2	-4.44
(111)	Ir	Pd	Pd2Ir2	Pd2Ir1	-7.30
(111)	Ir	Pd	Pd3Ir1	Pd2Ir1	-4.17
(111)	Ir	Pd	Pd3Ir1	Pd3Ir0	-6.78
(111)	Ir	Pt	Pt1Ir0	Clean Ir	-4.17
(111)	Ir	Pt	Pt2Ir0	Pt1Ir0	-5.04
(111)	Ir	Pt	Pt3Ir0	Pt2Ir0	-5.47
(111)	Ir	Pt	Pt4Ir0	Pt3Ir0	-5.80
(111)	Ir	Pt	Pt1Ir1	Pt0Ir1	-5.34
(111)	Ir	Pt	Pt1Ir1	Pt1Ir0	-5.96
(111)	Ir	Pt	Pt1Ir2	Pt0Ir2	
(111)	Ir	Pt	Pt1Ir2	Pt1Ir1	
(111)	Ir	Pt	Pt2Ir1	Pt1Ir1	-5.69
(111)	Ir	Pt	Pt2Ir1	Pt2Ir0	-6.61
(111)	Ir	Pt	Pt1Ir3	Pt0Ir3	-6.62
(111)	Ir	Pt	Pt1Ir3	Pt1Ir2	
(111)	Ir	Pt	Pt2Ir2	Pt1Ir2	
(111)	Ir	Pt	Pt2Ir2	Pt2Ir1	-7.58
(111)	Ir	Pt	Pt3Ir1	Pt2Ir1	-6.08
(111)	Ir	Pt	Pt3Ir1	Pt3Ir0	-7.22
(111)	Ir	Rh	Rh1Ir0	Clean Ir	-4.13
(111)	Ir	Rh	Rh2Ir0	Rh1Ir0	-5.02
(111)	Ir	Rh	Rh3Ir0	Rh2Ir0	-5.62
(111)	Ir	Rh	Rh4Ir0	Rh3Ir0	-6.36
(111)	Ir	Rh	Rh1Ir1	Rh0Ir1	-5.32
(111)	Ir	Rh	Rh1Ir1	Rh1Ir0	-5.99
(111)	Ir	Rh	Rh1Ir2	Rh0Ir2	-6.00
(111)	Ir	Rh	Rh1Ir2	Rh1Ir1	-7.01
(111)	Ir	Rh	Rh2Ir1	Rh1Ir1	-5.82
(111)	Ir	Rh	Rh2Ir1	Rh2Ir0	-6.79
(111)	Ir	Rh	Rh1Ir3	Rh0Ir3	-6.86
(111)	Ir	Rh	Rh1Ir3	Rh1Ir2	-8.06
(111)	Ir	Rh	Rh2Ir2	Rh1Ir2	-6.70
(111)	Ir	Rh	Rh2Ir2	Rh2Ir1	-7.89
(111)	Ir	Rh	Rh3Ir1	Rh2Ir1	-6.53
(111)	Ir	Rh	Rh3Ir1	Rh3Ir0	-7.71

Surface Orientation	Host Slab	Heteroatom	Top Layer Configuration	Reference Configuration	Adsorption Energy (eV)
(111)	Pd	Ag	Ag1Pd0	Clean Pd	-1.87
(111)	Pd	Ag	Ag2Pd0	Ag1Pd0	-2.21
(111)	Pd	Ag	Ag3Pd0	Ag2Pd0	-2.44
(111)	Pd	Ag	Ag4Pd0	Ag3Pd0	-2.53
(111)	Pd	Ag	Ag1Pd1	Ag0Pd1	-2.37
(111)	Pd	Ag	Ag1Pd1	Ag1Pd0	-2.76
(111)	Pd	Ag	Ag1Pd2	Ag0Pd2	-2.79
(111)	Pd	Ag	Ag1Pd2	Ag1Pd1	-3.31
(111)	Pd	Ag	Ag2Pd1	Ag1Pd1	-2.64
(111)	Pd	Ag	Ag2Pd1	Ag2Pd0	-3.19
(111)	Pd	Ag	Ag1Pd3	Ag0Pd3	-3.11
(111)	Pd	Ag	Ag1Pd3	Ag1Pd2	-3.79
(111)	Pd	Ag	Ag2Pd2	Ag1Pd2	-2.95
(111)	Pd	Ag	Ag2Pd2	Ag2Pd1	-3.62
(111)	Pd	Ag	Ag3Pd1	Ag2Pd1	-2.76
(111)	Pd	Ag	Ag3Pd1	Ag3Pd0	-3.50
(111)	Pd	Au	Au1Pd0	Clean Pd	-2.22
(111)	Pd	Au	Au2Pd0	Au1Pd0	-2.81
(111)	Pd	Au	Au3Pd0	Au2Pd0	-3.09
(111)	Pd	Au	Au4Pd0	Au3Pd0	-3.07
(111)	Pd	Au	Au1Pd1	Au0Pd1	-2.88
(111)	Pd	Au	Au1Pd1	Au1Pd0	-2.90
(111)	Pd	Au	Au1Pd2	Au0Pd2	-3.37
(111)	Pd	Au	Au1Pd2	Au1Pd1	-3.40
(111)	Pd	Au	Au2Pd1	Au1Pd1	-3.23
(111)	Pd	Au	Au2Pd1	Au2Pd0	-3.32
(111)	Pd	Au	Au1Pd3	Au0Pd3	-3.71
(111)	Pd	Au	Au1Pd3	Au1Pd2	-3.81
(111)	Pd	Au	Au2Pd2	Au1Pd2	-3.52
(111)	Pd	Au	Au2Pd2	Au2Pd1	-3.68
(111)	Pd	Au	Au3Pd1	Au2Pd1	-3.32
(111)	Pd	Au	Au3Pd1	Au3Pd0	-3.55
(111)	Pd	Cu	Cu1Pd0	Clean Pd	-2.43
(111)	Pd	Cu	Cu2Pd0	Cu1Pd0	-2.88
(111)	Pd	Cu	Cu3Pd0	Cu2Pd0	-3.29
(111)	Pd	Cu	Cu4Pd0	Cu3Pd0	-3.66
(111)	Pd	Cu	Cu1Pd1	Cu0Pd1	-3.03
(111)	Pd	Cu	Cu1Pd1	Cu1Pd0	-2.85
(111)	Pd	Cu	Cu1Pd2	Cu0Pd2	-3.54
(111)	Pd	Cu	Cu1Pd2	Cu1Pd1	-3.42
(111)	Pd	Cu	Cu2Pd1	Cu1Pd1	-3.43
(111)	Pd	Cu	Cu2Pd1	Cu2Pd0	-3.40
(111)	Pd	Cu	Cu1Pd3	Cu0Pd3	-3.98
(111)	Pd	Cu	Cu1Pd3	Cu1Pd2	-3.91
(111)	Pd	Cu	Cu2Pd2	Cu1Pd2	-3.88
(111)	Pd	Cu	Cu2Pd2	Cu2Pd1	-3.87
(111)	Pd	Cu	Cu3Pd1	Cu2Pd1	-3.77
(111)	Pd	Cu	Cu3Pd1	Cu3Pd0	-3.89

Surface Orientation	Host Slab	Heteroatom	Top Layer Configuration	Reference Configuration	Adsorption Energy (eV)
(111)	Pd	Ir	Ir1Pd0	Clean Pd	-3.65
(111)	Pd	Ir	Ir2Pd0	Ir1Pd0	
(111)	Pd	Ir	Ir3Pd0	Ir2Pd0	
(111)	Pd	Ir	Ir4Pd0	Ir3Pd0	
(111)	Pd	Ir	Ir1Pd1	Ir0Pd1	-4.77
(111)	Pd	Ir	Ir1Pd1	Ir1Pd0	-3.38
(111)	Pd	Ir	Ir1Pd2	Ir0Pd2	-5.72
(111)	Pd	Ir	Ir1Pd2	Ir1Pd1	-3.85
(111)	Pd	Ir	Ir2Pd1	Ir1Pd1	
(111)	Pd	Ir	Ir2Pd1	Ir2Pd0	
(111)	Pd	Ir	Ir1Pd3	Ir0Pd3	-6.50
(111)	Pd	Ir	Ir1Pd3	Ir1Pd2	-4.25
(111)	Pd	Ir	Ir2Pd2	Ir1Pd2	-7.02
(111)	Pd	Ir	Ir2Pd2	Ir2Pd1	
(111)	Pd	Ir	Ir3Pd1	Ir2Pd1	
(111)	Pd	Ir	Ir3Pd1	Ir3Pd0	
(111)	Pd	Pt	Pt1Pd0	Clean Pd	-3.36
(111)	Pd	Pt	Pt2Pd0	Pt1Pd0	-4.52
(111)	Pd	Pt	Pt3Pd0	Pt2Pd0	-5.35
(111)	Pd	Pt	Pt4Pd0	Pt3Pd0	-5.91
(111)	Pd	Pt	Pt1Pd1	Pt0Pd1	-4.26
(111)	Pd	Pt	Pt1Pd1	Pt1Pd0	-3.15
(111)	Pd	Pt	Pt1Pd2	Pt0Pd2	-5.00
(111)	Pd	Pt	Pt1Pd2	Pt1Pd1	-3.64
(111)	Pd	Pt	Pt2Pd1	Pt1Pd1	-5.18
(111)	Pd	Pt	Pt2Pd1	Pt2Pd0	-3.80
(111)	Pd	Pt	Pt1Pd3	Pt0Pd3	-5.56
(111)	Pd	Pt	Pt1Pd3	Pt1Pd2	-4.03
(111)	Pd	Pt	Pt2Pd2	Pt1Pd2	-5.68
(111)	Pd	Pt	Pt2Pd2	Pt2Pd1	-4.14
(111)	Pd	Pt	Pt3Pd1	Pt2Pd1	-5.79
(111)	Pd	Pt	Pt3Pd1	Pt3Pd0	-4.25
(111)	Pd	Rh	Rh1Pd0	Clean Pd	-3.12
(111)	Pd	Rh	Rh2Pd0	Rh1Pd0	-4.32
(111)	Pd	Rh	Rh3Pd0	Rh2Pd0	
(111)	Pd	Rh	Rh4Pd0	Rh3Pd0	
(111)	Pd	Rh	Rh1Pd1	Rh0Pd1	-3.99
(111)	Pd	Rh	Rh1Pd1	Rh1Pd0	-3.12
(111)	Pd	Rh	Rh1Pd2	Rh0Pd2	-4.73
(111)	Pd	Rh	Rh1Pd2	Rh1Pd1	-3.65
(111)	Pd	Rh	Rh2Pd1	Rh1Pd1	
(111)	Pd	Rh	Rh2Pd1	Rh2Pd0	
(111)	Pd	Rh	Rh1Pd3	Rh0Pd3	-5.35
(111)	Pd	Rh	Rh1Pd3	Rh1Pd2	-4.09
(111)	Pd	Rh	Rh2Pd2	Rh1Pd2	-5.59
(111)	Pd	Rh	Rh2Pd2	Rh2Pd1	
(111)	Pd	Rh	Rh3Pd1	Rh2Pd1	
(111)	Pd	Rh	Rh3Pd1	Rh3Pd0	

Surface Orientation	Host Slab	Heteroatom	Top Layer Configuration	Reference Configuration	Adsorption Energy (eV)
(111)	Pt	Ag	Ag1Pt0	Clean Pt	-2.01
(111)	Pt	Ag	Ag2Pt0	Ag1Pt0	-2.15
(111)	Pt	Ag	Ag3Pt0	Ag2Pt0	-2.38
(111)	Pt	Ag	Ag4Pt0	Ag3Pt0	-2.48
(111)	Pt	Ag	Ag1Pt1	Ag0Pt1	-2.41
(111)	Pt	Ag	Ag1Pt1	Ag1Pt0	-4.14
(111)	Pt	Ag	Ag1Pt2	Ag0Pt2	-2.80
(111)	Pt	Ag	Ag1Pt2	Ag1Pt1	-4.94
(111)	Pt	Ag	Ag2Pt1	Ag1Pt1	-2.61
(111)	Pt	Ag	Ag2Pt1	Ag2Pt0	-4.61
(111)	Pt	Ag	Ag1Pt3	Ag0Pt3	-3.11
(111)	Pt	Ag	Ag1Pt3	Ag1Pt2	-5.47
(111)	Pt	Ag	Ag2Pt2	Ag1Pt2	-2.92
(111)	Pt	Ag	Ag2Pt2	Ag2Pt1	-5.25
(111)	Pt	Ag	Ag3Pt1	Ag2Pt1	-2.72
(111)	Pt	Ag	Ag3Pt1	Ag3Pt0	-4.95
(111)	Pt	Au	Au1Pt0	Clean Pt	-2.27
(111)	Pt	Au	Au2Pt0	Au1Pt0	-2.70
(111)	Pt	Au	Au3Pt0	Au2Pt0	-2.96
(111)	Pt	Au	Au4Pt0	Au3Pt0	-2.97
(111)	Pt	Au	Au1Pt1	Au0Pt1	-2.85
(111)	Pt	Au	Au1Pt1	Au1Pt0	-4.31
(111)	Pt	Au	Au1Pt2	Au0Pt2	-3.27
(111)	Pt	Au	Au1Pt2	Au1Pt1	-4.98
(111)	Pt	Au	Au2Pt1	Au1Pt1	-3.13
(111)	Pt	Au	Au2Pt1	Au2Pt0	-4.74
(111)	Pt	Au	Au1Pt3	Au0Pt3	-3.56
(111)	Pt	Au	Au1Pt3	Au1Pt2	-5.44
(111)	Pt	Au	Au2Pt2	Au1Pt2	-3.38
(111)	Pt	Au	Au2Pt2	Au2Pt1	-5.22
(111)	Pt	Au	Au3Pt1	Au2Pt1	-3.19
(111)	Pt	Au	Au3Pt1	Au3Pt0	-4.97
(111)	Pt	Cu	Cu1Pt0	Clean Pt	-2.71
(111)	Pt	Cu	Cu2Pt0	Cu1Pt0	-2.93
(111)	Pt	Cu	Cu3Pt0	Cu2Pt0	-3.29
(111)	Pt	Cu	Cu4Pt0	Cu3Pt0	-3.62
(111)	Pt	Cu	Cu1Pt1	Cu0Pt1	-3.19
(111)	Pt	Cu	Cu1Pt1	Cu1Pt0	-4.21
(111)	Pt	Cu	Cu1Pt2	Cu0Pt2	-3.66
(111)	Pt	Cu	Cu1Pt2	Cu1Pt1	-5.03
(111)	Pt	Cu	Cu2Pt1	Cu1Pt1	-3.51
(111)	Pt	Cu	Cu2Pt1	Cu2Pt0	-4.80
(111)	Pt	Cu	Cu1Pt3	Cu0Pt3	-4.09
(111)	Pt	Cu	Cu1Pt3	Cu1Pt2	-5.59
(111)	Pt	Cu	Cu2Pt2	Cu1Pt2	-3.95
(111)	Pt	Cu	Cu2Pt2	Cu2Pt1	-5.47
(111)	Pt	Cu	Cu3Pt1	Cu2Pt1	-3.81
(111)	Pt	Cu	Cu3Pt1	Cu3Pt0	-5.31

Surface Orientation	Host Slab	Heteroatom	Top Layer Configuration	Reference Configuration	Adsorption Energy (eV)
(111)	Pt	Ir	Ir1Pt0	Clean Pt	-4.21
(111)	Pt	Ir	Ir2Pt0	Ir1Pt0	
(111)	Pt	Ir	Ir3Pt0	Ir2Pt0	
(111)	Pt	Ir	Ir4Pt0	Ir3Pt0	
(111)	Pt	Ir	Ir1Pt1	Ir0Pt1	-5.32
(111)	Pt	Ir	Ir1Pt1	Ir1Pt0	-4.85
(111)	Pt	Ir	Ir1Pt2	Ir0Pt2	-6.15
(111)	Pt	Ir	Ir1Pt2	Ir1Pt1	-5.38
(111)	Pt	Ir	Ir2Pt1	Ir1Pt1	
(111)	Pt	Ir	Ir2Pt1	Ir2Pt0	
(111)	Pt	Ir	Ir1Pt3	Ir0Pt3	-6.90
(111)	Pt	Ir	Ir1Pt3	Ir1Pt2	-5.91
(111)	Pt	Ir	Ir2Pt2	Ir1Pt2	-7.18
(111)	Pt	Ir	Ir2Pt2	Ir2Pt1	
(111)	Pt	Ir	Ir3Pt1	Ir2Pt1	
(111)	Pt	Ir	Ir3Pt1	Ir3Pt0	
(111)	Pt	Pd	Pd1Pt0	Clean Pt	-2.63
(111)	Pt	Pd	Pd2Pt0	Pd1Pt0	-2.98
(111)	Pt	Pd	Pd3Pt0	Pd2Pt0	-3.38
(111)	Pt	Pd	Pd4Pt0	Pd3Pt0	-3.79
(111)	Pt	Pd	Pd1Pt1	Pd0Pt1	-3.20
(111)	Pt	Pd	Pd1Pt1	Pd1Pt0	-4.31
(111)	Pt	Pd	Pd1Pt2	Pd0Pt2	-3.66
(111)	Pt	Pd	Pd1Pt2	Pd1Pt1	-5.02
(111)	Pt	Pd	Pd2Pt1	Pd1Pt1	-3.53
(111)	Pt	Pd	Pd2Pt1	Pd2Pt0	-4.86
(111)	Pt	Pd	Pd1Pt3	Pd0Pt3	-4.08
(111)	Pt	Pd	Pd1Pt3	Pd1Pt2	-5.58
(111)	Pt	Pd	Pd2Pt2	Pd1Pt2	-3.99
(111)	Pt	Pd	Pd2Pt2	Pd2Pt1	-5.48
(111)	Pt	Pd	Pd3Pt1	Pd2Pt1	-3.90
(111)	Pt	Pd	Pd3Pt1	Pd3Pt0	-5.37
(111)	Pt	Rh	Rh1Pt0	Clean Pt	-3.69
(111)	Pt	Rh	Rh2Pt0	Rh1Pt0	-4.51
(111)	Pt	Rh	Rh3Pt0	Rh2Pt0	-5.17
(111)	Pt	Rh	Rh4Pt0	Rh3Pt0	-5.92
(111)	Pt	Rh	Rh1Pt1	Rh0Pt1	-4.53
(111)	Pt	Rh	Rh1Pt1	Rh1Pt0	-4.57
(111)	Pt	Rh	Rh1Pt2	Rh0Pt2	-5.16
(111)	Pt	Rh	Rh1Pt2	Rh1Pt1	-5.19
(111)	Pt	Rh	Rh2Pt1	Rh1Pt1	-5.17
(111)	Pt	Rh	Rh2Pt1	Rh2Pt0	-5.24
(111)	Pt	Rh	Rh1Pt3	Rh0Pt3	-5.76
(111)	Pt	Rh	Rh1Pt3	Rh1Pt2	-5.77
(111)	Pt	Rh	Rh2Pt2	Rh1Pt2	-5.83
(111)	Pt	Rh	Rh2Pt2	Rh2Pt1	-5.85
(111)	Pt	Rh	Rh3Pt1	Rh2Pt1	-5.87
(111)	Pt	Rh	Rh3Pt1	Rh3Pt0	-5.94

Surface Orientation	Host Slab	Heteroatom	Top Layer Configuration	Reference Configuration	Adsorption Energy (eV)
(111)	Rh	Ag	Ag1Rh0	Clean Rh	-1.92
(111)	Rh	Ag	Ag2Rh0	Ag1Rh0	-2.15
(111)	Rh	Ag	Ag3Rh0	Ag2Rh0	-2.29
(111)	Rh	Ag	Ag4Rh0	Ag3Rh0	-2.26
(111)	Rh	Ag	Ag1Rh1	Ag0Rh1	-2.42
(111)	Rh	Ag	Ag1Rh1	Ag1Rh0	-4.25
(111)	Rh	Ag	Ag1Rh2	Ag0Rh2	-2.75
(111)	Rh	Ag	Ag1Rh2	Ag1Rh1	-5.19
(111)	Rh	Ag	Ag2Rh1	Ag1Rh1	-2.57
(111)	Rh	Ag	Ag2Rh1	Ag2Rh0	-4.67
(111)	Rh	Ag	Ag1Rh3	Ag0Rh3	-3.08
(111)	Rh	Ag	Ag1Rh3	Ag1Rh2	-5.94
(111)	Rh	Ag	Ag2Rh2	Ag1Rh2	-2.84
(111)	Rh	Ag	Ag2Rh2	Ag2Rh1	-5.46
(111)	Rh	Ag	Ag3Rh1	Ag2Rh1	-2.53
(111)	Rh	Ag	Ag3Rh1	Ag3Rh0	-4.91
(111)	Rh	Au	Au1Rh0	Clean Rh	-2.43
(111)	Rh	Au	Au2Rh0	Au1Rh0	-2.87
(111)	Rh	Au	Au3Rh0	Au2Rh0	-2.97
(111)	Rh	Au	Au4Rh0	Au3Rh0	-2.71
(111)	Rh	Au	Au1Rh1	Au0Rh1	-3.16
(111)	Rh	Au	Au1Rh1	Au1Rh0	-4.47
(111)	Rh	Au	Au1Rh2	Au0Rh2	-3.56
(111)	Rh	Au	Au1Rh2	Au1Rh1	-5.28
(111)	Rh	Au	Au2Rh1	Au1Rh1	-3.26
(111)	Rh	Au	Au2Rh1	Au2Rh0	-4.86
(111)	Rh	Au	Au1Rh3	Au0Rh3	-3.93
(111)	Rh	Au	Au1Rh3	Au1Rh2	-5.98
(111)	Rh	Au	Au2Rh2	Au1Rh2	-3.54
(111)	Rh	Au	Au2Rh2	Au2Rh1	-5.56
(111)	Rh	Au	Au3Rh1	Au2Rh1	-3.15
(111)	Rh	Au	Au3Rh1	Au3Rh0	-5.04
(111)	Rh	Cu	Cu1Rh0	Clean Rh	-2.55
(111)	Rh	Cu	Cu2Rh0	Cu1Rh0	-3.00
(111)	Rh	Cu	Cu3Rh0	Cu2Rh0	-3.43
(111)	Rh	Cu	Cu4Rh0	Cu3Rh0	-3.80
(111)	Rh	Cu	Cu1Rh1	Cu0Rh1	-3.26
(111)	Rh	Cu	Cu1Rh1	Cu1Rh0	-4.45
(111)	Rh	Cu	Cu1Rh2	Cu0Rh2	-3.78
(111)	Rh	Cu	Cu1Rh2	Cu1Rh1	-5.39
(111)	Rh	Cu	Cu2Rh1	Cu1Rh1	-3.63
(111)	Rh	Cu	Cu2Rh1	Cu2Rh0	-5.08
(111)	Rh	Cu	Cu1Rh3	Cu0Rh3	-4.28
(111)	Rh	Cu	Cu1Rh3	Cu1Rh2	-6.11
(111)	Rh	Cu	Cu2Rh2	Cu1Rh2	-4.12
(111)	Rh	Cu	Cu2Rh2	Cu2Rh1	-5.88
(111)	Rh	Cu	Cu3Rh1	Cu2Rh1	-3.96
(111)	Rh	Cu	Cu3Rh1	Cu3Rh0	-5.62

Surface Orientation	Host Slab	Heteroatom	Top Layer Configuration	Reference Configuration	Adsorption Energy (eV)
(111)	Rh	Ir	Ir1Rh0	Clean Rh	-4.47
(111)	Rh	Ir	Ir2Rh0	Ir1Rh0	-6.25
(111)	Rh	Ir	Ir3Rh0	Ir2Rh0	-7.29
(111)	Rh	Ir	Ir4Rh0	Ir3Rh0	-8.27
(111)	Rh	Ir	Ir1Rh1	Ir0Rh1	-5.90
(111)	Rh	Ir	Ir1Rh1	Ir1Rh0	-5.18
(111)	Rh	Ir	Ir1Rh2	Ir0Rh2	-6.85
(111)	Rh	Ir	Ir1Rh2	Ir1Rh1	-5.82
(111)	Rh	Ir	Ir2Rh1	Ir1Rh1	-7.09
(111)	Rh	Ir	Ir2Rh1	Ir2Rh0	-6.02
(111)	Rh	Ir	Ir1Rh3	Ir0Rh3	-7.78
(111)	Rh	Ir	Ir1Rh3	Ir1Rh2	-6.54
(111)	Rh	Ir	Ir2Rh2	Ir1Rh2	-7.96
(111)	Rh	Ir	Ir2Rh2	Ir2Rh1	-6.69
(111)	Rh	Ir	Ir3Rh1	Ir2Rh1	-8.12
(111)	Rh	Ir	Ir3Rh1	Ir3Rh0	-6.84
(111)	Rh	Pd	Pd1Rh0	Clean Rh	-2.65
(111)	Rh	Pd	Pd2Rh0	Pd1Rh0	-3.20
(111)	Rh	Pd	Pd3Rh0	Pd2Rh0	-3.60
(111)	Rh	Pd	Pd4Rh0	Pd3Rh0	-3.92
(111)	Rh	Pd	Pd1Rh1	Pd0Rh1	-3.43
(111)	Rh	Pd	Pd1Rh1	Pd1Rh0	-4.53
(111)	Rh	Pd	Pd1Rh2	Pd0Rh2	-3.94
(111)	Rh	Pd	Pd1Rh2	Pd1Rh1	-5.38
(111)	Rh	Pd	Pd2Rh1	Pd1Rh1	-3.78
(111)	Rh	Pd	Pd2Rh1	Pd2Rh0	-5.10
(111)	Rh	Pd	Pd1Rh3	Pd0Rh3	-4.46
(111)	Rh	Pd	Pd1Rh3	Pd1Rh2	-6.13
(111)	Rh	Pd	Pd2Rh2	Pd1Rh2	-4.28
(111)	Rh	Pd	Pd2Rh2	Pd2Rh1	-5.88
(111)	Rh	Pd	Pd3Rh1	Pd2Rh1	-4.11
(111)	Rh	Pd	Pd3Rh1	Pd3Rh0	-5.61
(111)	Rh	Pt	Pt1Rh0	Clean Rh	-3.93
(111)	Rh	Pt	Pt2Rh0	Pt1Rh0	-5.00
(111)	Rh	Pt	Pt3Rh0	Pt2Rh0	-5.58
(111)	Rh	Pt	Pt4Rh0	Pt3Rh0	-5.94
(111)	Rh	Pt	Pt1Rh1	Pt0Rh1	-5.05
(111)	Rh	Pt	Pt1Rh1	Pt1Rh0	-4.87
(111)	Rh	Pt	Pt1Rh2	Pt0Rh2	-5.74
(111)	Rh	Pt	Pt1Rh2	Pt1Rh1	-5.55
(111)	Rh	Pt	Pt2Rh1	Pt1Rh1	-5.64
(111)	Rh	Pt	Pt2Rh1	Pt2Rh0	-5.51
(111)	Rh	Pt	Pt1Rh3	Pt0Rh3	-6.40
(111)	Rh	Pt	Pt1Rh3	Pt1Rh2	-6.27
(111)	Rh	Pt	Pt2Rh2	Pt1Rh2	-6.26
(111)	Rh	Pt	Pt2Rh2	Pt2Rh1	-6.17
(111)	Rh	Pt	Pt3Rh1	Pt2Rh1	-6.11
(111)	Rh	Pt	Pt3Rh1	Pt3Rh0	-6.04

Table S6: DFT-calculated adsorption energies for bimetallic systems, 2x2 fcc (100) surfaces. The (A) and (D) configurations of atoms refer to arrangements in which two atoms are adjacent (A) or along the surface diagonal (D). See Figure S6 for an illustration of structures (A) and (D). Empty rows correspond to cases of reconstruction.

Surface Orientation	Host Slab	Heteroatom	Top Layer Configuration	Reference Configuration	Adsorption Energy (eV)
(100)	Ag	Au	Au1Ag0	Clean Ag	-2.35
(100)	Ag	Au	Au(2D)Ag0	Au1Ag0	-2.21
(100)	Ag	Au	Au(2A)Ag0	Au1Ag0	-2.65
(100)	Ag	Au	Au(3)Ag0	Au(2A)Ag0	-2.50
(100)	Ag	Au	Au(3)Ag0	Au(2D)Ag0	-2.94
(100)	Ag	Au	Au(4)Ag0	Au3Ag0	-2.73
(100)	Ag	Au	Au1Ag1 (D)	Au0Ag1	-2.34
(100)	Ag	Au	Au1Ag1 (D)	Au1Ag0	-1.66
(100)	Ag	Au	Au1Ag1 (A)	Au0Ag1	-2.75
(100)	Ag	Au	Au1Ag1 (A)	Au1Ag0	-2.07
(100)	Ag	Au	Au1Ag(2A)	Au0Ag(2A)	-2.66
(100)	Ag	Au	Au1Ag(2A)	Au1Ag1 (A)	-1.96
(100)	Ag	Au	Au1Ag(2A)	Au1Ag1 (D)	-2.38
(100)	Ag	Au	Au1Ag(2D)	Au0Ag(2D)	-3.10
(100)	Ag	Au	Au1Ag(2D)	Au1Ag1 (A)	-2.06
(100)	Ag	Au	Au(2A)Ag1	Au1Ag1 (A)	-2.59
(100)	Ag	Au	Au(2A)Ag1	Au1Ag1 (D)	-3.01
(100)	Ag	Au	Au(2A)Ag1	Au(2A)Ag0	-2.02
(100)	Ag	Au	Au(2D)Ag1	Au1Ag1 (A)	-2.55
(100)	Ag	Au	Au(2D)Ag1	Au(2D)Ag0	-2.41
(100)	Ag	Au	Au1Ag3	Au0Ag3	-2.91
(100)	Ag	Au	Au1Ag3	Au1Ag(2D)	-2.19
(100)	Ag	Au	Au1Ag3	Au1Ag(2A)	-2.29
(100)	Ag	Au	Au2Ag2 (A)	Au1Ag(2A)	-2.85
(100)	Ag	Au	Au2Ag2 (A)	Au(2A)Ag1	-2.22
(100)	Ag	Au	Au2Ag2 (D)	Au1Ag(2D)	-2.82
(100)	Ag	Au	Au2Ag2 (D)	Au(2D)Ag1	-2.33
(100)	Ag	Au	Au3Ag1	Au(2D)Ag1	-2.81
(100)	Ag	Au	Au3Ag1	Au(2A)Ag1	-2.76
(100)	Ag	Au	Au3Ag1	Au3Ag0	-2.28
(100)	Ag	Cu	Cu1Ag0	Clean Ag	-2.17
(100)	Ag	Cu	Cu(2D)Ag0	Cu1Ag0	-2.18
(100)	Ag	Cu	Cu(2A)Ag0	Cu1Ag0	-2.58
(100)	Ag	Cu	Cu(3)Ag0	Cu(2A)Ag0	-2.52
(100)	Ag	Cu	Cu(3)Ag0	Cu(2D)Ag0	-2.92
(100)	Ag	Cu	Cu(4)Ag0	Cu3Ag0	
(100)	Ag	Cu	Cu1Ag1 (D)	Cu0Ag1	-2.20
(100)	Ag	Cu	Cu1Ag1 (D)	Cu1Ag0	-1.69
(100)	Ag	Cu	Cu1Ag1 (A)	Cu0Ag1	-2.57
(100)	Ag	Cu	Cu1Ag1 (A)	Cu1Ag0	-2.07
(100)	Ag	Cu	Cu1Ag(2A)	Cu0Ag(2A)	-2.52
(100)	Ag	Cu	Cu1Ag(2A)	Cu1Ag1 (A)	-2.01
(100)	Ag	Cu	Cu1Ag(2A)	Cu1Ag1 (D)	-2.39
(100)	Ag	Cu	Cu1Ag(2D)	Cu0Ag(2D)	-2.92
(100)	Ag	Cu	Cu1Ag(2D)	Cu1Ag1 (A)	-2.06

Surface Orientation	Host Slab	Heteroatom	Top Layer Configuration	Reference Configuration	Adsorption Energy (eV)
(100)	Ag	Cu	Cu(2A)Ag1	Cu1Ag1 (A)	-2.54
(100)	Ag	Cu	Cu(2A)Ag1	Cu1Ag1 (D)	-2.92
(100)	Ag	Cu	Cu(2A)Ag1	Cu(2A)Ag0	-2.03
(100)	Ag	Cu	Cu(2D)Ag1	Cu1Ag1 (A)	-2.51
(100)	Ag	Cu	Cu(2D)Ag1	Cu(2D)Ag0	-2.40
(100)	Ag	Cu	Cu1Ag3	Cu0Ag3	-2.79
(100)	Ag	Cu	Cu1Ag3	Cu1Ag(2D)	-2.25
(100)	Ag	Cu	Cu1Ag3	Cu1Ag(2A)	-2.30
(100)	Ag	Cu	Cu2Ag2 (A)	Cu1Ag(2A)	-2.81
(100)	Ag	Cu	Cu2Ag2 (A)	Cu(2A)Ag1	-2.28
(100)	Ag	Cu	Cu2Ag2 (D)	Cu1Ag(2D)	-2.78
(100)	Ag	Cu	Cu2Ag2 (D)	Cu(2D)Ag1	-2.33
(100)	Ag	Cu	Cu3Ag1	Cu(2D)Ag1	-2.82
(100)	Ag	Cu	Cu3Ag1	Cu(2A)Ag1	-2.79
(100)	Ag	Cu	Cu3Ag1	Cu3Ag0	-2.30
(100)	Ag	Ir	Ir1Ag0	Clean Ag	-3.36
(100)	Ag	Ir	Ir(2D)Ag0	Ir1Ag0	-2.87
(100)	Ag	Ir	Ir(2A)Ag0	Ir1Ag0	
(100)	Ag	Ir	Ir(3)Ag0	Ir(2A)Ag0	
(100)	Ag	Ir	Ir(3)Ag0	Ir(2D)Ag0	
(100)	Ag	Ir	Ir(4)Ag0	Ir3Ag0	
(100)	Ag	Ir	Ir1Ag1 (D)	Ir0Ag1	-3.36
(100)	Ag	Ir	Ir1Ag1 (D)	Ir1Ag0	-1.66
(100)	Ag	Ir	Ir1Ag1 (A)	Ir0Ag1	-4.07
(100)	Ag	Ir	Ir1Ag1 (A)	Ir1Ag0	-2.37
(100)	Ag	Ir	Ir1Ag(2A)	Ir0Ag(2A)	-4.02
(100)	Ag	Ir	Ir1Ag(2A)	Ir1Ag1 (A)	-2.01
(100)	Ag	Ir	Ir1Ag(2A)	Ir1Ag1 (D)	-2.72
(100)	Ag	Ir	Ir1Ag(2D)	Ir0Ag(2D)	-4.78
(100)	Ag	Ir	Ir1Ag(2D)	Ir1Ag1 (A)	-2.42
(100)	Ag	Ir	Ir(2A)Ag1	Ir1Ag1 (A)	
(100)	Ag	Ir	Ir(2A)Ag1	Ir1Ag1 (D)	
(100)	Ag	Ir	Ir(2A)Ag1	Ir(2A)Ag0	
(100)	Ag	Ir	Ir(2D)Ag1	Ir1Ag1 (A)	-3.53
(100)	Ag	Ir	Ir(2D)Ag1	Ir(2D)Ag0	-3.04
(100)	Ag	Ir	Ir1Ag3	Ir0Ag3	-4.65
(100)	Ag	Ir	Ir1Ag3	Ir1Ag(2D)	-2.25
(100)	Ag	Ir	Ir1Ag3	Ir1Ag(2A)	-2.66
(100)	Ag	Ir	Ir2Ag2 (A)	Ir1Ag(2A)	
(100)	Ag	Ir	Ir2Ag2 (A)	Ir(2A)Ag1	
(100)	Ag	Ir	Ir2Ag2 (D)	Ir1Ag(2D)	-4.15
(100)	Ag	Ir	Ir2Ag2 (D)	Ir(2D)Ag1	-3.04
(100)	Ag	Ir	Ir3Ag1	Ir(2D)Ag1	
(100)	Ag	Ir	Ir3Ag1	Ir(2A)Ag1	
(100)	Ag	Ir	Ir3Ag1	Ir3Ag0	

Surface Orientation	Host Slab	Heteroatom	Top Layer Configuration	Reference Configuration	Adsorption Energy (eV)
(100)	Ag	Pd	Pd1Ag0	Clean Ag	-2.40
(100)	Ag	Pd	Pd(2D)Ag0	Pd1Ag0	-2.31
(100)	Ag	Pd	Pd(2A)Ag0	Pd1Ag0	-2.82
(100)	Ag	Pd	Pd(3)Ag0	Pd(2A)Ag0	-2.80
(100)	Ag	Pd	Pd(3)Ag0	Pd(2D)Ag0	-3.32
(100)	Ag	Pd	Pd(4)Ag0	Pd3Ag0	-3.24
(100)	Ag	Pd	Pd1Ag1 (D)	Pd0Ag1	-2.41
(100)	Ag	Pd	Pd1Ag1 (D)	Pd1Ag0	-1.68
(100)	Ag	Pd	Pd1Ag1 (A)	Pd0Ag1	-2.91
(100)	Ag	Pd	Pd1Ag1 (A)	Pd1Ag0	-2.18
(100)	Ag	Pd	Pd1Ag(2A)	Pd0Ag(2A)	-2.86
(100)	Ag	Pd	Pd1Ag(2A)	Pd1Ag1 (A)	-2.01
(100)	Ag	Pd	Pd1Ag(2A)	Pd1Ag1 (D)	-2.51
(100)	Ag	Pd	Pd1Ag(2D)	Pd0Ag(2D)	-3.39
(100)	Ag	Pd	Pd1Ag(2D)	Pd1Ag1 (A)	-2.20
(100)	Ag	Pd	Pd(2A)Ag1	Pd1Ag1 (A)	-2.86
(100)	Ag	Pd	Pd(2A)Ag1	Pd1Ag1 (D)	-3.36
(100)	Ag	Pd	Pd(2A)Ag1	Pd(2A)Ag0	-2.21
(100)	Ag	Pd	Pd(2D)Ag1	Pd1Ag1 (A)	-2.76
(100)	Ag	Pd	Pd(2D)Ag1	Pd(2D)Ag0	-2.64
(100)	Ag	Pd	Pd1Ag3	Pd0Ag3	-3.27
(100)	Ag	Pd	Pd1Ag3	Pd1Ag(2D)	-2.25
(100)	Ag	Pd	Pd1Ag3	Pd1Ag(2A)	-2.44
(100)	Ag	Pd	Pd2Ag2 (A)	Pd1Ag(2A)	-3.28
(100)	Ag	Pd	Pd2Ag2 (A)	Pd(2A)Ag1	-2.43
(100)	Ag	Pd	Pd2Ag2 (D)	Pd1Ag(2D)	-3.18
(100)	Ag	Pd	Pd2Ag2 (D)	Pd(2D)Ag1	-2.62
(100)	Ag	Pd	Pd3Ag1	Pd(2D)Ag1	-3.28
(100)	Ag	Pd	Pd3Ag1	Pd(2A)Ag1	-3.18
(100)	Ag	Pd	Pd3Ag1	Pd3Ag0	-2.60
(100)	Ag	Pt	Pt1Ag0	Clean Ag	-3.58
(100)	Ag	Pt	Pt(2D)Ag0	Pt1Ag0	-3.15
(100)	Ag	Pt	Pt(2A)Ag0	Pt1Ag0	-4.14
(100)	Ag	Pt	Pt(3)Ag0	Pt(2A)Ag0	-3.94
(100)	Ag	Pt	Pt(3)Ag0	Pt(2D)Ag0	-4.93
(100)	Ag	Pt	Pt(4)Ag0	Pt3Ag0	-4.70
(100)	Ag	Pt	Pt1Ag1 (D)	Pt0Ag1	-3.56
(100)	Ag	Pt	Pt1Ag1 (D)	Pt1Ag0	-1.65
(100)	Ag	Pt	Pt1Ag1 (A)	Pt0Ag1	-4.20
(100)	Ag	Pt	Pt1Ag1 (A)	Pt1Ag0	-2.28
(100)	Ag	Pt	Pt1Ag(2A)	Pt0Ag(2A)	-4.09
(100)	Ag	Pt	Pt1Ag(2A)	Pt1Ag1 (A)	-1.95
(100)	Ag	Pt	Pt1Ag(2A)	Pt1Ag1 (D)	-2.58
(100)	Ag	Pt	Pt1Ag(2D)	Pt0Ag(2D)	-4.77
(100)	Ag	Pt	Pt1Ag(2D)	Pt1Ag1 (A)	-2.30

Surface Orientation	Host Slab	Heteroatom	Top Layer Configuration	Reference Configuration	Adsorption Energy (eV)
(100)	Ag	Pt	Pt(2A)Ag1	Pt1Ag1 (A)	-4.19
(100)	Ag	Pt	Pt(2A)Ag1	Pt1Ag1 (D)	-4.82
(100)	Ag	Pt	Pt(2A)Ag1	Pt(2A)Ag0	-2.33
(100)	Ag	Pt	Pt(2D)Ag1	Pt1Ag1 (A)	-3.71
(100)	Ag	Pt	Pt(2D)Ag1	Pt(2D)Ag0	-2.84
(100)	Ag	Pt	Pt1Ag3	Pt0Ag3	-4.58
(100)	Ag	Pt	Pt1Ag3	Pt1Ag(2D)	-2.18
(100)	Ag	Pt	Pt1Ag3	Pt1Ag(2A)	-2.52
(100)	Ag	Pt	Pt2Ag2 (A)	Pt1Ag(2A)	-4.69
(100)	Ag	Pt	Pt2Ag2 (A)	Pt(2A)Ag1	-2.45
(100)	Ag	Pt	Pt2Ag2 (D)	Pt1Ag(2D)	-4.24
(100)	Ag	Pt	Pt2Ag2 (D)	Pt(2D)Ag1	-2.82
(100)	Ag	Pt	Pt3Ag1	Pt(2D)Ag1	-4.86
(100)	Ag	Pt	Pt3Ag1	Pt(2A)Ag1	-4.38
(100)	Ag	Pt	Pt3Ag1	Pt3Ag0	-2.77
(100)	Ag	Rh	Rh1Ag0	Clean Ag	-2.93
(100)	Ag	Rh	Rh(2D)Ag0	Rh1Ag0	-2.71
(100)	Ag	Rh	Rh(2A)Ag0	Rh1Ag0	
(100)	Ag	Rh	Rh(3)Ag0	Rh(2A)Ag0	
(100)	Ag	Rh	Rh(3)Ag0	Rh(2D)Ag0	
(100)	Ag	Rh	Rh(4)Ag0	Rh3Ag0	
(100)	Ag	Rh	Rh1Ag1 (D)	Rh0Ag1	-2.94
(100)	Ag	Rh	Rh1Ag1 (D)	Rh1Ag0	-1.68
(100)	Ag	Rh	Rh1Ag1 (A)	Rh0Ag1	-3.53
(100)	Ag	Rh	Rh1Ag1 (A)	Rh1Ag0	-2.27
(100)	Ag	Rh	Rh1Ag(2A)	Rh0Ag(2A)	-3.51
(100)	Ag	Rh	Rh1Ag(2A)	Rh1Ag1 (A)	-2.04
(100)	Ag	Rh	Rh1Ag(2A)	Rh1Ag1 (D)	-2.64
(100)	Ag	Rh	Rh1Ag(2D)	Rh0Ag(2D)	-4.14
(100)	Ag	Rh	Rh1Ag(2D)	Rh1Ag1 (A)	-2.33
(100)	Ag	Rh	Rh(2A)Ag1	Rh1Ag1 (A)	
(100)	Ag	Rh	Rh(2A)Ag1	Rh1Ag1 (D)	
(100)	Ag	Rh	Rh(2A)Ag1	Rh(2A)Ag0	
(100)	Ag	Rh	Rh(2D)Ag1	Rh1Ag1 (A)	-3.30
(100)	Ag	Rh	Rh(2D)Ag1	Rh(2D)Ag0	-2.86
(100)	Ag	Rh	Rh1Ag3	Rh0Ag3	-4.05
(100)	Ag	Rh	Rh1Ag3	Rh1Ag(2D)	-2.29
(100)	Ag	Rh	Rh1Ag3	Rh1Ag(2A)	-2.57
(100)	Ag	Rh	Rh2Ag2 (A)	Rh1Ag(2A)	
(100)	Ag	Rh	Rh2Ag2 (A)	Rh(2A)Ag1	
(100)	Ag	Rh	Rh2Ag2 (D)	Rh1Ag(2D)	-3.81
(100)	Ag	Rh	Rh2Ag2 (D)	Rh(2D)Ag1	-2.84
(100)	Ag	Rh	Rh3Ag1	Rh(2D)Ag1	
(100)	Ag	Rh	Rh3Ag1	Rh(2A)Ag1	
(100)	Ag	Rh	Rh3Ag1	Rh3Ag0	

Surface Orientation	Host Slab	Heteroatom	Top Layer Configuration	Reference Configuration	Adsorption Energy (eV)
(100)	Au	Ag	Ag1Au0	Clean Au	-1.90
(100)	Au	Ag	Ag(2D)Au0	Ag1Au0	-1.85
(100)	Au	Ag	Ag(2A)Au0	Ag1Au0	-2.11
(100)	Au	Ag	Ag(3)Au0	Ag(2A)Au0	-2.07
(100)	Au	Ag	Ag(3)Au0	Ag(2D)Au0	-2.33
(100)	Au	Ag	Ag(4)Au0	Ag3Au0	-2.23
(100)	Au	Ag	Ag1Au1 (D)	Ag0Au1	-1.83
(100)	Au	Ag	Ag1Au1 (D)	Ag1Au0	-2.22
(100)	Au	Ag	Ag1Au1 (A)	Ag0Au1	-2.20
(100)	Au	Ag	Ag1Au1 (A)	Ag1Au0	-2.59
(100)	Au	Ag	Ag1Au(2A)	Ag0Au(2A)	-2.12
(100)	Au	Ag	Ag1Au(2A)	Ag1Au1 (A)	-2.49
(100)	Au	Ag	Ag1Au(2A)	Ag1Au1 (D)	-2.86
(100)	Au	Ag	Ag1Au(2D)	Ag0Au(2D)	-2.46
(100)	Au	Ag	Ag1Au(2D)	Ag1Au1 (A)	-2.37
(100)	Au	Ag	Ag(2A)Au1	Ag1Au1 (A)	-2.01
(100)	Au	Ag	Ag(2A)Au1	Ag1Au1 (D)	-2.38
(100)	Au	Ag	Ag(2A)Au1	Ag(2A)Au0	-2.49
(100)	Au	Ag	Ag(2D)Au1	Ag1Au1 (A)	-2.16
(100)	Au	Ag	Ag(2D)Au1	Ag(2D)Au0	-2.90
(100)	Au	Ag	Ag1Au3	Ag0Au3	-2.34
(100)	Au	Ag	Ag1Au3	Ag1Au(2D)	-2.74
(100)	Au	Ag	Ag1Au3	Ag1Au(2A)	-2.61
(100)	Au	Ag	Ag2Au2 (A)	Ag1Au(2A)	-2.23
(100)	Au	Ag	Ag2Au2 (A)	Ag(2A)Au1	-2.71
(100)	Au	Ag	Ag2Au2 (D)	Ag1Au(2D)	-2.39
(100)	Au	Ag	Ag2Au2 (D)	Ag(2D)Au1	-2.61
(100)	Au	Ag	Ag3Au1	Ag(2D)Au1	-2.15
(100)	Au	Ag	Ag3Au1	Ag(2A)Au1	-2.30
(100)	Au	Ag	Ag3Au1	Ag3Au0	-2.72
(100)	Au	Cu	Cu1Au0	Clean Au	-2.62
(100)	Au	Cu	Cu(2D)Au0	Cu1Au0	-2.51
(100)	Au	Cu	Cu(2A)Au0	Cu1Au0	-2.83
(100)	Au	Cu	Cu(3)Au0	Cu(2A)Au0	-2.68
(100)	Au	Cu	Cu(3)Au0	Cu(2D)Au0	-3.01
(100)	Au	Cu	Cu(4)Au0	Cu3Au0	-2.85
(100)	Au	Cu	Cu1Au1 (D)	Cu0Au1	-2.48
(100)	Au	Cu	Cu1Au1 (D)	Cu1Au0	-2.14
(100)	Au	Cu	Cu1Au1 (A)	Cu0Au1	-2.88
(100)	Au	Cu	Cu1Au1 (A)	Cu1Au0	-2.54
(100)	Au	Cu	Cu1Au(2A)	Cu0Au(2A)	-2.74
(100)	Au	Cu	Cu1Au(2A)	Cu1Au1 (A)	-2.43
(100)	Au	Cu	Cu1Au(2A)	Cu1Au1 (D)	-2.83
(100)	Au	Cu	Cu1Au(2D)	Cu0Au(2D)	-3.12
(100)	Au	Cu	Cu1Au(2D)	Cu1Au1 (A)	-2.35

Surface Orientation	Host Slab	Heteroatom	Top Layer Configuration	Reference Configuration	Adsorption Energy (eV)
(100)	Au	Cu	Cu(2A)Au1	Cu1Au1 (A)	-2.66
(100)	Au	Cu	Cu(2A)Au1	Cu1Au1 (D)	-3.06
(100)	Au	Cu	Cu(2A)Au1	Cu(2A)Au0	-2.37
(100)	Au	Cu	Cu(2D)Au1	Cu1Au1 (A)	-2.77
(100)	Au	Cu	Cu(2D)Au1	Cu(2D)Au0	-2.81
(100)	Au	Cu	Cu1Au3	Cu0Au3	-2.96
(100)	Au	Cu	Cu1Au3	Cu1Au(2D)	-2.70
(100)	Au	Cu	Cu1Au3	Cu1Au(2A)	-2.62
(100)	Au	Cu	Cu2Au2 (A)	Cu1Au(2A)	-2.89
(100)	Au	Cu	Cu2Au2 (A)	Cu(2A)Au1	-2.67
(100)	Au	Cu	Cu2Au2 (D)	Cu1Au(2D)	-3.01
(100)	Au	Cu	Cu2Au2 (D)	Cu(2D)Au1	-2.58
(100)	Au	Cu	Cu3Au1	Cu(2D)Au1	-2.82
(100)	Au	Cu	Cu3Au1	Cu(2A)Au1	-2.93
(100)	Au	Cu	Cu3Au1	Cu3Au0	-2.62
(100)	Au	Ir	Ir1Au0	Clean Au	-3.87
(100)	Au	Ir	Ir(2D)Au0	Ir1Au0	-3.27
(100)	Au	Ir	Ir(2A)Au0	Ir1Au0	
(100)	Au	Ir	Ir(3)Au0	Ir(2A)Au0	
(100)	Au	Ir	Ir(3)Au0	Ir(2D)Au0	
(100)	Au	Ir	Ir(4)Au0	Ir3Au0	
(100)	Au	Ir	Ir1Au1 (D)	Ir0Au1	-3.53
(100)	Au	Ir	Ir1Au1 (D)	Ir1Au0	-1.95
(100)	Au	Ir	Ir1Au1 (A)	Ir0Au1	-4.34
(100)	Au	Ir	Ir1Au1 (A)	Ir1Au0	-2.75
(100)	Au	Ir	Ir1Au(2A)	Ir0Au(2A)	-4.09
(100)	Au	Ir	Ir1Au(2A)	Ir1Au1 (A)	-2.33
(100)	Au	Ir	Ir1Au(2A)	Ir1Au1 (D)	-3.13
(100)	Au	Ir	Ir1Au(2D)	Ir0Au(2D)	-4.91
(100)	Au	Ir	Ir1Au(2D)	Ir1Au1 (A)	-2.68
(100)	Au	Ir	Ir(2A)Au1	Ir1Au1 (A)	
(100)	Au	Ir	Ir(2A)Au1	Ir1Au1 (D)	
(100)	Au	Ir	Ir(2A)Au1	Ir(2A)Au0	
(100)	Au	Ir	Ir(2D)Au1	Ir1Au1 (A)	-3.91
(100)	Au	Ir	Ir(2D)Au1	Ir(2D)Au0	-3.39
(100)	Au	Ir	Ir1Au3	Ir0Au3	-4.65
(100)	Au	Ir	Ir1Au3	Ir1Au(2D)	-2.61
(100)	Au	Ir	Ir1Au3	Ir1Au(2A)	-2.96
(100)	Au	Ir	Ir2Au2 (A)	Ir1Au(2A)	
(100)	Au	Ir	Ir2Au2 (A)	Ir(2A)Au1	
(100)	Au	Ir	Ir2Au2 (D)	Ir1Au(2D)	-4.47
(100)	Au	Ir	Ir2Au2 (D)	Ir(2D)Au1	-3.25
(100)	Au	Ir	Ir3Au1	Ir(2D)Au1	
(100)	Au	Ir	Ir3Au1	Ir(2A)Au1	
(100)	Au	Ir	Ir3Au1	Ir3Au0	

Surface Orientation	Host Slab	Heteroatom	Top Layer Configuration	Reference Configuration	Adsorption Energy (eV)
(100)	Au	Pd	Pd1Au0	Clean Au	-2.62
(100)	Au	Pd	Pd(2D)Au0	Pd1Au0	-2.47
(100)	Au	Pd	Pd(2A)Au0	Pd1Au0	-2.87
(100)	Au	Pd	Pd(3)Au0	Pd(2A)Au0	-2.84
(100)	Au	Pd	Pd(3)Au0	Pd(2D)Au0	-3.24
(100)	Au	Pd	Pd(4)Au0	Pd3Au0	-3.15
(100)	Au	Pd	Pd1Au1 (D)	Pd0Au1	-2.46
(100)	Au	Pd	Pd1Au1 (D)	Pd1Au0	-2.13
(100)	Au	Pd	Pd1Au1 (A)	Pd0Au1	-2.98
(100)	Au	Pd	Pd1Au1 (A)	Pd1Au0	-2.64
(100)	Au	Pd	Pd1Au(2A)	Pd0Au(2A)	-2.84
(100)	Au	Pd	Pd1Au(2A)	Pd1Au1 (A)	-2.43
(100)	Au	Pd	Pd1Au(2A)	Pd1Au1 (D)	-2.95
(100)	Au	Pd	Pd1Au(2D)	Pd0Au(2D)	-3.36
(100)	Au	Pd	Pd1Au(2D)	Pd1Au1 (A)	-2.49
(100)	Au	Pd	Pd(2A)Au1	Pd1Au1 (A)	-2.78
(100)	Au	Pd	Pd(2A)Au1	Pd1Au1 (D)	-3.30
(100)	Au	Pd	Pd(2A)Au1	Pd(2A)Au0	-2.56
(100)	Au	Pd	Pd(2D)Au1	Pd1Au1 (A)	-2.88
(100)	Au	Pd	Pd(2D)Au1	Pd(2D)Au0	-3.05
(100)	Au	Pd	Pd1Au3	Pd0Au3	-3.19
(100)	Au	Pd	Pd1Au3	Pd1Au(2D)	-2.69
(100)	Au	Pd	Pd1Au3	Pd1Au(2A)	-2.75
(100)	Au	Pd	Pd2Au2 (A)	Pd1Au(2A)	-3.13
(100)	Au	Pd	Pd2Au2 (A)	Pd(2A)Au1	-2.78
(100)	Au	Pd	Pd2Au2 (D)	Pd1Au(2D)	-3.22
(100)	Au	Pd	Pd2Au2 (D)	Pd(2D)Au1	-2.84
(100)	Au	Pd	Pd3Au1	Pd(2D)Au1	-3.06
(100)	Au	Pd	Pd3Au1	Pd(2A)Au1	-3.16
(100)	Au	Pd	Pd3Au1	Pd3Au0	-2.88
(100)	Au	Pt	Pt1Au0	Clean Au	-3.71
(100)	Au	Pt	Pt(2D)Au0	Pt1Au0	-3.30
(100)	Au	Pt	Pt(2A)Au0	Pt1Au0	-4.13
(100)	Au	Pt	Pt(3)Au0	Pt(2A)Au0	-3.94
(100)	Au	Pt	Pt(3)Au0	Pt(2D)Au0	-4.76
(100)	Au	Pt	Pt(4)Au0	Pt3Au0	-4.49
(100)	Au	Pt	Pt1Au1 (D)	Pt0Au1	-3.45
(100)	Au	Pt	Pt1Au1 (D)	Pt1Au0	-2.02
(100)	Au	Pt	Pt1Au1 (A)	Pt0Au1	-4.13
(100)	Au	Pt	Pt1Au1 (A)	Pt1Au0	-2.70
(100)	Au	Pt	Pt1Au(2A)	Pt0Au(2A)	-3.90
(100)	Au	Pt	Pt1Au(2A)	Pt1Au1 (A)	-2.34
(100)	Au	Pt	Pt1Au(2A)	Pt1Au1 (D)	-3.02
(100)	Au	Pt	Pt1Au(2D)	Pt0Au(2D)	-4.61
(100)	Au	Pt	Pt1Au(2D)	Pt1Au1 (A)	-2.58

Surface Orientation	Host Slab	Heteroatom	Top Layer Configuration	Reference Configuration	Adsorption Energy (eV)
(100)	Au	Pt	Pt(2A)Au1	Pt1Au1 (A)	-4.00
(100)	Au	Pt	Pt(2A)Au1	Pt1Au1 (D)	-4.68
(100)	Au	Pt	Pt(2A)Au1	Pt(2A)Au0	-2.57
(100)	Au	Pt	Pt(2D)Au1	Pt1Au1 (A)	-3.77
(100)	Au	Pt	Pt(2D)Au1	Pt(2D)Au0	-3.18
(100)	Au	Pt	Pt1Au3	Pt0Au3	-4.34
(100)	Au	Pt	Pt1Au3	Pt1Au(2D)	-2.60
(100)	Au	Pt	Pt1Au3	Pt1Au(2A)	-2.84
(100)	Au	Pt	Pt2Au2 (A)	Pt1Au(2A)	-4.43
(100)	Au	Pt	Pt2Au2 (A)	Pt(2A)Au1	-2.78
(100)	Au	Pt	Pt2Au2 (D)	Pt1Au(2D)	-4.19
(100)	Au	Pt	Pt2Au2 (D)	Pt(2D)Au1	-3.01
(100)	Au	Pt	Pt3Au1	Pt(2D)Au1	-4.53
(100)	Au	Pt	Pt3Au1	Pt(2A)Au1	-4.31
(100)	Au	Pt	Pt3Au1	Pt3Au0	-2.94
(100)	Au	Rh	Rh1Au0	Clean Au	-3.43
(100)	Au	Rh	Rh(2D)Au0	Rh1Au0	-3.09
(100)	Au	Rh	Rh(2A)Au0	Rh1Au0	
(100)	Au	Rh	Rh(3)Au0	Rh(2A)Au0	
(100)	Au	Rh	Rh(3)Au0	Rh(2D)Au0	
(100)	Au	Rh	Rh(4)Au0	Rh3Au0	
(100)	Au	Rh	Rh1Au1 (D)	Rh0Au1	-3.19
(100)	Au	Rh	Rh1Au1 (D)	Rh1Au0	-2.05
(100)	Au	Rh	Rh1Au1 (A)	Rh0Au1	-3.83
(100)	Au	Rh	Rh1Au1 (A)	Rh1Au0	-2.69
(100)	Au	Rh	Rh1Au(2A)	Rh0Au(2A)	-3.66
(100)	Au	Rh	Rh1Au(2A)	Rh1Au1 (A)	-2.41
(100)	Au	Rh	Rh1Au(2A)	Rh1Au1 (D)	-3.05
(100)	Au	Rh	Rh1Au(2D)	Rh0Au(2D)	-4.32
(100)	Au	Rh	Rh1Au(2D)	Rh1Au1 (A)	-2.59
(100)	Au	Rh	Rh(2A)Au1	Rh1Au1 (A)	
(100)	Au	Rh	Rh(2A)Au1	Rh1Au1 (D)	
(100)	Au	Rh	Rh(2A)Au1	Rh(2A)Au0	
(100)	Au	Rh	Rh(2D)Au1	Rh1Au1 (A)	-3.64
(100)	Au	Rh	Rh(2D)Au1	Rh(2D)Au0	-3.24
(100)	Au	Rh	Rh1Au3	Rh0Au3	-4.12
(100)	Au	Rh	Rh1Au3	Rh1Au(2D)	-2.67
(100)	Au	Rh	Rh1Au3	Rh1Au(2A)	-2.86
(100)	Au	Rh	Rh2Au2 (A)	Rh1Au(2A)	
(100)	Au	Rh	Rh2Au2 (A)	Rh(2A)Au1	
(100)	Au	Rh	Rh2Au2 (D)	Rh1Au(2D)	-4.10
(100)	Au	Rh	Rh2Au2 (D)	Rh(2D)Au1	-3.05
(100)	Au	Rh	Rh3Au1	Rh(2D)Au1	
(100)	Au	Rh	Rh3Au1	Rh(2A)Au1	
(100)	Au	Rh	Rh3Au1	Rh3Au0	

Surface Orientation	Host Slab	Heteroatom	Top Layer Configuration	Reference Configuration	Adsorption Energy (eV)
(100)	Cu	Ag	Ag1Cu0	Clean Cu	-1.88
(100)	Cu	Ag	Ag(2D)Cu0	Ag1Cu0	-2.11
(100)	Cu	Ag	Ag(2A)Cu0	Ag1Cu0	-2.02
(100)	Cu	Ag	Ag(3)Cu0	Ag(2A)Cu0	
(100)	Cu	Ag	Ag(3)Cu0	Ag(2D)Cu0	
(100)	Cu	Ag	Ag(4)Cu0	Ag3Cu0	
(100)	Cu	Ag	Ag1Cu1 (D)	Ag0Cu1	-2.07
(100)	Cu	Ag	Ag1Cu1 (D)	Ag1Cu0	-2.67
(100)	Cu	Ag	Ag1Cu1 (A)	Ag0Cu1	-2.35
(100)	Cu	Ag	Ag1Cu1 (A)	Ag1Cu0	-2.95
(100)	Cu	Ag	Ag1Cu(2A)	Ag0Cu(2A)	-2.37
(100)	Cu	Ag	Ag1Cu(2A)	Ag1Cu1 (A)	-3.14
(100)	Cu	Ag	Ag1Cu(2A)	Ag1Cu1 (D)	-3.42
(100)	Cu	Ag	Ag1Cu(2D)	Ag0Cu(2D)	-2.63
(100)	Cu	Ag	Ag1Cu(2D)	Ag1Cu1 (A)	-2.92
(100)	Cu	Ag	Ag(2A)Cu1	Ag1Cu1 (A)	-2.02
(100)	Cu	Ag	Ag(2A)Cu1	Ag1Cu1 (D)	-2.29
(100)	Cu	Ag	Ag(2A)Cu1	Ag(2A)Cu0	-2.95
(100)	Cu	Ag	Ag(2D)Cu1	Ag1Cu1 (A)	-2.41
(100)	Cu	Ag	Ag(2D)Cu1	Ag(2D)Cu0	-3.25
(100)	Cu	Ag	Ag1Cu3	Ag0Cu3	-2.51
(100)	Cu	Ag	Ag1Cu3	Ag1Cu(2D)	-3.46
(100)	Cu	Ag	Ag1Cu3	Ag1Cu(2A)	-3.24
(100)	Cu	Ag	Ag2Cu2 (A)	Ag1Cu(2A)	-2.15
(100)	Cu	Ag	Ag2Cu2 (A)	Ag(2A)Cu1	-3.28
(100)	Cu	Ag	Ag2Cu2 (D)	Ag1Cu(2D)	-2.56
(100)	Cu	Ag	Ag2Cu2 (D)	Ag(2D)Cu1	-3.07
(100)	Cu	Ag	Ag3Cu1	Ag(2D)Cu1	
(100)	Cu	Ag	Ag3Cu1	Ag(2A)Cu1	
(100)	Cu	Ag	Ag3Cu1	Ag3Cu0	
(100)	Cu	Au	Au1Cu0	Clean Cu	-2.67
(100)	Cu	Au	Au(2D)Cu0	Au1Cu0	-2.67
(100)	Cu	Au	Au(2A)Cu0	Au1Cu0	-2.85
(100)	Cu	Au	Au(3)Cu0	Au(2A)Cu0	-2.60
(100)	Cu	Au	Au(3)Cu0	Au(2D)Cu0	-2.78
(100)	Cu	Au	Au(4)Cu0	Au3Cu0	
(100)	Cu	Au	Au1Cu1 (D)	Au0Cu1	-2.77
(100)	Cu	Au	Au1Cu1 (D)	Au1Cu0	-2.58
(100)	Cu	Au	Au1Cu1 (A)	Au0Cu1	-3.24
(100)	Cu	Au	Au1Cu1 (A)	Au1Cu0	-3.05
(100)	Cu	Au	Au1Cu(2A)	Au0Cu(2A)	-3.14
(100)	Cu	Au	Au1Cu(2A)	Au1Cu1 (A)	-3.02
(100)	Cu	Au	Au1Cu(2A)	Au1Cu1 (D)	-3.49
(100)	Cu	Au	Au1Cu(2D)	Au0Cu(2D)	-3.62
(100)	Cu	Au	Au1Cu(2D)	Au1Cu1 (A)	-3.02

Surface Orientation	Host Slab	Heteroatom	Top Layer Configuration	Reference Configuration	Adsorption Energy (eV)
(100)	Cu	Au	Au(2A)Cu1	Au1Cu1 (A)	-2.73
(100)	Cu	Au	Au(2A)Cu1	Au1Cu1 (D)	-3.19
(100)	Cu	Au	Au(2A)Cu1	Au(2A)Cu0	-2.93
(100)	Cu	Au	Au(2D)Cu1	Au1Cu1 (A)	-3.03
(100)	Cu	Au	Au(2D)Cu1	Au(2D)Cu0	-3.41
(100)	Cu	Au	Au1Cu3	Au0Cu3	-3.36
(100)	Cu	Au	Au1Cu3	Au1Cu(2D)	-3.32
(100)	Cu	Au	Au1Cu3	Au1Cu(2A)	-3.32
(100)	Cu	Au	Au2Cu2 (A)	Au1Cu(2A)	-2.92
(100)	Cu	Au	Au2Cu2 (A)	Au(2A)Cu1	-3.22
(100)	Cu	Au	Au2Cu2 (D)	Au1Cu(2D)	-3.23
(100)	Cu	Au	Au2Cu2 (D)	Au(2D)Cu1	-3.22
(100)	Cu	Au	Au3Cu1	Au(2D)Cu1	
(100)	Cu	Au	Au3Cu1	Au(2A)Cu1	
(100)	Cu	Au	Au3Cu1	Au3Cu0	
(100)	Cu	Ir	Ir1Cu0	Clean Cu	-4.41
(100)	Cu	Ir	Ir(2D)Cu0	Ir1Cu0	
(100)	Cu	Ir	Ir(2A)Cu0	Ir1Cu0	-6.35
(100)	Cu	Ir	Ir(3)Cu0	Ir(2A)Cu0	-5.84
(100)	Cu	Ir	Ir(3)Cu0	Ir(2D)Cu0	
(100)	Cu	Ir	Ir(4)Cu0	Ir3Cu0	
(100)	Cu	Ir	Ir1Cu1 (D)	Ir0Cu1	-4.50
(100)	Cu	Ir	Ir1Cu1 (D)	Ir1Cu0	-2.57
(100)	Cu	Ir	Ir1Cu1 (A)	Ir0Cu1	-5.41
(100)	Cu	Ir	Ir1Cu1 (A)	Ir1Cu0	-3.49
(100)	Cu	Ir	Ir1Cu(2A)	Ir0Cu(2A)	-5.39
(100)	Cu	Ir	Ir1Cu(2A)	Ir1Cu1 (A)	-3.10
(100)	Cu	Ir	Ir1Cu(2A)	Ir1Cu1 (D)	-4.02
(100)	Cu	Ir	Ir1Cu(2D)	Ir0Cu(2D)	-6.34
(100)	Cu	Ir	Ir1Cu(2D)	Ir1Cu1 (A)	-3.57
(100)	Cu	Ir	Ir(2A)Cu1	Ir1Cu1 (A)	-6.42
(100)	Cu	Ir	Ir(2A)Cu1	Ir1Cu1 (D)	-7.34
(100)	Cu	Ir	Ir(2A)Cu1	Ir(2A)Cu0	-3.56
(100)	Cu	Ir	Ir(2D)Cu1	Ir1Cu1 (A)	-6.42
(100)	Cu	Ir	Ir(2D)Cu1	Ir(2D)Cu0	
(100)	Cu	Ir	Ir1Cu3	Ir0Cu3	-6.15
(100)	Cu	Ir	Ir1Cu3	Ir1Cu(2D)	-3.39
(100)	Cu	Ir	Ir1Cu3	Ir1Cu(2A)	-3.86
(100)	Cu	Ir	Ir2Cu2 (A)	Ir1Cu(2A)	-6.94
(100)	Cu	Ir	Ir2Cu2 (A)	Ir(2A)Cu1	-3.61
(100)	Cu	Ir	Ir2Cu2 (D)	Ir1Cu(2D)	-5.75
(100)	Cu	Ir	Ir2Cu2 (D)	Ir(2D)Cu1	-2.90
(100)	Cu	Ir	Ir3Cu1	Ir(2D)Cu1	-6.29
(100)	Cu	Ir	Ir3Cu1	Ir(2A)Cu1	-6.29
(100)	Cu	Ir	Ir3Cu1	Ir3Cu0	-4.01

Surface Orientation	Host Slab	Heteroatom	Top Layer Configuration	Reference Configuration	Adsorption Energy (eV)
(100)	Cu	Pd	Pd1Cu0	Clean Cu	-2.87
(100)	Cu	Pd	Pd(2D)Cu0	Pd1Cu0	-2.93
(100)	Cu	Pd	Pd(2A)Cu0	Pd1Cu0	-3.19
(100)	Cu	Pd	Pd(3)Cu0	Pd(2A)Cu0	-3.27
(100)	Cu	Pd	Pd(3)Cu0	Pd(2D)Cu0	-3.53
(100)	Cu	Pd	Pd(4)Cu0	Pd3Cu0	-3.45
(100)	Cu	Pd	Pd1Cu1 (D)	Pd0Cu1	-3.01
(100)	Cu	Pd	Pd1Cu1 (D)	Pd1Cu0	-2.62
(100)	Cu	Pd	Pd1Cu1 (A)	Pd0Cu1	-3.52
(100)	Cu	Pd	Pd1Cu1 (A)	Pd1Cu0	-3.13
(100)	Cu	Pd	Pd1Cu(2A)	Pd0Cu(2A)	-3.51
(100)	Cu	Pd	Pd1Cu(2A)	Pd1Cu1 (A)	-3.11
(100)	Cu	Pd	Pd1Cu(2A)	Pd1Cu1 (D)	-3.62
(100)	Cu	Pd	Pd1Cu(2D)	Pd0Cu(2D)	-4.06
(100)	Cu	Pd	Pd1Cu(2D)	Pd1Cu1 (A)	-3.19
(100)	Cu	Pd	Pd(2A)Cu1	Pd1Cu1 (A)	-3.27
(100)	Cu	Pd	Pd(2A)Cu1	Pd1Cu1 (D)	-3.79
(100)	Cu	Pd	Pd(2A)Cu1	Pd(2A)Cu0	-3.21
(100)	Cu	Pd	Pd(2D)Cu1	Pd1Cu1 (A)	-3.49
(100)	Cu	Pd	Pd(2D)Cu1	Pd(2D)Cu0	-3.70
(100)	Cu	Pd	Pd1Cu3	Pd0Cu3	-3.90
(100)	Cu	Pd	Pd1Cu3	Pd1Cu(2D)	-3.41
(100)	Cu	Pd	Pd1Cu3	Pd1Cu(2A)	-3.49
(100)	Cu	Pd	Pd2Cu2 (A)	Pd1Cu(2A)	-3.62
(100)	Cu	Pd	Pd2Cu2 (A)	Pd(2A)Cu1	-3.45
(100)	Cu	Pd	Pd2Cu2 (D)	Pd1Cu(2D)	-3.87
(100)	Cu	Pd	Pd2Cu2 (D)	Pd(2D)Cu1	-3.56
(100)	Cu	Pd	Pd3Cu1	Pd(2D)Cu1	-3.37
(100)	Cu	Pd	Pd3Cu1	Pd(2A)Cu1	-3.59
(100)	Cu	Pd	Pd3Cu1	Pd3Cu0	-3.53
(100)	Cu	Pt	Pt1Cu0	Clean Cu	-4.28
(100)	Cu	Pt	Pt(2D)Cu0	Pt1Cu0	-3.97
(100)	Cu	Pt	Pt(2A)Cu0	Pt1Cu0	-5.01
(100)	Cu	Pt	Pt(3)Cu0	Pt(2A)Cu0	
(100)	Cu	Pt	Pt(3)Cu0	Pt(2D)Cu0	
(100)	Cu	Pt	Pt(4)Cu0	Pt3Cu0	
(100)	Cu	Pt	Pt1Cu1 (D)	Pt0Cu1	-4.36
(100)	Cu	Pt	Pt1Cu1 (D)	Pt1Cu0	-2.56
(100)	Cu	Pt	Pt1Cu1 (A)	Pt0Cu1	-5.13
(100)	Cu	Pt	Pt1Cu1 (A)	Pt1Cu0	-3.33
(100)	Cu	Pt	Pt1Cu(2A)	Pt0Cu(2A)	-5.04
(100)	Cu	Pt	Pt1Cu(2A)	Pt1Cu1 (A)	-3.03
(100)	Cu	Pt	Pt1Cu(2A)	Pt1Cu1 (D)	-3.79
(100)	Cu	Pt	Pt1Cu(2D)	Pt0Cu(2D)	-5.84
(100)	Cu	Pt	Pt1Cu(2D)	Pt1Cu1 (A)	-3.36

Surface Orientation	Host Slab	Heteroatom	Top Layer Configuration	Reference Configuration	Adsorption Energy (eV)
(100)	Cu	Pt	Pt(2A)Cu1	Pt1Cu1 (A)	-4.99
(100)	Cu	Pt	Pt(2A)Cu1	Pt1Cu1 (D)	-5.75
(100)	Cu	Pt	Pt(2A)Cu1	Pt(2A)Cu0	-3.30
(100)	Cu	Pt	Pt(2D)Cu1	Pt1Cu1 (A)	-4.72
(100)	Cu	Pt	Pt(2D)Cu1	Pt(2D)Cu0	-4.07
(100)	Cu	Pt	Pt1Cu3	Pt0Cu3	-5.57
(100)	Cu	Pt	Pt1Cu3	Pt1Cu(2D)	-3.31
(100)	Cu	Pt	Pt1Cu3	Pt1Cu(2A)	-3.64
(100)	Cu	Pt	Pt2Cu2 (A)	Pt1Cu(2A)	-5.41
(100)	Cu	Pt	Pt2Cu2 (A)	Pt(2A)Cu1	-3.45
(100)	Cu	Pt	Pt2Cu2 (D)	Pt1Cu(2D)	-5.26
(100)	Cu	Pt	Pt2Cu2 (D)	Pt(2D)Cu1	-3.90
(100)	Cu	Pt	Pt3Cu1	Pt(2D)Cu1	
(100)	Cu	Pt	Pt3Cu1	Pt(2A)Cu1	
(100)	Cu	Pt	Pt3Cu1	Pt3Cu0	
(100)	Cu	Rh	Rh1Cu0	Clean Cu	-3.71
(100)	Cu	Rh	Rh(2D)Cu0	Rh1Cu0	-3.59
(100)	Cu	Rh	Rh(2A)Cu0	Rh1Cu0	-4.79
(100)	Cu	Rh	Rh(3)Cu0	Rh(2A)Cu0	-4.72
(100)	Cu	Rh	Rh(3)Cu0	Rh(2D)Cu0	-5.92
(100)	Cu	Rh	Rh(4)Cu0	Rh3Cu0	-5.57
(100)	Cu	Rh	Rh1Cu1 (D)	Rh0Cu1	-3.82
(100)	Cu	Rh	Rh1Cu1 (D)	Rh1Cu0	-2.60
(100)	Cu	Rh	Rh1Cu1 (A)	Rh0Cu1	-4.53
(100)	Cu	Rh	Rh1Cu1 (A)	Rh1Cu0	-3.30
(100)	Cu	Rh	Rh1Cu(2A)	Rh0Cu(2A)	-4.55
(100)	Cu	Rh	Rh1Cu(2A)	Rh1Cu1 (A)	-3.14
(100)	Cu	Rh	Rh1Cu(2A)	Rh1Cu1 (D)	-3.84
(100)	Cu	Rh	Rh1Cu(2D)	Rh0Cu(2D)	-5.28
(100)	Cu	Rh	Rh1Cu(2D)	Rh1Cu1 (A)	-3.39
(100)	Cu	Rh	Rh(2A)Cu1	Rh1Cu1 (A)	-4.89
(100)	Cu	Rh	Rh(2A)Cu1	Rh1Cu1 (D)	-5.60
(100)	Cu	Rh	Rh(2A)Cu1	Rh(2A)Cu0	-3.41
(100)	Cu	Rh	Rh(2D)Cu1	Rh1Cu1 (A)	-4.38
(100)	Cu	Rh	Rh(2D)Cu1	Rh(2D)Cu0	-4.09
(100)	Cu	Rh	Rh1Cu3	Rh0Cu3	-5.14
(100)	Cu	Rh	Rh1Cu3	Rh1Cu(2D)	-3.44
(100)	Cu	Rh	Rh1Cu3	Rh1Cu(2A)	-3.70
(100)	Cu	Rh	Rh2Cu2 (A)	Rh1Cu(2A)	-5.33
(100)	Cu	Rh	Rh2Cu2 (A)	Rh(2A)Cu1	-3.58
(100)	Cu	Rh	Rh2Cu2 (D)	Rh1Cu(2D)	-5.00
(100)	Cu	Rh	Rh2Cu2 (D)	Rh(2D)Cu1	-4.02
(100)	Cu	Rh	Rh3Cu1	Rh(2D)Cu1	-5.70
(100)	Cu	Rh	Rh3Cu1	Rh(2A)Cu1	-5.18
(100)	Cu	Rh	Rh3Cu1	Rh3Cu0	-3.86

Surface Orientation	Host Slab	Heteroatom	Top Layer Configuration	Reference Configuration	Adsorption Energy (eV)
(100)	Ir	Ag	Ag1Ir0	Clean Ir	-2.45
(100)	Ir	Ag	Ag(2D)Ir0	Ag1Ir0	-2.44
(100)	Ir	Ag	Ag(2A)Ir0	Ag1Ir0	-2.47
(100)	Ir	Ag	Ag(3)Ir0	Ag(2A)Ir0	-2.47
(100)	Ir	Ag	Ag(3)Ir0	Ag(2D)Ir0	-2.50
(100)	Ir	Ag	Ag(4)Ir0	Ag3Ir0	-2.45
(100)	Ir	Ag	Ag1Ir1 (D)	Ag0Ir1	-2.38
(100)	Ir	Ag	Ag1Ir1 (D)	Ag1Ir0	-5.81
(100)	Ir	Ag	Ag1Ir1 (A)	Ag0Ir1	-2.58
(100)	Ir	Ag	Ag1Ir1 (A)	Ag1Ir0	-6.01
(100)	Ir	Ag	Ag1Ir(2A)	Ag0Ir(2A)	-2.52
(100)	Ir	Ag	Ag1Ir(2A)	Ag1Ir1 (A)	-6.87
(100)	Ir	Ag	Ag1Ir(2A)	Ag1Ir1 (D)	-7.07
(100)	Ir	Ag	Ag1Ir(2D)	Ag0Ir(2D)	
(100)	Ir	Ag	Ag1Ir(2D)	Ag1Ir1 (A)	
(100)	Ir	Ag	Ag(2A)Ir1	Ag1Ir1 (A)	-2.42
(100)	Ir	Ag	Ag(2A)Ir1	Ag1Ir1 (D)	-2.61
(100)	Ir	Ag	Ag(2A)Ir1	Ag(2A)Ir0	-5.96
(100)	Ir	Ag	Ag(2D)Ir1	Ag1Ir1 (A)	-2.58
(100)	Ir	Ag	Ag(2D)Ir1	Ag(2D)Ir0	-6.15
(100)	Ir	Ag	Ag1Ir3	Ag0Ir3	
(100)	Ir	Ag	Ag1Ir3	Ag1Ir(2D)	
(100)	Ir	Ag	Ag1Ir3	Ag1Ir(2A)	
(100)	Ir	Ag	Ag2Ir2 (A)	Ag1Ir(2A)	-2.44
(100)	Ir	Ag	Ag2Ir2 (A)	Ag(2A)Ir1	-6.90
(100)	Ir	Ag	Ag2Ir2 (D)	Ag1Ir(2D)	
(100)	Ir	Ag	Ag2Ir2 (D)	Ag(2D)Ir1	
(100)	Ir	Ag	Ag3Ir1	Ag(2D)Ir1	-2.37
(100)	Ir	Ag	Ag3Ir1	Ag(2A)Ir1	-2.54
(100)	Ir	Ag	Ag3Ir1	Ag3Ir0	-6.03
(100)	Ir	Au	Au1Ir0	Clean Ir	-2.96
(100)	Ir	Au	Au(2D)Ir0	Au1Ir0	-2.82
(100)	Ir	Au	Au(2A)Ir0	Au1Ir0	-3.07
(100)	Ir	Au	Au(3)Ir0	Au(2A)Ir0	-2.90
(100)	Ir	Au	Au(3)Ir0	Au(2D)Ir0	-3.15
(100)	Ir	Au	Au(4)Ir0	Au3Ir0	-2.90
(100)	Ir	Au	Au1Ir1 (D)	Au0Ir1	-2.79
(100)	Ir	Au	Au1Ir1 (D)	Au1Ir0	-5.72
(100)	Ir	Au	Au1Ir1 (A)	Au0Ir1	-3.27
(100)	Ir	Au	Au1Ir1 (A)	Au1Ir0	-6.20
(100)	Ir	Au	Au1Ir(2A)	Au0Ir(2A)	-3.03
(100)	Ir	Au	Au1Ir(2A)	Au1Ir1 (A)	-6.69
(100)	Ir	Au	Au1Ir(2A)	Au1Ir1 (D)	-7.18
(100)	Ir	Au	Au1Ir(2D)	Au0Ir(2D)	-3.63
(100)	Ir	Au	Au1Ir(2D)	Au1Ir1 (A)	-6.03

Surface Orientation	Host Slab	Heteroatom	Top Layer Configuration	Reference Configuration	Adsorption Energy (eV)
(100)	Ir	Au	Au(2A)Ir1	Au1Ir1 (A)	-2.88
(100)	Ir	Au	Au(2A)Ir1	Au1Ir1 (D)	-3.36
(100)	Ir	Au	Au(2A)Ir1	Au(2A)Ir0	-6.01
(100)	Ir	Au	Au(2D)Ir1	Au1Ir1 (A)	-3.09
(100)	Ir	Au	Au(2D)Ir1	Au(2D)Ir0	-6.47
(100)	Ir	Au	Au1Ir3	Au0Ir3	-3.24
(100)	Ir	Au	Au1Ir3	Au1Ir(2D)	-7.41
(100)	Ir	Au	Au1Ir3	Au1Ir(2A)	-6.75
(100)	Ir	Au	Au2Ir2 (A)	Au1Ir(2A)	-3.02
(100)	Ir	Au	Au2Ir2 (A)	Au(2A)Ir1	-6.83
(100)	Ir	Au	Au2Ir2 (D)	Au1Ir(2D)	-3.38
(100)	Ir	Au	Au2Ir2 (D)	Au(2D)Ir1	-6.33
(100)	Ir	Au	Au3Ir1	Au(2D)Ir1	-2.87
(100)	Ir	Au	Au3Ir1	Au(2A)Ir1	-3.08
(100)	Ir	Au	Au3Ir1	Au3Ir0	-6.19
(100)	Ir	Cu	Cu1Ir0	Clean Ir	-3.36
(100)	Ir	Cu	Cu(2D)Ir0	Cu1Ir0	-3.37
(100)	Ir	Cu	Cu(2A)Ir0	Cu1Ir0	-3.63
(100)	Ir	Cu	Cu(3)Ir0	Cu(2A)Ir0	-3.56
(100)	Ir	Cu	Cu(3)Ir0	Cu(2D)Ir0	-3.81
(100)	Ir	Cu	Cu(4)Ir0	Cu3Ir0	-3.65
(100)	Ir	Cu	Cu1Ir1 (D)	Cu0Ir1	-3.27
(100)	Ir	Cu	Cu1Ir1 (D)	Cu1Ir0	-5.80
(100)	Ir	Cu	Cu1Ir1 (A)	Cu0Ir1	-3.69
(100)	Ir	Cu	Cu1Ir1 (A)	Cu1Ir0	-6.22
(100)	Ir	Cu	Cu1Ir(2A)	Cu0Ir(2A)	-3.54
(100)	Ir	Cu	Cu1Ir(2A)	Cu1Ir1 (A)	-6.78
(100)	Ir	Cu	Cu1Ir(2A)	Cu1Ir1 (D)	-7.20
(100)	Ir	Cu	Cu1Ir(2D)	Cu0Ir(2D)	-4.02
(100)	Ir	Cu	Cu1Ir(2D)	Cu1Ir1 (A)	-6.00
(100)	Ir	Cu	Cu(2A)Ir1	Cu1Ir1 (A)	-3.46
(100)	Ir	Cu	Cu(2A)Ir1	Cu1Ir1 (D)	-3.88
(100)	Ir	Cu	Cu(2A)Ir1	Cu(2A)Ir0	-6.06
(100)	Ir	Cu	Cu(2D)Ir1	Cu1Ir1 (A)	-3.63
(100)	Ir	Cu	Cu(2D)Ir1	Cu(2D)Ir0	-6.48
(100)	Ir	Cu	Cu1Ir3	Cu0Ir3	-3.76
(100)	Ir	Cu	Cu1Ir3	Cu1Ir(2D)	-7.53
(100)	Ir	Cu	Cu1Ir3	Cu1Ir(2A)	-6.76
(100)	Ir	Cu	Cu2Ir2 (A)	Cu1Ir(2A)	-3.61
(100)	Ir	Cu	Cu2Ir2 (A)	Cu(2A)Ir1	-6.93
(100)	Ir	Cu	Cu2Ir2 (D)	Cu1Ir(2D)	-3.92
(100)	Ir	Cu	Cu2Ir2 (D)	Cu(2D)Ir1	-6.29
(100)	Ir	Cu	Cu3Ir1	Cu(2D)Ir1	-3.56
(100)	Ir	Cu	Cu3Ir1	Cu(2A)Ir1	-3.73
(100)	Ir	Cu	Cu3Ir1	Cu3Ir0	-6.22

Surface Orientation	Host Slab	Heteroatom	Top Layer Configuration	Reference Configuration	Adsorption Energy (eV)
(100)	Ir	Pd	Pd1Ir0	Clean Ir	-3.51
(100)	Ir	Pd	Pd(2D)Ir0	Pd1Ir0	-3.46
(100)	Ir	Pd	Pd(2A)Ir0	Pd1Ir0	-3.62
(100)	Ir	Pd	Pd(3)Ir0	Pd(2A)Ir0	-3.65
(100)	Ir	Pd	Pd(3)Ir0	Pd(2D)Ir0	-3.81
(100)	Ir	Pd	Pd(4)Ir0	Pd3Ir0	-3.75
(100)	Ir	Pd	Pd1Ir1 (D)	Pd0Ir1	-3.41
(100)	Ir	Pd	Pd1Ir1 (D)	Pd1Ir0	-5.79
(100)	Ir	Pd	Pd1Ir1 (A)	Pd0Ir1	-3.96
(100)	Ir	Pd	Pd1Ir1 (A)	Pd1Ir0	-6.34
(100)	Ir	Pd	Pd1Ir(2A)	Pd0Ir(2A)	-3.80
(100)	Ir	Pd	Pd1Ir(2A)	Pd1Ir1 (A)	-6.76
(100)	Ir	Pd	Pd1Ir(2A)	Pd1Ir1 (D)	-7.31
(100)	Ir	Pd	Pd1Ir(2D)	Pd0Ir(2D)	-4.38
(100)	Ir	Pd	Pd1Ir(2D)	Pd1Ir1 (A)	-6.09
(100)	Ir	Pd	Pd(2A)Ir1	Pd1Ir1 (A)	-3.59
(100)	Ir	Pd	Pd(2A)Ir1	Pd1Ir1 (D)	-4.13
(100)	Ir	Pd	Pd(2A)Ir1	Pd(2A)Ir0	-6.30
(100)	Ir	Pd	Pd(2D)Ir1	Pd1Ir1 (A)	-3.90
(100)	Ir	Pd	Pd(2D)Ir1	Pd(2D)Ir0	-6.77
(100)	Ir	Pd	Pd1Ir3	Pd0Ir3	-4.00
(100)	Ir	Pd	Pd1Ir3	Pd1Ir(2D)	-7.42
(100)	Ir	Pd	Pd1Ir3	Pd1Ir(2A)	-6.75
(100)	Ir	Pd	Pd2Ir2 (A)	Pd1Ir(2A)	-3.86
(100)	Ir	Pd	Pd2Ir2 (A)	Pd(2A)Ir1	-7.03
(100)	Ir	Pd	Pd2Ir2 (D)	Pd1Ir(2D)	-4.15
(100)	Ir	Pd	Pd2Ir2 (D)	Pd(2D)Ir1	-6.35
(100)	Ir	Pd	Pd3Ir1	Pd(2D)Ir1	-3.66
(100)	Ir	Pd	Pd3Ir1	Pd(2A)Ir1	-3.97
(100)	Ir	Pd	Pd3Ir1	Pd3Ir0	-6.63
(100)	Ir	Pt	Pt1Ir0	Clean Ir	-4.96
(100)	Ir	Pt	Pt(2D)Ir0	Pt1Ir0	-4.79
(100)	Ir	Pt	Pt(2A)Ir0	Pt1Ir0	-5.41
(100)	Ir	Pt	Pt(3)Ir0	Pt(2A)Ir0	-5.21
(100)	Ir	Pt	Pt(3)Ir0	Pt(2D)Ir0	-5.83
(100)	Ir	Pt	Pt(4)Ir0	Pt3Ir0	-5.45
(100)	Ir	Pt	Pt1Ir1 (D)	Pt0Ir1	-4.78
(100)	Ir	Pt	Pt1Ir1 (D)	Pt1Ir0	-5.71
(100)	Ir	Pt	Pt1Ir1 (A)	Pt0Ir1	-5.66
(100)	Ir	Pt	Pt1Ir1 (A)	Pt1Ir0	-6.59
(100)	Ir	Pt	Pt1Ir(2A)	Pt0Ir(2A)	-5.35
(100)	Ir	Pt	Pt1Ir(2A)	Pt1Ir1 (A)	-6.62
(100)	Ir	Pt	Pt1Ir(2A)	Pt1Ir1 (D)	-7.50
(100)	Ir	Pt	Pt1Ir(2D)	Pt0Ir(2D)	-6.31
(100)	Ir	Pt	Pt1Ir(2D)	Pt1Ir1 (A)	-6.32

Surface Orientation	Host Slab	Heteroatom	Top Layer Configuration	Reference Configuration	Adsorption Energy (eV)
(100)	Ir	Pt	Pt(2A)Ir1	Pt1Ir1 (A)	-5.20
(100)	Ir	Pt	Pt(2A)Ir1	Pt1Ir1 (D)	-6.08
(100)	Ir	Pt	Pt(2A)Ir1	Pt(2A)Ir0	-6.38
(100)	Ir	Pt	Pt(2D)Ir1	Pt1Ir1 (A)	-5.38
(100)	Ir	Pt	Pt(2D)Ir1	Pt(2D)Ir0	-7.19
(100)	Ir	Pt	Pt1Ir3	Pt0Ir3	-5.70
(100)	Ir	Pt	Pt1Ir3	Pt1Ir(2D)	-7.18
(100)	Ir	Pt	Pt1Ir3	Pt1Ir(2A)	-6.89
(100)	Ir	Pt	Pt2Ir2 (A)	Pt1Ir(2A)	-5.56
(100)	Ir	Pt	Pt2Ir2 (A)	Pt(2A)Ir1	-6.98
(100)	Ir	Pt	Pt2Ir2 (D)	Pt1Ir(2D)	-5.76
(100)	Ir	Pt	Pt2Ir2 (D)	Pt(2D)Ir1	-6.70
(100)	Ir	Pt	Pt3Ir1	Pt(2D)Ir1	-5.42
(100)	Ir	Pt	Pt3Ir1	Pt(2A)Ir1	-5.60
(100)	Ir	Pt	Pt3Ir1	Pt3Ir0	-6.78
(100)	Ir	Rh	Rh1Ir0	Clean Ir	-5.00
(100)	Ir	Rh	Rh(2D)Ir0	Rh1Ir0	-4.94
(100)	Ir	Rh	Rh(2A)Ir0	Rh1Ir0	-5.54
(100)	Ir	Rh	Rh(3)Ir0	Rh(2A)Ir0	-5.45
(100)	Ir	Rh	Rh(3)Ir0	Rh(2D)Ir0	-6.06
(100)	Ir	Rh	Rh(4)Ir0	Rh3Ir0	-5.73
(100)	Ir	Rh	Rh1Ir1 (D)	Rh0Ir1	-4.88
(100)	Ir	Rh	Rh1Ir1 (D)	Rh1Ir0	-5.77
(100)	Ir	Rh	Rh1Ir1 (A)	Rh0Ir1	-5.79
(100)	Ir	Rh	Rh1Ir1 (A)	Rh1Ir0	-6.68
(100)	Ir	Rh	Rh1Ir(2A)	Rh0Ir(2A)	-5.54
(100)	Ir	Rh	Rh1Ir(2A)	Rh1Ir1 (A)	-6.68
(100)	Ir	Rh	Rh1Ir(2A)	Rh1Ir1 (D)	-7.59
(100)	Ir	Rh	Rh1Ir(2D)	Rh0Ir(2D)	-6.44
(100)	Ir	Rh	Rh1Ir(2D)	Rh1Ir1 (A)	-6.33
(100)	Ir	Rh	Rh(2A)Ir1	Rh1Ir1 (A)	-5.34
(100)	Ir	Rh	Rh(2A)Ir1	Rh1Ir1 (D)	-6.25
(100)	Ir	Rh	Rh(2A)Ir1	Rh(2A)Ir0	-6.48
(100)	Ir	Rh	Rh(2D)Ir1	Rh1Ir1 (A)	-5.64
(100)	Ir	Rh	Rh(2D)Ir1	Rh(2D)Ir0	-7.38
(100)	Ir	Rh	Rh1Ir3	Rh0Ir3	-5.92
(100)	Ir	Rh	Rh1Ir3	Rh1Ir(2D)	-7.28
(100)	Ir	Rh	Rh1Ir3	Rh1Ir(2A)	-6.92
(100)	Ir	Rh	Rh2Ir2 (A)	Rh1Ir(2A)	-5.76
(100)	Ir	Rh	Rh2Ir2 (A)	Rh(2A)Ir1	-7.10
(100)	Ir	Rh	Rh2Ir2 (D)	Rh1Ir(2D)	-6.05
(100)	Ir	Rh	Rh2Ir2 (D)	Rh(2D)Ir1	-6.74
(100)	Ir	Rh	Rh3Ir1	Rh(2D)Ir1	-5.59
(100)	Ir	Rh	Rh3Ir1	Rh(2A)Ir1	-5.89
(100)	Ir	Rh	Rh3Ir1	Rh3Ir0	-6.92

Surface Orientation	Host Slab	Heteroatom	Top Layer Configuration	Reference Configuration	Adsorption Energy (eV)
(100)	Pd	Ag	Ag1Pd0	Clean Pd	-2.11
(100)	Pd	Ag	Ag(2D)Pd0	Ag1Pd0	-2.20
(100)	Pd	Ag	Ag(2A)Pd0	Ag1Pd0	-2.44
(100)	Pd	Ag	Ag(3)Pd0	Ag(2A)Pd0	-2.43
(100)	Pd	Ag	Ag(3)Pd0	Ag(2D)Pd0	-2.67
(100)	Pd	Ag	Ag(4)Pd0	Ag3Pd0	-2.56
(100)	Pd	Ag	Ag1Pd1 (D)	Ag0Pd1	-2.16
(100)	Pd	Ag	Ag1Pd1 (D)	Ag1Pd0	-2.68
(100)	Pd	Ag	Ag1Pd1 (A)	Ag0Pd1	-2.50
(100)	Pd	Ag	Ag1Pd1 (A)	Ag1Pd0	-3.02
(100)	Pd	Ag	Ag1Pd(2A)	Ag0Pd(2A)	-2.60
(100)	Pd	Ag	Ag1Pd(2A)	Ag1Pd1 (A)	-3.19
(100)	Pd	Ag	Ag1Pd(2A)	Ag1Pd1 (D)	-3.53
(100)	Pd	Ag	Ag1Pd(2D)	Ag0Pd(2D)	-2.88
(100)	Pd	Ag	Ag1Pd(2D)	Ag1Pd1 (A)	-2.99
(100)	Pd	Ag	Ag(2A)Pd1	Ag1Pd1 (A)	-2.44
(100)	Pd	Ag	Ag(2A)Pd1	Ag1Pd1 (D)	-2.78
(100)	Pd	Ag	Ag(2A)Pd1	Ag(2A)Pd0	-3.02
(100)	Pd	Ag	Ag(2D)Pd1	Ag1Pd1 (A)	-2.61
(100)	Pd	Ag	Ag(2D)Pd1	Ag(2D)Pd0	-3.43
(100)	Pd	Ag	Ag1Pd3	Ag0Pd3	-2.89
(100)	Pd	Ag	Ag1Pd3	Ag1Pd(2D)	-3.63
(100)	Pd	Ag	Ag1Pd3	Ag1Pd(2A)	-3.44
(100)	Pd	Ag	Ag2Pd2 (A)	Ag1Pd(2A)	-2.72
(100)	Pd	Ag	Ag2Pd2 (A)	Ag(2A)Pd1	-3.46
(100)	Pd	Ag	Ag2Pd2 (D)	Ag1Pd(2D)	-2.90
(100)	Pd	Ag	Ag2Pd2 (D)	Ag(2D)Pd1	-3.29
(100)	Pd	Ag	Ag3Pd1	Ag(2D)Pd1	-2.58
(100)	Pd	Ag	Ag3Pd1	Ag(2A)Pd1	-2.74
(100)	Pd	Ag	Ag3Pd1	Ag3Pd0	-3.33
(100)	Pd	Au	Au1Pd0	Clean Pd	-2.57
(100)	Pd	Au	Au(2D)Pd0	Au1Pd0	-2.49
(100)	Pd	Au	Au(2A)Pd0	Au1Pd0	-3.01
(100)	Pd	Au	Au(3)Pd0	Au(2A)Pd0	-2.85
(100)	Pd	Au	Au(3)Pd0	Au(2D)Pd0	-3.37
(100)	Pd	Au	Au(4)Pd0	Au3Pd0	-3.08
(100)	Pd	Au	Au1Pd1 (D)	Au0Pd1	-2.53
(100)	Pd	Au	Au1Pd1 (D)	Au1Pd0	-2.59
(100)	Pd	Au	Au1Pd1 (A)	Au0Pd1	-3.04
(100)	Pd	Au	Au1Pd1 (A)	Au1Pd0	-3.10
(100)	Pd	Au	Au1Pd(2A)	Au0Pd(2A)	-3.04
(100)	Pd	Au	Au1Pd(2A)	Au1Pd1 (A)	-3.10
(100)	Pd	Au	Au1Pd(2A)	Au1Pd1 (D)	-3.60
(100)	Pd	Au	Au1Pd(2D)	Au0Pd(2D)	-3.52
(100)	Pd	Au	Au1Pd(2D)	Au1Pd1 (A)	-3.10

Surface Orientation	Host Slab	Heteroatom	Top Layer Configuration	Reference Configuration	Adsorption Energy (eV)
(100)	Pd	Au	Au(2A)Pd1	Au1Pd1 (A)	-2.92
(100)	Pd	Au	Au(2A)Pd1	Au1Pd1 (D)	-3.43
(100)	Pd	Au	Au(2A)Pd1	Au(2A)Pd0	-3.01
(100)	Pd	Au	Au(2D)Pd1	Au1Pd1 (A)	-2.99
(100)	Pd	Au	Au(2D)Pd1	Au(2D)Pd0	-3.60
(100)	Pd	Au	Au1Pd3	Au0Pd3	-3.44
(100)	Pd	Au	Au1Pd3	Au1Pd(2D)	-3.54
(100)	Pd	Au	Au1Pd3	Au1Pd(2A)	-3.54
(100)	Pd	Au	Au2Pd2 (A)	Au1Pd(2A)	-3.26
(100)	Pd	Au	Au2Pd2 (A)	Au(2A)Pd1	-3.44
(100)	Pd	Au	Au2Pd2 (D)	Au1Pd(2D)	-3.36
(100)	Pd	Au	Au2Pd2 (D)	Au(2D)Pd1	-3.47
(100)	Pd	Au	Au3Pd1	Au(2D)Pd1	-3.14
(100)	Pd	Au	Au3Pd1	Au(2A)Pd1	-3.20
(100)	Pd	Au	Au3Pd1	Au3Pd0	-3.36
(100)	Pd	Cu	Cu1Pd0	Clean Pd	-2.80
(100)	Pd	Cu	Cu(2D)Pd0	Cu1Pd0	-2.85
(100)	Pd	Cu	Cu(2A)Pd0	Cu1Pd0	-3.23
(100)	Pd	Cu	Cu(3)Pd0	Cu(2A)Pd0	-3.21
(100)	Pd	Cu	Cu(3)Pd0	Cu(2D)Pd0	-3.59
(100)	Pd	Cu	Cu(4)Pd0	Cu3Pd0	-3.47
(100)	Pd	Cu	Cu1Pd1 (D)	Cu0Pd1	-2.81
(100)	Pd	Cu	Cu1Pd1 (D)	Cu1Pd0	-2.65
(100)	Pd	Cu	Cu1Pd1 (A)	Cu0Pd1	-3.27
(100)	Pd	Cu	Cu1Pd1 (A)	Cu1Pd0	-3.10
(100)	Pd	Cu	Cu1Pd(2A)	Cu0Pd(2A)	-3.32
(100)	Pd	Cu	Cu1Pd(2A)	Cu1Pd1 (A)	-3.15
(100)	Pd	Cu	Cu1Pd(2A)	Cu1Pd1 (D)	-3.60
(100)	Pd	Cu	Cu1Pd(2D)	Cu0Pd(2D)	-3.73
(100)	Pd	Cu	Cu1Pd(2D)	Cu1Pd1 (A)	-3.09
(100)	Pd	Cu	Cu(2A)Pd1	Cu1Pd1 (A)	-3.20
(100)	Pd	Cu	Cu(2A)Pd1	Cu1Pd1 (D)	-3.66
(100)	Pd	Cu	Cu(2A)Pd1	Cu(2A)Pd0	-3.08
(100)	Pd	Cu	Cu(2D)Pd1	Cu1Pd1 (A)	-3.33
(100)	Pd	Cu	Cu(2D)Pd1	Cu(2D)Pd0	-3.57
(100)	Pd	Cu	Cu1Pd3	Cu0Pd3	-3.71
(100)	Pd	Cu	Cu1Pd3	Cu1Pd(2D)	-3.60
(100)	Pd	Cu	Cu1Pd3	Cu1Pd(2A)	-3.54
(100)	Pd	Cu	Cu2Pd2 (A)	Cu1Pd(2A)	-3.59
(100)	Pd	Cu	Cu2Pd2 (A)	Cu(2A)Pd1	-3.53
(100)	Pd	Cu	Cu2Pd2 (D)	Cu1Pd(2D)	-3.72
(100)	Pd	Cu	Cu2Pd2 (D)	Cu(2D)Pd1	-3.48
(100)	Pd	Cu	Cu3Pd1	Cu(2D)Pd1	-3.48
(100)	Pd	Cu	Cu3Pd1	Cu(2A)Pd1	-3.60
(100)	Pd	Cu	Cu3Pd1	Cu3Pd0	-3.46

Surface Orientation	Host Slab	Heteroatom	Top Layer Configuration	Reference Configuration	Adsorption Energy (eV)
(100)	Pd	Ir	Ir1Pd0	Clean Pd	-4.47
(100)	Pd	Ir	Ir(2D)Pd0	Ir1Pd0	-4.07
(100)	Pd	Ir	Ir(2A)Pd0	Ir1Pd0	
(100)	Pd	Ir	Ir(3)Pd0	Ir(2A)Pd0	
(100)	Pd	Ir	Ir(3)Pd0	Ir(2D)Pd0	-7.29
(100)	Pd	Ir	Ir(4)Pd0	Ir3Pd0	
(100)	Pd	Ir	Ir1Pd1 (D)	Ir0Pd1	-4.38
(100)	Pd	Ir	Ir1Pd1 (D)	Ir1Pd0	-2.54
(100)	Pd	Ir	Ir1Pd1 (A)	Ir0Pd1	-5.28
(100)	Pd	Ir	Ir1Pd1 (A)	Ir1Pd0	-3.43
(100)	Pd	Ir	Ir1Pd(2A)	Ir0Pd(2A)	-5.23
(100)	Pd	Ir	Ir1Pd(2A)	Ir1Pd1 (A)	-3.05
(100)	Pd	Ir	Ir1Pd(2A)	Ir1Pd1 (D)	-3.95
(100)	Pd	Ir	Ir1Pd(2D)	Ir0Pd(2D)	-6.12
(100)	Pd	Ir	Ir1Pd(2D)	Ir1Pd1 (A)	-3.47
(100)	Pd	Ir	Ir(2A)Pd1	Ir1Pd1 (A)	
(100)	Pd	Ir	Ir(2A)Pd1	Ir1Pd1 (D)	
(100)	Pd	Ir	Ir(2A)Pd1	Ir(2A)Pd0	
(100)	Pd	Ir	Ir(2D)Pd1	Ir1Pd1 (A)	-4.92
(100)	Pd	Ir	Ir(2D)Pd1	Ir(2D)Pd0	-4.29
(100)	Pd	Ir	Ir1Pd3	Ir0Pd3	-6.05
(100)	Pd	Ir	Ir1Pd3	Ir1Pd(2D)	-3.55
(100)	Pd	Ir	Ir1Pd3	Ir1Pd(2A)	-3.97
(100)	Pd	Ir	Ir2Pd2 (A)	Ir1Pd(2A)	
(100)	Pd	Ir	Ir2Pd2 (A)	Ir(2A)Pd1	
(100)	Pd	Ir	Ir2Pd2 (D)	Ir1Pd(2D)	-5.72
(100)	Pd	Ir	Ir2Pd2 (D)	Ir(2D)Pd1	-4.27
(100)	Pd	Ir	Ir3Pd1	Ir(2D)Pd1	-7.17
(100)	Pd	Ir	Ir3Pd1	Ir(2A)Pd1	
(100)	Pd	Ir	Ir3Pd1	Ir3Pd0	-4.16
(100)	Pd	Pt	Pt1Pd0	Clean Pd	-3.93
(100)	Pd	Pt	Pt(2D)Pd0	Pt1Pd0	-3.71
(100)	Pd	Pt	Pt(2A)Pd0	Pt1Pd0	-4.71
(100)	Pd	Pt	Pt(3)Pd0	Pt(2A)Pd0	-4.58
(100)	Pd	Pt	Pt(3)Pd0	Pt(2D)Pd0	-5.58
(100)	Pd	Pt	Pt(4)Pd0	Pt3Pd0	-5.35
(100)	Pd	Pt	Pt1Pd1 (D)	Pt0Pd1	-3.85
(100)	Pd	Pt	Pt1Pd1 (D)	Pt1Pd0	-2.55
(100)	Pd	Pt	Pt1Pd1 (A)	Pt0Pd1	-4.56
(100)	Pd	Pt	Pt1Pd1 (A)	Pt1Pd0	-3.26
(100)	Pd	Pt	Pt1Pd(2A)	Pt0Pd(2A)	-4.53
(100)	Pd	Pt	Pt1Pd(2A)	Pt1Pd1 (A)	-3.07
(100)	Pd	Pt	Pt1Pd(2A)	Pt1Pd1 (D)	-3.78
(100)	Pd	Pt	Pt1Pd(2D)	Pt0Pd(2D)	-5.24
(100)	Pd	Pt	Pt1Pd(2D)	Pt1Pd1 (A)	-3.30

Surface Orientation	Host Slab	Heteroatom	Top Layer Configuration	Reference Configuration	Adsorption Energy (eV)
(100)	Pd	Pt	Pt(2A)Pd1	Pt1Pd1 (A)	-4.69
(100)	Pd	Pt	Pt(2A)Pd1	Pt1Pd1 (D)	-5.40
(100)	Pd	Pt	Pt(2A)Pd1	Pt(2A)Pd0	-3.24
(100)	Pd	Pt	Pt(2D)Pd1	Pt1Pd1 (A)	-4.41
(100)	Pd	Pt	Pt(2D)Pd1	Pt(2D)Pd0	-3.96
(100)	Pd	Pt	Pt1Pd3	Pt0Pd3	-5.18
(100)	Pd	Pt	Pt1Pd3	Pt1Pd(2D)	-3.56
(100)	Pd	Pt	Pt1Pd3	Pt1Pd(2A)	-3.79
(100)	Pd	Pt	Pt2Pd2 (A)	Pt1Pd(2A)	-5.33
(100)	Pd	Pt	Pt2Pd2 (A)	Pt(2A)Pd1	-3.71
(100)	Pd	Pt	Pt2Pd2 (D)	Pt1Pd(2D)	-5.05
(100)	Pd	Pt	Pt2Pd2 (D)	Pt(2D)Pd1	-3.94
(100)	Pd	Pt	Pt3Pd1	Pt(2D)Pd1	-5.48
(100)	Pd	Pt	Pt3Pd1	Pt(2A)Pd1	-5.20
(100)	Pd	Pt	Pt3Pd1	Pt3Pd0	-3.86
(100)	Pd	Rh	Rh1Pd0	Clean Pd	-3.71
(100)	Pd	Rh	Rh(2D)Pd0	Rh1Pd0	-3.58
(100)	Pd	Rh	Rh(2A)Pd0	Rh1Pd0	-4.55
(100)	Pd	Rh	Rh(3)Pd0	Rh(2A)Pd0	-4.52
(100)	Pd	Rh	Rh(3)Pd0	Rh(2D)Pd0	-5.49
(100)	Pd	Rh	Rh(4)Pd0	Rh3Pd0	-5.44
(100)	Pd	Rh	Rh1Pd1 (D)	Rh0Pd1	-3.67
(100)	Pd	Rh	Rh1Pd1 (D)	Rh1Pd0	-2.59
(100)	Pd	Rh	Rh1Pd1 (A)	Rh0Pd1	-4.32
(100)	Pd	Rh	Rh1Pd1 (A)	Rh1Pd0	-3.24
(100)	Pd	Rh	Rh1Pd(2A)	Rh0Pd(2A)	-4.35
(100)	Pd	Rh	Rh1Pd(2A)	Rh1Pd1 (A)	-3.12
(100)	Pd	Rh	Rh1Pd(2A)	Rh1Pd1 (D)	-3.77
(100)	Pd	Rh	Rh1Pd(2D)	Rh0Pd(2D)	-4.99
(100)	Pd	Rh	Rh1Pd(2D)	Rh1Pd1 (A)	-3.28
(100)	Pd	Rh	Rh(2A)Pd1	Rh1Pd1 (A)	-4.57
(100)	Pd	Rh	Rh(2A)Pd1	Rh1Pd1 (D)	-5.22
(100)	Pd	Rh	Rh(2A)Pd1	Rh(2A)Pd0	-3.26
(100)	Pd	Rh	Rh(2D)Pd1	Rh1Pd1 (A)	-4.27
(100)	Pd	Rh	Rh(2D)Pd1	Rh(2D)Pd0	-3.93
(100)	Pd	Rh	Rh1Pd3	Rh0Pd3	-5.01
(100)	Pd	Rh	Rh1Pd3	Rh1Pd(2D)	-3.64
(100)	Pd	Rh	Rh1Pd3	Rh1Pd(2A)	-3.80
(100)	Pd	Rh	Rh2Pd2 (A)	Rh1Pd(2A)	-5.25
(100)	Pd	Rh	Rh2Pd2 (A)	Rh(2A)Pd1	-3.80
(100)	Pd	Rh	Rh2Pd2 (D)	Rh1Pd(2D)	-4.94
(100)	Pd	Rh	Rh2Pd2 (D)	Rh(2D)Pd1	-3.95
(100)	Pd	Rh	Rh3Pd1	Rh(2D)Pd1	-5.50
(100)	Pd	Rh	Rh3Pd1	Rh(2A)Pd1	-5.19
(100)	Pd	Rh	Rh3Pd1	Rh3Pd0	-3.94

Surface Orientation	Host Slab	Heteroatom	Top Layer Configuration	Reference Configuration	Adsorption Energy (eV)
(100)	Pt	Ag	Ag1Pt0	Clean Pt	-2.39
(100)	Pt	Ag	Ag(2D)Pt0	Ag1Pt0	-2.33
(100)	Pt	Ag	Ag(2A)Pt0	Ag1Pt0	-2.47
(100)	Pt	Ag	Ag(3)Pt0	Ag(2A)Pt0	-2.45
(100)	Pt	Ag	Ag(3)Pt0	Ag(2D)Pt0	-2.58
(100)	Pt	Ag	Ag(4)Pt0	Ag3Pt0	-2.50
(100)	Pt	Ag	Ag1Pt1 (D)	Ag0Pt1	-2.26
(100)	Pt	Ag	Ag1Pt1 (D)	Ag1Pt0	-4.37
(100)	Pt	Ag	Ag1Pt1 (A)	Ag0Pt1	-2.56
(100)	Pt	Ag	Ag1Pt1 (A)	Ag1Pt0	-4.67
(100)	Pt	Ag	Ag1Pt(2A)	Ag0Pt(2A)	-2.57
(100)	Pt	Ag	Ag1Pt(2A)	Ag1Pt1 (A)	-4.84
(100)	Pt	Ag	Ag1Pt(2A)	Ag1Pt1 (D)	-5.15
(100)	Pt	Ag	Ag1Pt(2D)	Ag0Pt(2D)	-2.84
(100)	Pt	Ag	Ag1Pt(2D)	Ag1Pt1 (A)	-4.36
(100)	Pt	Ag	Ag(2A)Pt1	Ag1Pt1 (A)	-2.37
(100)	Pt	Ag	Ag(2A)Pt1	Ag1Pt1 (D)	-2.68
(100)	Pt	Ag	Ag(2A)Pt1	Ag(2A)Pt0	-4.58
(100)	Pt	Ag	Ag(2D)Pt1	Ag1Pt1 (A)	-2.60
(100)	Pt	Ag	Ag(2D)Pt1	Ag(2D)Pt0	-4.94
(100)	Pt	Ag	Ag1Pt3	Ag0Pt3	-2.78
(100)	Pt	Ag	Ag1Pt3	Ag1Pt(2D)	-5.32
(100)	Pt	Ag	Ag1Pt3	Ag1Pt(2A)	-4.84
(100)	Pt	Ag	Ag2Pt2 (A)	Ag1Pt(2A)	-2.56
(100)	Pt	Ag	Ag2Pt2 (A)	Ag(2A)Pt1	-5.03
(100)	Pt	Ag	Ag2Pt2 (D)	Ag1Pt(2D)	-2.86
(100)	Pt	Ag	Ag2Pt2 (D)	Ag(2D)Pt1	-4.62
(100)	Pt	Ag	Ag3Pt1	Ag(2D)Pt1	-2.42
(100)	Pt	Ag	Ag3Pt1	Ag(2A)Pt1	-2.65
(100)	Pt	Ag	Ag3Pt1	Ag3Pt0	-4.77
(100)	Pt	Au	Au1Pt0	Clean Pt	-2.75
(100)	Pt	Au	Au(2D)Pt0	Au1Pt0	-2.57
(100)	Pt	Au	Au(2A)Pt0	Au1Pt0	-2.96
(100)	Pt	Au	Au(3)Pt0	Au(2A)Pt0	-2.80
(100)	Pt	Au	Au(3)Pt0	Au(2D)Pt0	-3.19
(100)	Pt	Au	Au(4)Pt0	Au3Pt0	-2.94
(100)	Pt	Au	Au1Pt1 (D)	Au0Pt1	-2.48
(100)	Pt	Au	Au1Pt1 (D)	Au1Pt0	-4.23
(100)	Pt	Au	Au1Pt1 (A)	Au0Pt1	-2.98
(100)	Pt	Au	Au1Pt1 (A)	Au1Pt0	-4.73
(100)	Pt	Au	Au1Pt(2A)	Au0Pt(2A)	-2.86
(100)	Pt	Au	Au1Pt(2A)	Au1Pt1 (A)	-4.71
(100)	Pt	Au	Au1Pt(2A)	Au1Pt1 (D)	-5.21
(100)	Pt	Au	Au1Pt(2D)	Au0Pt(2D)	-3.38
(100)	Pt	Au	Au1Pt(2D)	Au1Pt1 (A)	-4.48

Surface Orientation	Host Slab	Heteroatom	Top Layer Configuration	Reference Configuration	Adsorption Energy (eV)
(100)	Pt	Au	Au(2A)Pt1	Au1Pt1 (A)	-2.76
(100)	Pt	Au	Au(2A)Pt1	Au1Pt1 (D)	-3.26
(100)	Pt	Au	Au(2A)Pt1	Au(2A)Pt0	-4.53
(100)	Pt	Au	Au(2D)Pt1	Au1Pt1 (A)	-2.90
(100)	Pt	Au	Au(2D)Pt1	Au(2D)Pt0	-5.06
(100)	Pt	Au	Au1Pt3	Au0Pt3	-3.18
(100)	Pt	Au	Au1Pt3	Au1Pt(2D)	-5.18
(100)	Pt	Au	Au1Pt3	Au1Pt(2A)	-4.95
(100)	Pt	Au	Au2Pt2 (A)	Au1Pt(2A)	-3.00
(100)	Pt	Au	Au2Pt2 (A)	Au(2A)Pt1	-4.96
(100)	Pt	Au	Au2Pt2 (D)	Au1Pt(2D)	-3.22
(100)	Pt	Au	Au2Pt2 (D)	Au(2D)Pt1	-4.81
(100)	Pt	Au	Au3Pt1	Au(2D)Pt1	-2.91
(100)	Pt	Au	Au3Pt1	Au(2A)Pt1	-3.05
(100)	Pt	Au	Au3Pt1	Au3Pt0	-4.78
(100)	Pt	Cu	Cu1Pt0	Clean Pt	-3.27
(100)	Pt	Cu	Cu(2D)Pt0	Cu1Pt0	-3.20
(100)	Pt	Cu	Cu(2A)Pt0	Cu1Pt0	-3.45
(100)	Pt	Cu	Cu(3)Pt0	Cu(2A)Pt0	-3.35
(100)	Pt	Cu	Cu(3)Pt0	Cu(2D)Pt0	-3.61
(100)	Pt	Cu	Cu(4)Pt0	Cu3Pt0	-3.45
(100)	Pt	Cu	Cu1Pt1 (D)	Cu0Pt1	-3.07
(100)	Pt	Cu	Cu1Pt1 (D)	Cu1Pt0	-4.30
(100)	Pt	Cu	Cu1Pt1 (A)	Cu0Pt1	-3.48
(100)	Pt	Cu	Cu1Pt1 (A)	Cu1Pt0	-4.71
(100)	Pt	Cu	Cu1Pt(2A)	Cu0Pt(2A)	-3.41
(100)	Pt	Cu	Cu1Pt(2A)	Cu1Pt1 (A)	-4.76
(100)	Pt	Cu	Cu1Pt(2A)	Cu1Pt1 (D)	-5.17
(100)	Pt	Cu	Cu1Pt(2D)	Cu0Pt(2D)	-3.78
(100)	Pt	Cu	Cu1Pt(2D)	Cu1Pt1 (A)	-4.37
(100)	Pt	Cu	Cu(2A)Pt1	Cu1Pt1 (A)	-3.26
(100)	Pt	Cu	Cu(2A)Pt1	Cu1Pt1 (D)	-3.66
(100)	Pt	Cu	Cu(2A)Pt1	Cu(2A)Pt0	-4.51
(100)	Pt	Cu	Cu(2D)Pt1	Cu1Pt1 (A)	-3.46
(100)	Pt	Cu	Cu(2D)Pt1	Cu(2D)Pt0	-4.97
(100)	Pt	Cu	Cu1Pt3	Cu0Pt3	-3.65
(100)	Pt	Cu	Cu1Pt3	Cu1Pt(2D)	-5.26
(100)	Pt	Cu	Cu1Pt3	Cu1Pt(2A)	-4.87
(100)	Pt	Cu	Cu2Pt2 (A)	Cu1Pt(2A)	-3.50
(100)	Pt	Cu	Cu2Pt2 (A)	Cu(2A)Pt1	-5.01
(100)	Pt	Cu	Cu2Pt2 (D)	Cu1Pt(2D)	-3.74
(100)	Pt	Cu	Cu2Pt2 (D)	Cu(2D)Pt1	-4.65
(100)	Pt	Cu	Cu3Pt1	Cu(2D)Pt1	-3.37
(100)	Pt	Cu	Cu3Pt1	Cu(2A)Pt1	-3.58
(100)	Pt	Cu	Cu3Pt1	Cu3Pt0	-4.74

Surface Orientation	Host Slab	Heteroatom	Top Layer Configuration	Reference Configuration	Adsorption Energy (eV)
(100)	Pt	Ir	Ir1Pt0	Clean Pt	-5.35
(100)	Pt	Ir	Ir(2D)Pt0	Ir1Pt0	-4.64
(100)	Pt	Ir	Ir(2A)Pt0	Ir1Pt0	-6.08
(100)	Pt	Ir	Ir(3)Pt0	Ir(2A)Pt0	-5.66
(100)	Pt	Ir	Ir(3)Pt0	Ir(2D)Pt0	-7.10
(100)	Pt	Ir	Ir(4)Pt0	Ir3Pt0	-6.61
(100)	Pt	Ir	Ir1Pt1 (D)	Ir0Pt1	-4.83
(100)	Pt	Ir	Ir1Pt1 (D)	Ir1Pt0	-3.98
(100)	Pt	Ir	Ir1Pt1 (A)	Ir0Pt1	-5.86
(100)	Pt	Ir	Ir1Pt1 (A)	Ir1Pt0	-5.00
(100)	Pt	Ir	Ir1Pt(2A)	Ir0Pt(2A)	-5.59
(100)	Pt	Ir	Ir1Pt(2A)	Ir1Pt1 (A)	-4.57
(100)	Pt	Ir	Ir1Pt(2A)	Ir1Pt1 (D)	-5.59
(100)	Pt	Ir	Ir1Pt(2D)	Ir0Pt(2D)	-6.52
(100)	Pt	Ir	Ir1Pt(2D)	Ir1Pt1 (A)	-4.74
(100)	Pt	Ir	Ir(2A)Pt1	Ir1Pt1 (A)	-5.77
(100)	Pt	Ir	Ir(2A)Pt1	Ir1Pt1 (D)	-6.79
(100)	Pt	Ir	Ir(2A)Pt1	Ir(2A)Pt0	-4.69
(100)	Pt	Ir	Ir(2D)Pt1	Ir1Pt1 (A)	-5.44
(100)	Pt	Ir	Ir(2D)Pt1	Ir(2D)Pt0	-5.81
(100)	Pt	Ir	Ir1Pt3	Ir0Pt3	-6.25
(100)	Pt	Ir	Ir1Pt3	Ir1Pt(2D)	-5.11
(100)	Pt	Ir	Ir1Pt3	Ir1Pt(2A)	-5.29
(100)	Pt	Ir	Ir2Pt2 (A)	Ir1Pt(2A)	-6.47
(100)	Pt	Ir	Ir2Pt2 (A)	Ir(2A)Pt1	-5.26
(100)	Pt	Ir	Ir2Pt2 (D)	Ir1Pt(2D)	-6.15
(100)	Pt	Ir	Ir2Pt2 (D)	Ir(2D)Pt1	-5.45
(100)	Pt	Ir	Ir3Pt1	Ir(2D)Pt1	-6.71
(100)	Pt	Ir	Ir3Pt1	Ir(2A)Pt1	-6.38
(100)	Pt	Ir	Ir3Pt1	Ir3Pt0	-5.41
(100)	Pt	Pd	Pd1Pt0	Clean Pt	-3.16
(100)	Pt	Pd	Pd(2D)Pt0	Pd1Pt0	-2.97
(100)	Pt	Pd	Pd(2A)Pt0	Pd1Pt0	-3.28
(100)	Pt	Pd	Pd(3)Pt0	Pd(2A)Pt0	-3.26
(100)	Pt	Pd	Pd(3)Pt0	Pd(2D)Pt0	-3.57
(100)	Pt	Pd	Pd(4)Pt0	Pd3Pt0	-3.55
(100)	Pt	Pd	Pd1Pt1 (D)	Pd0Pt1	-2.89
(100)	Pt	Pd	Pd1Pt1 (D)	Pd1Pt0	-4.23
(100)	Pt	Pd	Pd1Pt1 (A)	Pd0Pt1	-3.39
(100)	Pt	Pd	Pd1Pt1 (A)	Pd1Pt0	-4.73
(100)	Pt	Pd	Pd1Pt(2A)	Pd0Pt(2A)	-3.31
(100)	Pt	Pd	Pd1Pt(2A)	Pd1Pt1 (A)	-4.74
(100)	Pt	Pd	Pd1Pt(2A)	Pd1Pt1 (D)	-5.25
(100)	Pt	Pd	Pd1Pt(2D)	Pd0Pt(2D)	-3.81
(100)	Pt	Pd	Pd1Pt(2D)	Pd1Pt1 (A)	-4.50

Surface Orientation	Host Slab	Heteroatom	Top Layer Configuration	Reference Configuration	Adsorption Energy (eV)
(100)	Pt	Pd	Pd(2A)Pt1	Pd1Pt1 (A)	-3.18
(100)	Pt	Pd	Pd(2A)Pt1	Pd1Pt1 (D)	-3.68
(100)	Pt	Pd	Pd(2A)Pt1	Pd(2A)Pt0	-4.63
(100)	Pt	Pd	Pd(2D)Pt1	Pd1Pt1 (A)	-3.37
(100)	Pt	Pd	Pd(2D)Pt1	Pd(2D)Pt0	-5.13
(100)	Pt	Pd	Pd1Pt3	Pd0Pt3	-3.69
(100)	Pt	Pd	Pd1Pt3	Pd1Pt(2D)	-5.26
(100)	Pt	Pd	Pd1Pt3	Pd1Pt(2A)	-5.02
(100)	Pt	Pd	Pd2Pt2 (A)	Pd1Pt(2A)	-3.58
(100)	Pt	Pd	Pd2Pt2 (A)	Pd(2A)Pt1	-5.14
(100)	Pt	Pd	Pd2Pt2 (D)	Pd1Pt(2D)	-3.77
(100)	Pt	Pd	Pd2Pt2 (D)	Pd(2D)Pt1	-4.90
(100)	Pt	Pd	Pd3Pt1	Pd(2D)Pt1	-3.46
(100)	Pt	Pd	Pd3Pt1	Pd(2A)Pt1	-3.66
(100)	Pt	Pd	Pd3Pt1	Pd3Pt0	-5.03
(100)	Pt	Rh	Rh1Pt0	Clean Pt	-4.54
(100)	Pt	Rh	Rh(2D)Pt0	Rh1Pt0	-4.14
(100)	Pt	Rh	Rh(2A)Pt0	Rh1Pt0	-4.90
(100)	Pt	Rh	Rh(3)Pt0	Rh(2A)Pt0	-4.70
(100)	Pt	Rh	Rh(3)Pt0	Rh(2D)Pt0	-5.46
(100)	Pt	Rh	Rh(4)Pt0	Rh3Pt0	-5.31
(100)	Pt	Rh	Rh1Pt1 (D)	Rh0Pt1	-4.16
(100)	Pt	Rh	Rh1Pt1 (D)	Rh1Pt0	-4.11
(100)	Pt	Rh	Rh1Pt1 (A)	Rh0Pt1	-4.89
(100)	Pt	Rh	Rh1Pt1 (A)	Rh1Pt0	-4.85
(100)	Pt	Rh	Rh1Pt(2A)	Rh0Pt(2A)	-4.74
(100)	Pt	Rh	Rh1Pt(2A)	Rh1Pt1 (A)	-4.68
(100)	Pt	Rh	Rh1Pt(2A)	Rh1Pt1 (D)	-5.42
(100)	Pt	Rh	Rh1Pt(2D)	Rh0Pt(2D)	-5.40
(100)	Pt	Rh	Rh1Pt(2D)	Rh1Pt1 (A)	-4.59
(100)	Pt	Rh	Rh(2A)Pt1	Rh1Pt1 (A)	-4.69
(100)	Pt	Rh	Rh(2A)Pt1	Rh1Pt1 (D)	-5.42
(100)	Pt	Rh	Rh(2A)Pt1	Rh(2A)Pt0	-4.64
(100)	Pt	Rh	Rh(2D)Pt1	Rh1Pt1 (A)	-4.76
(100)	Pt	Rh	Rh(2D)Pt1	Rh(2D)Pt0	-5.47
(100)	Pt	Rh	Rh1Pt3	Rh0Pt3	-5.25
(100)	Pt	Rh	Rh1Pt3	Rh1Pt(2D)	-5.23
(100)	Pt	Rh	Rh1Pt3	Rh1Pt(2A)	-5.13
(100)	Pt	Rh	Rh2Pt2 (A)	Rh1Pt(2A)	-5.24
(100)	Pt	Rh	Rh2Pt2 (A)	Rh(2A)Pt1	-5.23
(100)	Pt	Rh	Rh2Pt2 (D)	Rh1Pt(2D)	-5.33
(100)	Pt	Rh	Rh2Pt2 (D)	Rh(2D)Pt1	-5.16
(100)	Pt	Rh	Rh3Pt1	Rh(2D)Pt1	-5.24
(100)	Pt	Rh	Rh3Pt1	Rh(2A)Pt1	-5.31
(100)	Pt	Rh	Rh3Pt1	Rh3Pt0	-5.26

Surface Orientation	Host Slab	Heteroatom	Top Layer Configuration	Reference Configuration	Adsorption Energy (eV)
(100)	Rh	Ag	Ag1Rh0	Clean Rh	-2.22
(100)	Rh	Ag	Ag(2D)Rh0	Ag1Rh0	-2.31
(100)	Rh	Ag	Ag(2A)Rh0	Ag1Rh0	-2.41
(100)	Rh	Ag	Ag(3)Rh0	Ag(2A)Rh0	-2.43
(100)	Rh	Ag	Ag(3)Rh0	Ag(2D)Rh0	-2.53
(100)	Rh	Ag	Ag(4)Rh0	Ag3Rh0	-2.44
(100)	Rh	Ag	Ag1Rh1 (D)	Ag0Rh1	-2.29
(100)	Rh	Ag	Ag1Rh1 (D)	Ag1Rh0	-4.52
(100)	Rh	Ag	Ag1Rh1 (A)	Ag0Rh1	-2.47
(100)	Rh	Ag	Ag1Rh1 (A)	Ag1Rh0	-4.71
(100)	Rh	Ag	Ag1Rh(2A)	Ag0Rh(2A)	-2.56
(100)	Rh	Ag	Ag1Rh(2A)	Ag1Rh1 (A)	-5.31
(100)	Rh	Ag	Ag1Rh(2A)	Ag1Rh1 (D)	-5.50
(100)	Rh	Ag	Ag1Rh(2D)	Ag0Rh(2D)	-2.76
(100)	Rh	Ag	Ag1Rh(2D)	Ag1Rh1 (A)	-4.76
(100)	Rh	Ag	Ag(2A)Rh1	Ag1Rh1 (A)	-2.44
(100)	Rh	Ag	Ag(2A)Rh1	Ag1Rh1 (D)	-2.63
(100)	Rh	Ag	Ag(2A)Rh1	Ag(2A)Rh0	-4.74
(100)	Rh	Ag	Ag(2D)Rh1	Ag1Rh1 (A)	-2.57
(100)	Rh	Ag	Ag(2D)Rh1	Ag(2D)Rh0	-4.96
(100)	Rh	Ag	Ag1Rh3	Ag0Rh3	-2.75
(100)	Rh	Ag	Ag1Rh3	Ag1Rh(2D)	-5.93
(100)	Rh	Ag	Ag1Rh3	Ag1Rh(2A)	-5.38
(100)	Rh	Ag	Ag2Rh2 (A)	Ag1Rh(2A)	-2.55
(100)	Rh	Ag	Ag2Rh2 (A)	Ag(2A)Rh1	-5.42
(100)	Rh	Ag	Ag2Rh2 (D)	Ag1Rh(2D)	-2.78
(100)	Rh	Ag	Ag2Rh2 (D)	Ag(2D)Rh1	-4.97
(100)	Rh	Ag	Ag3Rh1	Ag(2D)Rh1	-2.45
(100)	Rh	Ag	Ag3Rh1	Ag(2A)Rh1	-2.57
(100)	Rh	Ag	Ag3Rh1	Ag3Rh0	-4.88
(100)	Rh	Au	Au1Rh0	Clean Rh	-2.81
(100)	Rh	Au	Au(2D)Rh0	Au1Rh0	-2.75
(100)	Rh	Au	Au(2A)Rh0	Au1Rh0	-3.09
(100)	Rh	Au	Au(3)Rh0	Au(2A)Rh0	-2.93
(100)	Rh	Au	Au(3)Rh0	Au(2D)Rh0	-3.27
(100)	Rh	Au	Au(4)Rh0	Au3Rh0	-2.96
(100)	Rh	Au	Au1Rh1 (D)	Au0Rh1	-2.81
(100)	Rh	Au	Au1Rh1 (D)	Au1Rh0	-4.45
(100)	Rh	Au	Au1Rh1 (A)	Au0Rh1	-3.23
(100)	Rh	Au	Au1Rh1 (A)	Au1Rh0	-4.87
(100)	Rh	Au	Au1Rh(2A)	Au0Rh(2A)	-3.19
(100)	Rh	Au	Au1Rh(2A)	Au1Rh1 (A)	-5.19
(100)	Rh	Au	Au1Rh(2A)	Au1Rh1 (D)	-5.61
(100)	Rh	Au	Au1Rh(2D)	Au0Rh(2D)	-3.67
(100)	Rh	Au	Au1Rh(2D)	Au1Rh1 (A)	-4.90

Surface Orientation	Host Slab	Heteroatom	Top Layer Configuration	Reference Configuration	Adsorption Energy (eV)
(100)	Rh	Au	Au(2A)Rh1	Au1Rh1 (A)	-3.00
(100)	Rh	Au	Au(2A)Rh1	Au1Rh1 (D)	-3.43
(100)	Rh	Au	Au(2A)Rh1	Au(2A)Rh0	-4.79
(100)	Rh	Au	Au(2D)Rh1	Au1Rh1 (A)	-3.14
(100)	Rh	Au	Au(2D)Rh1	Au(2D)Rh0	-5.25
(100)	Rh	Au	Au1Rh3	Au0Rh3	-3.48
(100)	Rh	Au	Au1Rh3	Au1Rh(2D)	-5.76
(100)	Rh	Au	Au1Rh3	Au1Rh(2A)	-5.47
(100)	Rh	Au	Au2Rh2 (A)	Au1Rh(2A)	-3.20
(100)	Rh	Au	Au2Rh2 (A)	Au(2A)Rh1	-5.39
(100)	Rh	Au	Au2Rh2 (D)	Au1Rh(2D)	-3.46
(100)	Rh	Au	Au2Rh2 (D)	Au(2D)Rh1	-5.22
(100)	Rh	Au	Au3Rh1	Au(2D)Rh1	-3.02
(100)	Rh	Au	Au3Rh1	Au(2A)Rh1	-3.16
(100)	Rh	Au	Au3Rh1	Au3Rh0	-5.01
(100)	Rh	Cu	Cu1Rh0	Clean Rh	-2.97
(100)	Rh	Cu	Cu(2D)Rh0	Cu1Rh0	-3.08
(100)	Rh	Cu	Cu(2A)Rh0	Cu1Rh0	-3.43
(100)	Rh	Cu	Cu(3)Rh0	Cu(2A)Rh0	-3.42
(100)	Rh	Cu	Cu(3)Rh0	Cu(2D)Rh0	-3.78
(100)	Rh	Cu	Cu(4)Rh0	Cu3Rh0	-3.64
(100)	Rh	Cu	Cu1Rh1 (D)	Cu0Rh1	-3.03
(100)	Rh	Cu	Cu1Rh1 (D)	Cu1Rh0	-4.51
(100)	Rh	Cu	Cu1Rh1 (A)	Cu0Rh1	-3.46
(100)	Rh	Cu	Cu1Rh1 (A)	Cu1Rh0	-4.94
(100)	Rh	Cu	Cu1Rh(2A)	Cu0Rh(2A)	-3.48
(100)	Rh	Cu	Cu1Rh(2A)	Cu1Rh1 (A)	-5.25
(100)	Rh	Cu	Cu1Rh(2A)	Cu1Rh1 (D)	-5.67
(100)	Rh	Cu	Cu1Rh(2D)	Cu0Rh(2D)	-3.92
(100)	Rh	Cu	Cu1Rh(2D)	Cu1Rh1 (A)	-4.94
(100)	Rh	Cu	Cu(2A)Rh1	Cu1Rh1 (A)	-3.40
(100)	Rh	Cu	Cu(2A)Rh1	Cu1Rh1 (D)	-3.82
(100)	Rh	Cu	Cu(2A)Rh1	Cu(2A)Rh0	-4.90
(100)	Rh	Cu	Cu(2D)Rh1	Cu1Rh1 (A)	-3.49
(100)	Rh	Cu	Cu(2D)Rh1	Cu(2D)Rh0	-5.35
(100)	Rh	Cu	Cu1Rh3	Cu0Rh3	-3.82
(100)	Rh	Cu	Cu1Rh3	Cu1Rh(2D)	-5.85
(100)	Rh	Cu	Cu1Rh3	Cu1Rh(2A)	-5.53
(100)	Rh	Cu	Cu2Rh2 (A)	Cu1Rh(2A)	-3.69
(100)	Rh	Cu	Cu2Rh2 (A)	Cu(2A)Rh1	-5.55
(100)	Rh	Cu	Cu2Rh2 (D)	Cu1Rh(2D)	-3.87
(100)	Rh	Cu	Cu2Rh2 (D)	Cu(2D)Rh1	-5.32
(100)	Rh	Cu	Cu3Rh1	Cu(2D)Rh1	-3.63
(100)	Rh	Cu	Cu3Rh1	Cu(2A)Rh1	-3.72
(100)	Rh	Cu	Cu3Rh1	Cu3Rh0	-5.21

Surface Orientation	Host Slab	Heteroatom	Top Layer Configuration	Reference Configuration	Adsorption Energy (eV)
(100)	Rh	Ir	Ir1Rh0	Clean Rh	-5.38
(100)	Rh	Ir	Ir(2D)Rh0	Ir1Rh0	-5.18
(100)	Rh	Ir	Ir(2A)Rh0	Ir1Rh0	-6.62
(100)	Rh	Ir	Ir(3)Rh0	Ir(2A)Rh0	-6.35
(100)	Rh	Ir	Ir(3)Rh0	Ir(2D)Rh0	-7.80
(100)	Rh	Ir	Ir(4)Rh0	Ir3Rh0	-7.25
(100)	Rh	Ir	Ir1Rh1 (D)	Ir0Rh1	-5.32
(100)	Rh	Ir	Ir1Rh1 (D)	Ir1Rh0	-4.39
(100)	Rh	Ir	Ir1Rh1 (A)	Ir0Rh1	-6.39
(100)	Rh	Ir	Ir1Rh1 (A)	Ir1Rh0	-5.46
(100)	Rh	Ir	Ir1Rh(2A)	Ir0Rh(2A)	-6.25
(100)	Rh	Ir	Ir1Rh(2A)	Ir1Rh1 (A)	-5.08
(100)	Rh	Ir	Ir1Rh(2A)	Ir1Rh1 (D)	-6.16
(100)	Rh	Ir	Ir1Rh(2D)	Ir0Rh(2D)	-7.33
(100)	Rh	Ir	Ir1Rh(2D)	Ir1Rh1 (A)	-5.40
(100)	Rh	Ir	Ir(2A)Rh1	Ir1Rh1 (A)	-6.48
(100)	Rh	Ir	Ir(2A)Rh1	Ir1Rh1 (D)	-7.55
(100)	Rh	Ir	Ir(2A)Rh1	Ir(2A)Rh0	-5.32
(100)	Rh	Ir	Ir(2D)Rh1	Ir1Rh1 (A)	-6.10
(100)	Rh	Ir	Ir(2D)Rh1	Ir(2D)Rh0	-6.39
(100)	Rh	Ir	Ir1Rh3	Ir0Rh3	-6.99
(100)	Rh	Ir	Ir1Rh3	Ir1Rh(2D)	-5.61
(100)	Rh	Ir	Ir1Rh3	Ir1Rh(2A)	-5.93
(100)	Rh	Ir	Ir2Rh2 (A)	Ir1Rh(2A)	-7.20
(100)	Rh	Ir	Ir2Rh2 (A)	Ir(2A)Rh1	-5.81
(100)	Rh	Ir	Ir2Rh2 (D)	Ir1Rh(2D)	-6.82
(100)	Rh	Ir	Ir2Rh2 (D)	Ir(2D)Rh1	-6.12
(100)	Rh	Ir	Ir3Rh1	Ir(2D)Rh1	-7.41
(100)	Rh	Ir	Ir3Rh1	Ir(2A)Rh1	-7.04
(100)	Rh	Ir	Ir3Rh1	Ir3Rh0	-6.00
(100)	Rh	Pd	Pd1Rh0	Clean Rh	-3.09
(100)	Rh	Pd	Pd(2D)Rh0	Pd1Rh0	-3.15
(100)	Rh	Pd	Pd(2A)Rh0	Pd1Rh0	-3.45
(100)	Rh	Pd	Pd(3)Rh0	Pd(2A)Rh0	-3.51
(100)	Rh	Pd	Pd(3)Rh0	Pd(2D)Rh0	-3.80
(100)	Rh	Pd	Pd(4)Rh0	Pd3Rh0	-3.75
(100)	Rh	Pd	Pd1Rh1 (D)	Pd0Rh1	-3.15
(100)	Rh	Pd	Pd1Rh1 (D)	Pd1Rh0	-4.50
(100)	Rh	Pd	Pd1Rh1 (A)	Pd0Rh1	-3.61
(100)	Rh	Pd	Pd1Rh1 (A)	Pd1Rh0	-4.96
(100)	Rh	Pd	Pd1Rh(2A)	Pd0Rh(2A)	-3.62
(100)	Rh	Pd	Pd1Rh(2A)	Pd1Rh1 (A)	-5.25
(100)	Rh	Pd	Pd1Rh(2A)	Pd1Rh1 (D)	-5.71
(100)	Rh	Pd	Pd1Rh(2D)	Pd0Rh(2D)	-4.11
(100)	Rh	Pd	Pd1Rh(2D)	Pd1Rh1 (A)	-4.98

Surface Orientation	Host Slab	Heteroatom	Top Layer Configuration	Reference Configuration	Adsorption Energy (eV)
(100)	Rh	Pd	Pd(2A)Rh1	Pd1Rh1 (A)	-3.51
(100)	Rh	Pd	Pd(2A)Rh1	Pd1Rh1 (D)	-3.97
(100)	Rh	Pd	Pd(2A)Rh1	Pd(2A)Rh0	-5.02
(100)	Rh	Pd	Pd(2D)Rh1	Pd1Rh1 (A)	-3.64
(100)	Rh	Pd	Pd(2D)Rh1	Pd(2D)Rh0	-5.46
(100)	Rh	Pd	Pd1Rh3	Pd0Rh3	-3.98
(100)	Rh	Pd	Pd1Rh3	Pd1Rh(2D)	-5.81
(100)	Rh	Pd	Pd1Rh3	Pd1Rh(2A)	-5.54
(100)	Rh	Pd	Pd2Rh2 (A)	Pd1Rh(2A)	-3.87
(100)	Rh	Pd	Pd2Rh2 (A)	Pd(2A)Rh1	-5.61
(100)	Rh	Pd	Pd2Rh2 (D)	Pd1Rh(2D)	-4.01
(100)	Rh	Pd	Pd2Rh2 (D)	Pd(2D)Rh1	-5.34
(100)	Rh	Pd	Pd3Rh1	Pd(2D)Rh1	-3.75
(100)	Rh	Pd	Pd3Rh1	Pd(2A)Rh1	-3.89
(100)	Rh	Pd	Pd3Rh1	Pd3Rh0	-5.40
(100)	Rh	Pt	Pt1Rh0	Clean Rh	-4.57
(100)	Rh	Pt	Pt(2D)Rh0	Pt1Rh0	-4.48
(100)	Rh	Pt	Pt(2A)Rh0	Pt1Rh0	-5.27
(100)	Rh	Pt	Pt(3)Rh0	Pt(2A)Rh0	-5.12
(100)	Rh	Pt	Pt(3)Rh0	Pt(2D)Rh0	-5.91
(100)	Rh	Pt	Pt(4)Rh0	Pt3Rh0	-5.53
(100)	Rh	Pt	Pt1Rh1 (D)	Pt0Rh1	-4.56
(100)	Rh	Pt	Pt1Rh1 (D)	Pt1Rh0	-4.44
(100)	Rh	Pt	Pt1Rh1 (A)	Pt0Rh1	-5.33
(100)	Rh	Pt	Pt1Rh1 (A)	Pt1Rh0	-5.20
(100)	Rh	Pt	Pt1Rh(2A)	Pt0Rh(2A)	-5.24
(100)	Rh	Pt	Pt1Rh(2A)	Pt1Rh1 (A)	-5.14
(100)	Rh	Pt	Pt1Rh(2A)	Pt1Rh1 (D)	-5.91
(100)	Rh	Pt	Pt1Rh(2D)	Pt0Rh(2D)	-6.05
(100)	Rh	Pt	Pt1Rh(2D)	Pt1Rh1 (A)	-5.19
(100)	Rh	Pt	Pt(2A)Rh1	Pt1Rh1 (A)	-5.21
(100)	Rh	Pt	Pt(2A)Rh1	Pt1Rh1 (D)	-5.97
(100)	Rh	Pt	Pt(2A)Rh1	Pt(2A)Rh0	-5.14
(100)	Rh	Pt	Pt(2D)Rh1	Pt1Rh1 (A)	-5.15
(100)	Rh	Pt	Pt(2D)Rh1	Pt(2D)Rh0	-5.88
(100)	Rh	Pt	Pt1Rh3	Pt0Rh3	-5.75
(100)	Rh	Pt	Pt1Rh3	Pt1Rh(2D)	-5.65
(100)	Rh	Pt	Pt1Rh3	Pt1Rh(2A)	-5.70
(100)	Rh	Pt	Pt2Rh2 (A)	Pt1Rh(2A)	-5.68
(100)	Rh	Pt	Pt2Rh2 (A)	Pt(2A)Rh1	-5.61
(100)	Rh	Pt	Pt2Rh2 (D)	Pt1Rh(2D)	-5.64
(100)	Rh	Pt	Pt2Rh2 (D)	Pt(2D)Rh1	-5.68
(100)	Rh	Pt	Pt3Rh1	Pt(2D)Rh1	-5.63
(100)	Rh	Pt	Pt3Rh1	Pt(2A)Rh1	-5.57
(100)	Rh	Pt	Pt3Rh1	Pt3Rh0	-5.60

Table S7: DFT-calculated adsorption energies for bimetallic systems, 1x3 fcc (211) surfaces. Empty rows correspond to cases of reconstruction.

Surface Orientation	Host Slab	Heteroatom	Top Layer Configuration	Reference Configuration	Adsorption Energy (eV)
(211)	Ag	Au	Au1Ag0	Clean Ag	-2.49
(211)	Ag	Au	Au2Ag0	Au1Ag0	-2.57
(211)	Ag	Au	Au3Ag0	Au2Ag0	-2.79
(211)	Ag	Au	Au1Ag1	Au0Ag1	-2.63
(211)	Ag	Au	Au1Ag1	Au1Ag0	-1.99
(211)	Ag	Au	Au1Ag2	Au0Ag2	-2.83
(211)	Ag	Au	Au1Ag2	Au1Ag1	-2.19
(211)	Ag	Au	Au2Ag1	Au1Ag1	-2.81
(211)	Ag	Au	Au2Ag1	Au2Ag0	-2.22
(211)	Ag	Cu	Cu1Ag0	Clean Ag	-2.38
(211)	Ag	Cu	Cu2Ag0	Cu1Ag0	-2.62
(211)	Ag	Cu	Cu3Ag0	Cu2Ag0	-2.63
(211)	Ag	Cu	Cu1Ag1	Cu0Ag1	-2.56
(211)	Ag	Cu	Cu1Ag1	Cu1Ag0	-2.03
(211)	Ag	Cu	Cu1Ag2	Cu0Ag2	-2.72
(211)	Ag	Cu	Cu1Ag2	Cu1Ag1	-2.15
(211)	Ag	Cu	Cu2Ag1	Cu1Ag1	-2.69
(211)	Ag	Cu	Cu2Ag1	Cu2Ag0	-2.10
(211)	Ag	Ir	Ir1Ag0	Clean Ag	-3.75
(211)	Ag	Ir	Ir2Ag0	Ir1Ag0	
(211)	Ag	Ir	Ir3Ag0	Ir2Ag0	
(211)	Ag	Ir	Ir1Ag1	Ir0Ag1	-4.10
(211)	Ag	Ir	Ir1Ag1	Ir1Ag0	-2.20
(211)	Ag	Ir	Ir1Ag2	Ir0Ag2	-4.54
(211)	Ag	Ir	Ir1Ag2	Ir1Ag1	-2.43
(211)	Ag	Ir	Ir2Ag1	Ir1Ag1	
(211)	Ag	Ir	Ir2Ag1	Ir2Ag0	
(211)	Ag	Pd	Pd1Ag0	Clean Ag	-2.68
(211)	Ag	Pd	Pd2Ag0	Pd1Ag0	-2.89
(211)	Ag	Pd	Pd3Ag0	Pd2Ag0	-3.15
(211)	Ag	Pd	Pd1Ag1	Pd0Ag1	-2.90
(211)	Ag	Pd	Pd1Ag1	Pd1Ag0	-2.07
(211)	Ag	Pd	Pd1Ag2	Pd0Ag2	-3.17
(211)	Ag	Pd	Pd1Ag2	Pd1Ag1	-2.25
(211)	Ag	Pd	Pd2Ag1	Pd1Ag1	-3.17
(211)	Ag	Pd	Pd2Ag1	Pd2Ag0	-2.35
(211)	Ag	Pt	Pt1Ag0	Clean Ag	-3.89
(211)	Ag	Pt	Pt2Ag0	Pt1Ag0	-4.21
(211)	Ag	Pt	Pt3Ag0	Pt2Ag0	
(211)	Ag	Pt	Pt1Ag1	Pt0Ag1	-4.16
(211)	Ag	Pt	Pt1Ag1	Pt1Ag0	-2.12
(211)	Ag	Pt	Pt1Ag2	Pt0Ag2	-4.50
(211)	Ag	Pt	Pt1Ag2	Pt1Ag1	-2.32
(211)	Ag	Pt	Pt2Ag1	Pt1Ag1	-4.56
(211)	Ag	Pt	Pt2Ag1	Pt2Ag0	-2.47
(211)	Ag	Rh	Rh1Ag0	Clean Ag	-3.27
(211)	Ag	Rh	Rh2Ag0	Rh1Ag0	
(211)	Ag	Rh	Rh3Ag0	Rh2Ag0	

Surface Orientation	Host Slab	Heteroatom	Top Layer Configuration	Reference Configuration	Adsorption Energy (eV)
(211)	Ag	Rh	Rh1Ag1	Rh0Ag1	-3.58
(211)	Ag	Rh	Rh1Ag1	Rh1Ag0	-2.15
(211)	Ag	Rh	Rh1Ag2	Rh0Ag2	-3.94
(211)	Ag	Rh	Rh1Ag2	Rh1Ag1	-2.34
(211)	Ag	Rh	Rh2Ag1	Rh1Ag1	-4.15
(211)	Ag	Rh	Rh2Ag1	Rh2Ag0	
(211)	Au	Ag	Ag1Au0	Clean Au	-2.01
(211)	Au	Ag	Ag2Au0	Ag1Au0	-2.07
(211)	Au	Ag	Ag3Au0	Ag2Au0	-2.17
(211)	Au	Ag	Ag1Au1	Ag0Au1	-2.14
(211)	Au	Ag	Ag1Au1	Ag1Au0	-2.46
(211)	Au	Ag	Ag1Au2	Ag0Au2	-2.29
(211)	Au	Ag	Ag1Au2	Ag1Au1	-2.60
(211)	Au	Ag	Ag2Au1	Ag1Au1	-2.22
(211)	Au	Ag	Ag2Au1	Ag2Au0	-2.60
(211)	Au	Cu	Cu1Au0	Clean Au	-2.73
(211)	Au	Cu	Cu2Au0	Cu1Au0	
(211)	Au	Cu	Cu3Au0	Cu2Au0	
(211)	Au	Cu	Cu1Au1	Cu0Au1	
(211)	Au	Cu	Cu1Au1	Cu1Au0	
(211)	Au	Cu	Cu1Au2	Cu0Au2	-2.99
(211)	Au	Cu	Cu1Au2	Cu1Au1	
(211)	Au	Cu	Cu2Au1	Cu1Au1	
(211)	Au	Cu	Cu2Au1	Cu2Au0	
(211)	Au	Ir	Ir1Au0	Clean Au	
(211)	Au	Ir	Ir2Au0	Ir1Au0	
(211)	Au	Ir	Ir3Au0	Ir2Au0	
(211)	Au	Ir	Ir1Au1	Ir0Au1	
(211)	Au	Ir	Ir1Au1	Ir1Au0	
(211)	Au	Ir	Ir1Au2	Ir0Au2	-4.73
(211)	Au	Ir	Ir1Au2	Ir1Au1	
(211)	Au	Ir	Ir2Au1	Ir1Au1	
(211)	Au	Ir	Ir2Au1	Ir2Au0	
(211)	Au	Pd	Pd1Au0	Clean Au	-2.75
(211)	Au	Pd	Pd2Au0	Pd1Au0	-2.92
(211)	Au	Pd	Pd3Au0	Pd2Au0	-3.12
(211)	Au	Pd	Pd1Au1	Pd0Au1	-2.94
(211)	Au	Pd	Pd1Au1	Pd1Au0	-2.52
(211)	Au	Pd	Pd1Au2	Pd0Au2	-3.17
(211)	Au	Pd	Pd1Au2	Pd1Au1	-2.68
(211)	Au	Pd	Pd2Au1	Pd1Au1	-3.15
(211)	Au	Pd	Pd2Au1	Pd2Au0	-2.74
(211)	Au	Pt	Pt1Au0	Clean Au	-3.85
(211)	Au	Pt	Pt2Au0	Pt1Au0	-4.18
(211)	Au	Pt	Pt3Au0	Pt2Au0	-4.41
(211)	Au	Pt	Pt1Au1	Pt0Au1	-4.08
(211)	Au	Pt	Pt1Au1	Pt1Au0	-2.56
(211)	Au	Pt	Pt1Au2	Pt0Au2	-4.35

Surface Orientation	Host Slab	Heteroatom	Top Layer Configuration	Reference Configuration	Adsorption Energy (eV)
(211)	Au	Pt	Pt1Au2	Pt1Au1	-2.73
(211)	Au	Pt	Pt2Au1	Pt1Au1	-4.42
(211)	Au	Pt	Pt2Au1	Pt2Au0	-2.80
(211)	Au	Rh	Rh1Au0	Clean Au	-3.57
(211)	Au	Rh	Rh2Au0	Rh1Au0	
(211)	Au	Rh	Rh3Au0	Rh2Au0	
(211)	Au	Rh	Rh1Au1	Rh0Au1	-3.83
(211)	Au	Rh	Rh1Au1	Rh1Au0	-2.59
(211)	Au	Rh	Rh1Au2	Rh0Au2	-4.13
(211)	Au	Rh	Rh1Au2	Rh1Au1	-2.75
(211)	Au	Rh	Rh2Au1	Rh1Au1	-4.26
(211)	Au	Rh	Rh2Au1	Rh2Au0	
(211)	Cu	Ag	Ag1Cu0	Clean Cu	-2.12
(211)	Cu	Ag	Ag2Cu0	Ag1Cu0	-2.20
(211)	Cu	Ag	Ag3Cu0	Ag2Cu0	-1.98
(211)	Cu	Ag	Ag1Cu1	Ag0Cu1	-2.26
(211)	Cu	Ag	Ag1Cu1	Ag1Cu0	-2.93
(211)	Cu	Ag	Ag1Cu2	Ag0Cu2	-2.46
(211)	Cu	Ag	Ag1Cu2	Ag1Cu1	-3.20
(211)	Cu	Ag	Ag2Cu1	Ag1Cu1	-2.31
(211)	Cu	Ag	Ag2Cu1	Ag2Cu0	-3.04
(211)	Cu	Au	Au1Cu0	Clean Cu	-2.86
(211)	Cu	Au	Au2Cu0	Au1Cu0	-2.86
(211)	Cu	Au	Au3Cu0	Au2Cu0	-2.93
(211)	Cu	Au	Au1Cu1	Au0Cu1	-3.02
(211)	Cu	Au	Au1Cu1	Au1Cu0	-2.95
(211)	Cu	Au	Au1Cu2	Au0Cu2	-3.30
(211)	Cu	Au	Au1Cu2	Au1Cu1	-3.29
(211)	Cu	Au	Au2Cu1	Au1Cu1	-3.19
(211)	Cu	Au	Au2Cu1	Au2Cu0	-3.28
(211)	Cu	Ir	Ir1Cu0	Clean Cu	-4.88
(211)	Cu	Ir	Ir2Cu0	Ir1Cu0	-5.78
(211)	Cu	Ir	Ir3Cu0	Ir2Cu0	-6.90
(211)	Cu	Ir	Ir1Cu1	Ir0Cu1	-5.31
(211)	Cu	Ir	Ir1Cu1	Ir1Cu0	-3.21
(211)	Cu	Ir	Ir1Cu2	Ir0Cu2	-5.88
(211)	Cu	Ir	Ir1Cu2	Ir1Cu1	-3.58
(211)	Cu	Ir	Ir2Cu1	Ir1Cu1	-6.27
(211)	Cu	Ir	Ir2Cu1	Ir2Cu0	-3.70
(211)	Cu	Pd	Pd1Cu0	Clean Cu	-3.21
(211)	Cu	Pd	Pd2Cu0	Pd1Cu0	-3.36
(211)	Cu	Pd	Pd3Cu0	Pd2Cu0	-3.49
(211)	Cu	Pd	Pd1Cu1	Pd0Cu1	-3.46
(211)	Cu	Pd	Pd1Cu1	Pd1Cu0	-3.04
(211)	Cu	Pd	Pd1Cu2	Pd0Cu2	-3.79
(211)	Cu	Pd	Pd1Cu2	Pd1Cu1	-3.34
(211)	Cu	Pd	Pd2Cu1	Pd1Cu1	-3.71
(211)	Cu	Pd	Pd2Cu1	Pd2Cu0	-3.39

Surface Orientation	Host Slab	Heteroatom	Top Layer Configuration	Reference Configuration	Adsorption Energy (eV)
(211)	Cu	Pt	Pt1Cu0	Clean Cu	-4.64
(211)	Cu	Pt	Pt2Cu0	Pt1Cu0	-4.80
(211)	Cu	Pt	Pt3Cu0	Pt2Cu0	-5.50
(211)	Cu	Pt	Pt1Cu1	Pt0Cu1	-4.95
(211)	Cu	Pt	Pt1Cu1	Pt1Cu0	-3.10
(211)	Cu	Pt	Pt1Cu2	Pt0Cu2	-5.40
(211)	Cu	Pt	Pt1Cu2	Pt1Cu1	-3.46
(211)	Cu	Pt	Pt2Cu1	Pt1Cu1	-5.44
(211)	Cu	Pt	Pt2Cu1	Pt2Cu0	-3.74
(211)	Cu	Rh	Rh1Cu0	Clean Cu	-4.15
(211)	Cu	Rh	Rh2Cu0	Rh1Cu0	-4.68
(211)	Cu	Rh	Rh3Cu0	Rh2Cu0	-5.22
(211)	Cu	Rh	Rh1Cu1	Rh0Cu1	-4.50
(211)	Cu	Rh	Rh1Cu1	Rh1Cu0	-3.14
(211)	Cu	Rh	Rh1Cu2	Rh0Cu2	-4.95
(211)	Cu	Rh	Rh1Cu2	Rh1Cu1	-3.45
(211)	Cu	Rh	Rh2Cu1	Rh1Cu1	-5.03
(211)	Cu	Rh	Rh2Cu1	Rh2Cu0	-3.49
(211)	Ir	Ag	Ag1Ir0	Clean Ir	-2.56
(211)	Ir	Ag	Ag2Ir0	Ag1Ir0	-2.56
(211)	Ir	Ag	Ag3Ir0	Ag2Ir0	-2.50
(211)	Ir	Ag	Ag1Ir1	Ag0Ir1	-2.55
(211)	Ir	Ag	Ag1Ir1	Ag1Ir0	-6.20
(211)	Ir	Ag	Ag1Ir2	Ag0Ir2	-2.88
(211)	Ir	Ag	Ag1Ir2	Ag1Ir1	-6.77
(211)	Ir	Ag	Ag2Ir1	Ag1Ir1	-2.62
(211)	Ir	Ag	Ag2Ir1	Ag2Ir0	-6.26
(211)	Ir	Au	Au1Ir0	Clean Ir	-3.01
(211)	Ir	Au	Au2Ir0	Au1Ir0	-3.01
(211)	Ir	Au	Au3Ir0	Au2Ir0	-3.16
(211)	Ir	Au	Au1Ir1	Au0Ir1	-3.02
(211)	Ir	Au	Au1Ir1	Au1Ir0	-6.22
(211)	Ir	Au	Au1Ir2	Au0Ir2	-3.51
(211)	Ir	Au	Au1Ir2	Au1Ir1	-6.93
(211)	Ir	Au	Au2Ir1	Au1Ir1	-3.32
(211)	Ir	Au	Au2Ir1	Au2Ir0	-6.52
(211)	Ir	Cu	Cu1Ir0	Clean Ir	-3.50
(211)	Ir	Cu	Cu2Ir0	Cu1Ir0	-3.58
(211)	Ir	Cu	Cu3Ir0	Cu2Ir0	-3.70
(211)	Ir	Cu	Cu1Ir1	Cu0Ir1	-3.57
(211)	Ir	Cu	Cu1Ir1	Cu1Ir0	-6.28
(211)	Ir	Cu	Cu1Ir2	Cu0Ir2	-3.96
(211)	Ir	Cu	Cu1Ir2	Cu1Ir1	-6.82
(211)	Ir	Cu	Cu2Ir1	Cu1Ir1	-3.78
(211)	Ir	Cu	Cu2Ir1	Cu2Ir0	-6.47
(211)	Ir	Pd	Pd1Ir0	Clean Ir	-3.66
(211)	Ir	Pd	Pd2Ir0	Pd1Ir0	-3.69
(211)	Ir	Pd	Pd3Ir0	Pd2Ir0	-3.85

Surface Orientation	Host Slab	Heteroatom	Top Layer Configuration	Reference Configuration	Adsorption Energy (eV)
(211)	Ir	Pd	Pd1Ir1	Pd0Ir1	-3.73
(211)	Ir	Pd	Pd1Ir1	Pd1Ir0	-6.28
(211)	Ir	Pd	Pd1Ir2	Pd0Ir2	-4.22
(211)	Ir	Pd	Pd1Ir2	Pd1Ir1	-6.93
(211)	Ir	Pd	Pd2Ir1	Pd1Ir1	-4.03
(211)	Ir	Pd	Pd2Ir1	Pd2Ir0	-6.62
(211)	Ir	Pt	Pt1Ir0	Clean Ir	-5.11
(211)	Ir	Pt	Pt2Ir0	Pt1Ir0	-5.18
(211)	Ir	Pt	Pt3Ir0	Pt2Ir0	-5.71
(211)	Ir	Pt	Pt1Ir1	Pt0Ir1	-5.23
(211)	Ir	Pt	Pt1Ir1	Pt1Ir0	-6.33
(211)	Ir	Pt	Pt1Ir2	Pt0Ir2	-5.89
(211)	Ir	Pt	Pt1Ir2	Pt1Ir1	-7.10
(211)	Ir	Pt	Pt2Ir1	Pt1Ir1	-5.82
(211)	Ir	Pt	Pt2Ir1	Pt2Ir0	-6.96
(211)	Ir	Rh	Rh1Ir0	Clean Ir	-5.27
(211)	Ir	Rh	Rh2Ir0	Rh1Ir0	-5.36
(211)	Ir	Rh	Rh3Ir0	Rh2Ir0	-5.77
(211)	Ir	Rh	Rh1Ir1	Rh0Ir1	-5.43
(211)	Ir	Rh	Rh1Ir1	Rh1Ir0	-6.37
(211)	Ir	Rh	Rh1Ir2	Rh0Ir2	-6.04
(211)	Ir	Rh	Rh1Ir2	Rh1Ir1	-7.04
(211)	Ir	Rh	Rh2Ir1	Rh1Ir1	-5.90
(211)	Ir	Rh	Rh2Ir1	Rh2Ir0	-6.91
(211)	Pd	Ag	Ag1Pd0	Clean Pd	-2.33
(211)	Pd	Ag	Ag2Pd0	Ag1Pd0	-2.43
(211)	Pd	Ag	Ag3Pd0	Ag2Pd0	-2.55
(211)	Pd	Ag	Ag1Pd1	Ag0Pd1	-2.49
(211)	Pd	Ag	Ag1Pd1	Ag1Pd0	-3.01
(211)	Pd	Ag	Ag1Pd2	Ag0Pd2	-2.72
(211)	Pd	Ag	Ag1Pd2	Ag1Pd1	-3.32
(211)	Pd	Ag	Ag2Pd1	Ag1Pd1	-2.64
(211)	Pd	Ag	Ag2Pd1	Ag2Pd0	-3.22
(211)	Pd	Au	Au1Pd0	Clean Pd	-2.74
(211)	Pd	Au	Au2Pd0	Au1Pd0	-2.84
(211)	Pd	Au	Au3Pd0	Au2Pd0	-3.20
(211)	Pd	Au	Au1Pd1	Au0Pd1	-2.92
(211)	Pd	Au	Au1Pd1	Au1Pd0	-3.04
(211)	Pd	Au	Au1Pd2	Au0Pd2	-3.25
(211)	Pd	Au	Au1Pd2	Au1Pd1	-3.41
(211)	Pd	Au	Au2Pd1	Au1Pd1	-3.22
(211)	Pd	Au	Au2Pd1	Au2Pd0	-3.42
(211)	Pd	Cu	Cu1Pd0	Clean Pd	-3.04
(211)	Pd	Cu	Cu2Pd0	Cu1Pd0	-3.24
(211)	Pd	Cu	Cu3Pd0	Cu2Pd0	-3.38
(211)	Pd	Cu	Cu1Pd1	Cu0Pd1	-3.28
(211)	Pd	Cu	Cu1Pd1	Cu1Pd0	-3.09
(211)	Pd	Cu	Cu1Pd2	Cu0Pd2	-3.53

Surface Orientation	Host Slab	Heteroatom	Top Layer Configuration	Reference Configuration	Adsorption Energy (eV)
(211)	Pd	Cu	Cu1Pd2	Cu1Pd1	-3.34
(211)	Pd	Cu	Cu2Pd1	Cu1Pd1	-3.44
(211)	Pd	Cu	Cu2Pd1	Cu2Pd0	-3.30
(211)	Pd	Ir	Ir1Pd0	Clean Pd	-4.83
(211)	Pd	Ir	Ir2Pd0	Ir1Pd0	-5.85
(211)	Pd	Ir	Ir3Pd0	Ir2Pd0	
(211)	Pd	Ir	Ir1Pd1	Ir0Pd1	-5.30
(211)	Pd	Ir	Ir1Pd1	Ir1Pd0	-3.32
(211)	Pd	Ir	Ir1Pd2	Ir0Pd2	-5.81
(211)	Pd	Ir	Ir1Pd2	Ir1Pd1	-3.60
(211)	Pd	Ir	Ir2Pd1	Ir1Pd1	
(211)	Pd	Ir	Ir2Pd1	Ir2Pd0	
(211)	Pd	Pt	Pt1Pd0	Clean Pd	-4.16
(211)	Pd	Pt	Pt2Pd0	Pt1Pd0	-4.57
(211)	Pd	Pt	Pt3Pd0	Pt2Pd0	-5.14
(211)	Pd	Pt	Pt1Pd1	Pt0Pd1	-4.48
(211)	Pd	Pt	Pt1Pd1	Pt1Pd0	-3.17
(211)	Pd	Pt	Pt1Pd2	Pt0Pd2	-4.92
(211)	Pd	Pt	Pt1Pd2	Pt1Pd1	-3.53
(211)	Pd	Pt	Pt2Pd1	Pt1Pd1	-5.03
(211)	Pd	Pt	Pt2Pd1	Pt2Pd0	-3.64
(211)	Pd	Rh	Rh1Pd0	Clean Pd	-4.00
(211)	Pd	Rh	Rh2Pd0	Rh1Pd0	-4.59
(211)	Pd	Rh	Rh3Pd0	Rh2Pd0	-4.83
(211)	Pd	Rh	Rh1Pd1	Rh0Pd1	-4.35
(211)	Pd	Rh	Rh1Pd1	Rh1Pd0	-3.20
(211)	Pd	Rh	Rh1Pd2	Rh0Pd2	-4.74
(211)	Pd	Rh	Rh1Pd2	Rh1Pd1	-3.49
(211)	Pd	Rh	Rh2Pd1	Rh1Pd1	-4.88
(211)	Pd	Rh	Rh2Pd1	Rh2Pd0	-3.48
(211)	Pt	Ag	Ag1Pt0	Clean Pt	-2.46
(211)	Pt	Ag	Ag2Pt0	Ag1Pt0	-2.47
(211)	Pt	Ag	Ag3Pt0	Ag2Pt0	-2.47
(211)	Pt	Ag	Ag1Pt1	Ag0Pt1	-2.56
(211)	Pt	Ag	Ag1Pt1	Ag1Pt0	-4.53
(211)	Pt	Ag	Ag1Pt2	Ag0Pt2	-2.81
(211)	Pt	Ag	Ag1Pt2	Ag1Pt1	-4.95
(211)	Pt	Ag	Ag2Pt1	Ag1Pt1	-2.63
(211)	Pt	Ag	Ag2Pt1	Ag2Pt0	-4.69
(211)	Pt	Au	Au1Pt0	Clean Pt	-2.72
(211)	Pt	Au	Au2Pt0	Au1Pt0	-2.79
(211)	Pt	Au	Au3Pt0	Au2Pt0	-3.00
(211)	Pt	Au	Au1Pt1	Au0Pt1	-2.85
(211)	Pt	Au	Au1Pt1	Au1Pt0	-4.56
(211)	Pt	Au	Au1Pt2	Au0Pt2	-3.20
(211)	Pt	Au	Au1Pt2	Au1Pt1	-5.05
(211)	Pt	Au	Au2Pt1	Au1Pt1	-3.10
(211)	Pt	Au	Au2Pt1	Au2Pt0	-4.87

Surface Orientation	Host Slab	Heteroatom	Top Layer Configuration	Reference Configuration	Adsorption Energy (eV)
(211)	Pt	Cu	Cu1Pt0	Clean Pt	-3.30
(211)	Pt	Cu	Cu2Pt0	Cu1Pt0	-3.40
(211)	Pt	Cu	Cu3Pt0	Cu2Pt0	-3.47
(211)	Pt	Cu	Cu1Pt1	Cu0Pt1	-3.49
(211)	Pt	Cu	Cu1Pt1	Cu1Pt0	-4.62
(211)	Pt	Cu	Cu1Pt2	Cu0Pt2	-3.72
(211)	Pt	Cu	Cu1Pt2	Cu1Pt1	-4.93
(211)	Pt	Cu	Cu2Pt1	Cu1Pt1	-3.57
(211)	Pt	Cu	Cu2Pt1	Cu2Pt0	-4.79
(211)	Pt	Ir	Ir1Pt0	Clean Pt	-5.31
(211)	Pt	Ir	Ir2Pt0	Ir1Pt0	-6.02
(211)	Pt	Ir	Ir3Pt0	Ir2Pt0	-6.38
(211)	Pt	Ir	Ir1Pt1	Ir0Pt1	-5.73
(211)	Pt	Ir	Ir1Pt1	Ir1Pt0	-4.86
(211)	Pt	Ir	Ir1Pt2	Ir0Pt2	-6.31
(211)	Pt	Ir	Ir1Pt2	Ir1Pt1	-5.28
(211)	Pt	Ir	Ir2Pt1	Ir1Pt1	-6.42
(211)	Pt	Ir	Ir2Pt1	Ir2Pt0	-5.25
(211)	Pt	Pd	Pd1Pt0	Clean Pt	-3.15
(211)	Pt	Pd	Pd2Pt0	Pd1Pt0	-3.27
(211)	Pt	Pd	Pd3Pt0	Pd2Pt0	-3.51
(211)	Pt	Pd	Pd1Pt1	Pd0Pt1	-3.34
(211)	Pt	Pd	Pd1Pt1	Pd1Pt0	-4.62
(211)	Pt	Pd	Pd1Pt2	Pd0Pt2	-3.73
(211)	Pt	Pd	Pd1Pt2	Pd1Pt1	-5.09
(211)	Pt	Pd	Pd2Pt1	Pd1Pt1	-3.62
(211)	Pt	Pd	Pd2Pt1	Pd2Pt0	-4.97
(211)	Pt	Rh	Rh1Pt0	Clean Pt	-4.49
(211)	Pt	Rh	Rh2Pt0	Rh1Pt0	-4.84
(211)	Pt	Rh	Rh3Pt0	Rh2Pt0	-5.21
(211)	Pt	Rh	Rh1Pt1	Rh0Pt1	-4.80
(211)	Pt	Rh	Rh1Pt1	Rh1Pt0	-4.74
(211)	Pt	Rh	Rh1Pt2	Rh0Pt2	-5.29
(211)	Pt	Rh	Rh1Pt2	Rh1Pt1	-5.19
(211)	Pt	Rh	Rh2Pt1	Rh1Pt1	-5.26
(211)	Pt	Rh	Rh2Pt1	Rh2Pt0	-5.16
(211)	Rh	Ag	Ag1Rh0	Clean Rh	-2.41
(211)	Rh	Ag	Ag2Rh0	Ag1Rh0	-2.47
(211)	Rh	Ag	Ag3Rh0	Ag2Rh0	-2.48
(211)	Rh	Ag	Ag1Rh1	Ag0Rh1	-2.48
(211)	Rh	Ag	Ag1Rh1	Ag1Rh0	-4.89
(211)	Rh	Ag	Ag1Rh2	Ag0Rh2	-2.73
(211)	Rh	Ag	Ag1Rh2	Ag1Rh1	-5.31
(211)	Rh	Ag	Ag2Rh1	Ag1Rh1	-2.58
(211)	Rh	Ag	Ag2Rh1	Ag2Rh0	-5.01
(211)	Rh	Au	Au1Rh0	Clean Rh	-2.96
(211)	Rh	Au	Au2Rh0	Au1Rh0	-2.99
(211)	Rh	Au	Au3Rh0	Au2Rh0	-3.26

Surface Orientation	Host Slab	Heteroatom	Top Layer Configuration	Reference Configuration	Adsorption Energy (eV)
(211)	Rh	Au	Au1Rh1	Au0Rh1	-3.05
(211)	Rh	Au	Au1Rh1	Au1Rh0	-4.92
(211)	Rh	Au	Au1Rh2	Au0Rh2	-3.46
(211)	Rh	Au	Au1Rh2	Au1Rh1	-5.46
(211)	Rh	Au	Au2Rh1	Au1Rh1	-3.36
(211)	Rh	Au	Au2Rh1	Au2Rh0	-5.28
(211)	Rh	Cu	Cu1Rh0	Clean Rh	-3.23
(211)	Rh	Cu	Cu2Rh0	Cu1Rh0	-3.38
(211)	Rh	Cu	Cu3Rh0	Cu2Rh0	-3.57
(211)	Rh	Cu	Cu1Rh1	Cu0Rh1	-3.39
(211)	Rh	Cu	Cu1Rh1	Cu1Rh0	-4.98
(211)	Rh	Cu	Cu1Rh2	Cu0Rh2	-3.72
(211)	Rh	Cu	Cu1Rh2	Cu1Rh1	-5.38
(211)	Rh	Cu	Cu2Rh1	Cu1Rh1	-3.63
(211)	Rh	Cu	Cu2Rh1	Cu2Rh0	-5.23
(211)	Rh	Ir	Ir1Rh0	Clean Rh	-5.81
(211)	Rh	Ir	Ir2Rh0	Ir1Rh0	-6.22
(211)	Rh	Ir	Ir3Rh0	Ir2Rh0	-7.00
(211)	Rh	Ir	Ir1Rh1	Ir0Rh1	-6.13
(211)	Rh	Ir	Ir1Rh1	Ir1Rh0	-5.15
(211)	Rh	Ir	Ir1Rh2	Ir0Rh2	-6.76
(211)	Rh	Ir	Ir1Rh2	Ir1Rh1	-5.68
(211)	Rh	Ir	Ir2Rh1	Ir1Rh1	-6.88
(211)	Rh	Ir	Ir2Rh1	Ir2Rh0	-5.80
(211)	Rh	Pd	Pd1Rh0	Clean Rh	-3.35
(211)	Rh	Pd	Pd2Rh0	Pd1Rh0	-3.46
(211)	Rh	Pd	Pd3Rh0	Pd2Rh0	-3.73
(211)	Rh	Pd	Pd1Rh1	Pd0Rh1	-3.49
(211)	Rh	Pd	Pd1Rh1	Pd1Rh0	-4.97
(211)	Rh	Pd	Pd1Rh2	Pd0Rh2	-3.89
(211)	Rh	Pd	Pd1Rh2	Pd1Rh1	-5.46
(211)	Rh	Pd	Pd2Rh1	Pd1Rh1	-3.82
(211)	Rh	Pd	Pd2Rh1	Pd2Rh0	-5.32
(211)	Rh	Pt	Pt1Rh0	Clean Rh	-4.84
(211)	Rh	Pt	Pt2Rh0	Pt1Rh0	-4.99
(211)	Rh	Pt	Pt3Rh0	Pt2Rh0	-5.70
(211)	Rh	Pt	Pt1Rh1	Pt0Rh1	-5.04
(211)	Rh	Pt	Pt1Rh1	Pt1Rh0	-5.02
(211)	Rh	Pt	Pt1Rh2	Pt0Rh2	-5.60
(211)	Rh	Pt	Pt1Rh2	Pt1Rh1	-5.62
(211)	Rh	Pt	Pt2Rh1	Pt1Rh1	-5.65
(211)	Rh	Pt	Pt2Rh1	Pt2Rh0	-5.68

Table S8: DFT-calculated adsorption energies for bimetallic systems, 3x3 bulk unit cell.

Host Metal	Heteroatom	Adsorption Energy (eV)
Ag	Au	-3.35
Ag	Cu	-3.36
Ag	Ir	-5.84
Ag	Pd	-3.99
Ag	Pt	-5.41
Ag	Rh	-5.08
Au	Ag	-2.54
Au	Cu	-3.41
Au	Ir	-5.64
Au	Pd	-3.74
Au	Pt	-4.96
Au	Rh	-5.00
Cu	Ag	-2.50
Cu	Au	-3.48
Cu	Ir	-7.36
Cu	Pd	-4.46
Cu	Pt	-6.31
Cu	Rh	-6.13
Ir	Ag	-2.20
Ir	Au	-2.93
Ir	Cu	-4.33
Ir	Pd	-4.57
Ir	Pt	-6.46
Ir	Rh	-7.16
Pd	Ag	-3.20
Pd	Au	-3.80
Pd	Cu	-4.46
Pd	Ir	-7.27
Pd	Pt	-6.03
Pd	Rh	-6.02
Pt	Ag	-2.45
Pt	Au	-2.82
Pt	Cu	-4.14
Pt	Ir	-7.02
Pt	Pd	-3.88
Pt	Rh	-5.87
Rh	Ag	-2.74
Rh	Au	-3.67
Rh	Cu	-4.58
Rh	Ir	-8.63
Rh	Pd	-4.75
Rh	Pt	-6.78

Table S9: Bond-associated energies corresponding to adsorption events, fcc(100) 2x2 unit cell. The first column denotes the configuration of adatoms in the top layer, and the second column denotes the configuration of top-layer atoms in a reference configuration (before a gas-phase metal atom is added). The remaining columns correspond to the *i*th bond added to atoms as a result of suface adsorption. Each number entry corresponds to the number of each type of bond added for a given adsorption; these are used in the least-squares fitting of the DFT-calculated adsorption energies to parameters in Table 1 of the main text. (A) and (D) configurations of atoms refer to arrangements in which two atoms are adjacent (A) or along the surface diagonal (D). See Figure S6 for illustrations of structures (A) and (D).

		α_i^B (Host Slab Metal)										α_i^A (Heteroatom Metal)									
Top Layer Config.	Reference Config.	1-3	4	5	6	7	8	9	10	11	12	1-3	4	5	6	7	8	9	10	11	12
B1	Clean B	1	1	0	0	0	0	4	0	0	0	0	0	0	0	0	0	0	0	0	0
B(2D)	B1	1	1	0	0	0	0	0	4	0	0	0	0	0	0	0	0	0	0	0	0
B(2A)	B1	1	1	2	2	0	0	0	4	0	0	0	0	0	0	0	0	0	0	0	0
B3	B(2A)	1	1	1	1	1	1	0	0	4	0	0	0	0	0	0	0	0	0	0	0
B3	B(2D)	1	1	3	3	1	1	0	0	4	0	0	0	0	0	0	0	0	0	0	0
B4	B3	1	1	1	1	3	3	0	0	0	4	0	0	0	0	0	0	0	0	0	0
A1B0	Clean B	0	0	0	0	0	0	4	0	0	0	1	1	0	0	0	0	0	0	0	0
A(2D)B0	A1B0	0	0	0	0	0	0	0	4	0	0	1	1	0	0	0	0	0	0	0	0
A(2A)B0	A1B0	0	0	0	0	0	0	0	4	0	0	1	1	2	2	0	0	0	0	0	0
A3B0	A(2A)B0	0	0	0	0	0	0	0	0	4	0	1	1	1	1	1	1	0	0	0	0
A3B0	A(2D)B0	0	0	0	0	0	0	0	0	4	0	1	1	3	3	1	1	0	0	0	0
A4B0	A3B0	0	0	0	0	0	0	0	0	0	4	1	1	1	1	3	3	0	0	0	0
A1B1 (D)	A0B1	0	0	0	0	0	0	0	4	0	0	1	1	0	0	0	0	0	0	0	0
A1B1 (D)	A1B0	1	1	0	0	0	0	0	4	0	0	0	0	0	0	0	0	0	0	0	0
A1B1 (A)	A0B1	0	0	1	1	0	0	0	4	0	0	1	1	1	1	0	0	0	0	0	0
A1B1 (A)	A1B0	1	1	1	1	0	0	0	4	0	0	0	0	1	1	0	0	0	0	0	0
A1B(2A)	A0B(2A)	0	0	0	0	1	1	0	0	4	0	1	1	1	1	0	0	0	0	0	0
A1B(2A)	A1B1 (A)	1	1	1	1	1	1	0	0	4	0	0	0	0	0	0	0	0	0	0	0
A1B(2A)	A1B1 (D)	1	1	2	2	1	1	0	0	4	0	0	0	1	1	0	0	0	0	0	0
A1B(2D)	A0B(2A)	0	0	2	2	0	0	0	0	4	0	1	1	1	1	1	1	0	0	0	0
A1B(2D)	A1B1 (A)	1	1	1	1	0	0	0	0	4	0	0	0	0	0	1	1	0	0	0	0
A(2A)B1	A1B1 (A)	0	0	0	0	0	0	0	0	4	0	1	1	1	1	1	1	0	0	0	0
A(2A)B1	A1B1 (D)	0	0	1	1	0	0	0	0	4	0	1	1	2	2	1	1	0	0	0	0
A(2A)B1	A(2A)B0	1	1	1	1	0	0	0	0	4	0	0	0	0	0	1	1	0	0	0	0
A(2D)B1	A1B1 (A)	0	0	0	0	1	1	0	0	4	0	1	1	1	1	0	0	0	0	0	0
A(2D)B1	A(2D)B0	1	1	1	1	1	1	0	0	4	0	0	0	2	2	0	0	0	0	0	0
A1B3	A0B3	0	0	0	0	2	2	0	0	0	4	1	1	1	1	1	1	0	0	0	0
A1B3	A1B(2D)	1	1	1	1	3	3	0	0	0	4	0	0	0	0	0	0	0	0	0	0
A1B3	A1B(2A)	1	1	1	1	2	2	0	0	0	4	0	0	0	0	1	1	0	0	0	0
A2B2 (A)	A1B(2A)	0	0	0	0	1	1	0	0	0	4	1	1	1	1	2	2	0	0	0	0
A2B2 (A)	A(2A)B1	1	1	1	1	2	2	0	0	0	4	0	0	0	0	1	1	0	0	0	0
A2B2 (D)	A1B(2D)	0	0	0	0	2	2	0	0	0	4	1	1	1	1	1	1	0	0	0	0
A2B2 (D)	A(2D)B1	1	1	1	1	1	1	0	0	0	4	0	0	0	0	2	2	0	0	0	0
A3B1	A(2D)B1	0	0	0	0	0	0	0	0	0	4	1	1	1	1	3	3	0	0	0	0
A3B1	A(2A)B1	0	0	0	0	1	1	0	0	0	4	1	1	1	1	2	2	0	0	0	0
A3B1	A3B0	1	1	1	1	1	1	0	0	0	4	0	0	0	0	2	2	0	0	0	0

Table S10: Bond-associated energies corresponding to adsorption events, fcc (111) 2x2 unit cell. A description of these entries is given in Table S9.

		α_i^B (Host Slab Metal)										α_i^A (Heteroatom Metal)									
Top Layer Config.	Reference Config.	1-3	4	5	6	7	8	9	10	11	12	1-3	4	5	6	7	8	9	10	11	12
B1	Clean B	1	0	0	0	0	0	0	3	0	0	0	0	0	0	0	0	0	0	0	0
B2	B1	1	2	2	0	0	0	0	1	2	0	0	0	0	0	0	0	0	0	0	0
B3	B2	1	1	1	3	3	0	0	0	2	1	0	0	0	0	0	0	0	0	0	0
B4	B3	1	1	1	1	1	4	4	0	0	3	0	0	0	0	0	0	0	0	0	0
A1B0	Clean B	0	0	0	0	0	0	0	3	0	0	1	0	0	0	0	0	0	0	0	0
A2B0	A1B0	0	0	0	0	0	0	0	1	2	0	1	2	2	0	0	0	0	0	0	0
A3B0	A2B0	0	0	0	0	0	0	0	0	2	1	1	1	1	3	3	0	0	0	0	0
A4B0	A3B0	0	0	0	0	0	0	0	0	0	3	1	1	1	1	1	4	4	0	0	0
A1B1	A0B1	0	1	1	0	0	0	0	1	2	0	1	1	1	0	0	0	0	0	0	0
A1B1	A1B0	1	1	1	0	0	0	0	1	2	0	0	1	1	0	0	0	0	0	0	0
A1B2	A0B2	0	0	0	2	2	0	0	0	2	1	1	1	1	1	1	0	0	0	0	0
A1B2	A1B1	1	1	1	2	2	0	0	0	2	1	0	0	0	1	1	0	0	0	0	0
A2B1	A1B1	0	0	0	1	1	0	0	0	2	1	1	1	1	2	2	0	0	0	0	0
A2B1	A2B0	1	1	1	1	1	0	0	0	2	1	0	0	0	2	2	0	0	0	0	0
A1B3	A0B3	0	0	0	0	0	3	3	0	0	3	1	1	1	1	1	1	1	0	0	0
A1B3	A1B2	1	1	1	1	1	3	3	0	0	3	0	0	0	0	0	1	1	0	0	0
A2B2	A1B2	0	0	0	0	0	2	2	0	0	3	1	1	1	1	1	2	2	0	0	0
A2B2	A2B1	1	1	1	1	1	2	2	0	0	3	0	0	0	0	0	2	2	0	0	0
A3B1	A2B1	0	0	0	0	0	1	1	0	0	3	1	1	1	1	1	3	3	0	0	0
A3B1	A3B0	1	1	1	1	1	1	1	0	0	3	0	0	0	0	0	3	3	0	0	0

Table S11: Bond-associated energies corresponding to adsorption events, fcc (211) 1x3 unit cell. A description of these entries is given in Table S9.

		α_i^B (Host Slab Metal)										α_i^A (Heteroatom Metal)									
Top Layer Config.	Reference Config.	1-3	4	5	6	7	8	9	10	11	12	1-3	4	5	6	7	8	9	10	11	12
B1	Clean B	1	1	1	0	0	2	0	1	2	0	0	0	0	0	0	0	0	0	0	0
B2	B1	1	1	1	2	0	1	1	1	1	1	0	0	0	0	0	0	0	0	0	0
B3	B2	1	1	1	1	3	0	2	1	0	2	0	0	0	0	0	0	0	0	0	0
A1B0	Clean B	0	0	0	0	0	2	0	1	2	0	1	1	1	0	0	0	0	0	0	1
A2B0	A1B0	0	0	0	0	0	1	1	1	1	1	1	1	1	2	0	0	0	0	0	1
A3B0	A2B0	0	0	0	0	0	0	2	1	0	2	1	1	1	1	3	0	0	0	0	1
A1B1	A0B1	0	0	0	1	0	1	1	1	1	1	1	1	1	1	0	0	0	0	0	1
A1B1	A1B0	1	1	1	1	0	1	1	1	1	1	0	0	0	1	0	0	0	0	0	0
A1B2	A0B2	0	0	0	0	2	0	2	1	0	2	1	1	1	1	1	0	0	0	0	1
A1B2	A1B1	1	1	1	1	2	0	2	1	0	2	0	0	0	0	1	0	0	0	0	0
A2B1	A1B1	0	0	0	0	1	0	2	1	0	2	1	1	1	1	2	0	0	0	0	1
A2B1	A2B0	1	1	1	1	1	0	2	1	0	2	0	0	0	0	2	0	0	0	0	0

Table S12: Bond-associated energies corresponding to adsorption events, 3x3 bulk unit cell. A description of these entries is given in Table S9.

		α_i^B (Host Slab Metal)										α_i^A (Heteroatom Metal)									
Adsorbed System	Reference System	1-3	4	5	6	7	8	9	10	11	12	1-3	4	5	6	7	8	9	10	11	12
A1B26	B26	0	0	0	0	0	0	0	0	0	12	1	1	1	1	1	1	1	1	1	1
B27	B26	1	1	1	1	1	1	1	1	1	13	0	0	0	0	0	0	0	0	0	0

Table S13: Description and energetics of all single-atom Pt-Pd swaps considered in the A_3B alloy structure.

Description	Model Energy (eV)	DFT Energy (eV)
Pt_3Pd, Pt-rich: Core Pd atom swapped with 3rd layer Pt atom	0.00	0.13
Pt_3Pd, Pt-rich: Swap of Pt into 1st subsurface layer from 2nd subsurface layer	0.12	0.15
Pt_3Pd, Pt-rich: Swap of Pd from 1st subsurface layer to surface corner site	-0.22	-0.17
Pt_3Pd, Pt-rich: Swap of Pd from 1st subsurface layer to surface 8-fold coordinated site	-0.09	-0.09
Pt_3Pd, Pd-rich: Core Pt atom swapped with 3rd layer Pd atom	0.00	-0.01
Pt_3Pd, Pd-rich: Swap of Pd from 2nd subsurface layer into 1st subsurface layer, (100) face	-0.03	0.02
Pt_3Pd, Pd-rich: Swap of Pd from 2nd subsurface layer into 1st subsurface layer, near edge	-0.04	0.03
Pt_3Pd, Pd-rich: Swap of Pt from 1st subsurface layer into surface 8-fold coordinated site	0.17	0.14
Pt_3Pd, Pd-rich: Swap of 8-fold coordinated surface atoms	0.01	-0.04
Pd_3Pt, Pd-rich: Core Pt atom swapped with 3rd layer Pd atom	0.00	-0.06
Pd_3Pt, Pd-rich: Swap of Pd into 1st subsurface layer from 2nd subsurface layer	0.00	-0.02
Pd_3Pt, Pd-rich: Swap of Pt from 1st subsurface layer to surface corner site	0.30	0.32
Pd_3Pt, Pd-rich: Swap of Pt from 1st subsurface layer to surface 8-fold coordinated site	0.12	0.16
Pd_3Pt, Pt-rich: Core Pd atom swapped with 3rd layer Pt atom	0.00	0.09
Pd_3Pt, Pt-rich: Swap of Pt from 2nd subsurface layer into 1st subsurface layer, (100) face	0.03	0.11
Pd_3Pt, Pt-rich: Swap of Pt from 2nd subsurface layer into 1st subsurface layer, near edge	0.02	0.11
Pd_3Pt, Pt-rich: Swap of Pd from 1st subsurface layer into surface 8-fold coordinated site	-0.10	-0.17
Pd_3Pt, Pt-rich: Swap of 8-fold coordinated surface atoms	0.00	-0.08

Table S14: Relative energies and cohesive energies of 147 atom cuboctahedral Pd-Pt core-shell random alloys calculated using DFT. All relative energies are referenced to structure mix-1. Cohesive energies per atom are referenced to gas phase Pt and Pd.

Structure: Pd (core), Pt (shell)	Relative energy, DFT, eV	Cohesive energy, DFT, eV/atom
mix-1	0.00	-3.5878
mix-2	-0.49	-3.5911
mix-3	0.88	-3.5818
mix-4	0.16	-3.5868
mix-5	0.97	-3.5812
mix-6	-0.05	-3.5882
mix-7	0.29	-3.5858
mix-8	-0.23	-3.5894
mix-9	-0.01	-3.5879
mix-10	1.22	-3.5795
mix-11	1.52	-3.5775
mix-12	2.58	-3.5703
mix-13	1.53	-3.5774
mix-14	1.75	-3.5759
mix-15	3.33	-3.5651
mix-16	3.30	-3.5653
mix-17	3.00	-3.5674
mix-18	2.28	-3.5723

Table S15: Relative energies and cohesive energies of 147 atom cuboctahedral Pd-Pt core-shell random alloys calculated using α_i^Z parameters. All relative energies are referenced to structure mix-1. Cohesive energies per atom are referenced to gas phase Pt and Pd. Residuals between model predictions and DFT calculations are also reported.

Structure: Pd (core), Pt (shell)	Relative energy, α_i^Z parameters, eV	Relative energy, α_i^Z parameters, eV	Residuals, Relative energy, eV	Residuals Cohesive energy, eV
mix-1	0.00	-3.7342	0.00	0.1464
mix-2	-0.16	-3.7353	0.32	0.1442
mix-3	1.07	-3.7270	0.18	0.1451
mix-4	0.35	-3.7318	0.20	0.1450
mix-5	0.78	-3.7289	0.19	0.1477
mix-6	-0.02	-3.7344	0.03	0.1462
mix-7	0.14	-3.7333	0.16	0.1475
mix-8	-0.33	-3.7364	0.10	0.1471
mix-9	0.13	-3.7333	0.14	0.1454
mix-10	1.53	-3.7238	0.31	0.1443
mix-11	1.44	-3.7245	0.09	0.1470
mix-12	2.30	-3.7186	0.28	0.1483
mix-13	1.34	-3.7251	0.19	0.1477
mix-14	1.78	-3.7221	0.03	0.1462
mix-15	2.73	-3.7156	0.60	0.1505
mix-16	2.83	-3.7150	0.48	0.1496
mix-17	2.68	-3.7160	0.32	0.1486
mix-18	2.01	-3.7205	0.26	0.1482

Table S16: Relative energies and cohesive energies of 147 atom cuboctahedral Pd-Pt core-shell random alloys calculated using the effective medium theory (EMT). All relative energies are referenced to structure mix-1. Cohesive energies per atom are referenced to gas phase Pt and Pd. Residuals between model predictions and DFT calculations are also reported.

Structure: Pd (core), Pt (shell)	Relative energy, EMT, eV	Cohesive energy, EMT, eV	Residuals, Relative energy, eV	Residuals Cohesive energy, eV
mix-1	0.00	-4.8209		
mix-2	0.31	-4.8187	0.80	1.2331
mix-3	1.10	-4.8134	0.22	1.2276
mix-4	0.54	-4.8172	0.38	1.2315
mix-5	0.81	-4.8154	0.16	1.2305
mix-6	0.29	-4.8189	0.34	1.2342
mix-7	0.33	-4.8186	0.04	1.2307
mix-8	0.38	-4.8183	0.61	1.2328
mix-9	0.73	-4.8159	0.74	1.2289
mix-10	1.39	-4.8114	0.17	1.2280
mix-11	1.13	-4.8132	0.39	1.2319
mix-12	1.89	-4.8080	0.69	1.2357
mix-13	1.10	-4.8134	0.43	1.2378
mix-14	1.36	-4.8116	0.39	1.2360
mix-15	2.64	-4.8029	0.69	1.2357
mix-16	2.19	-4.8060	1.11	1.2378
mix-17	1.85	-4.8083	1.15	1.2406
mix-18	1.71	-4.8093	0.57	1.2409

Table S17: Relative energies and cohesive energies of 147 atom cuboctahedral Pt-Pd core-shell random alloys calculated using DFT. All relative energies are referenced to structure mix-1. Cohesive energies per atom are referenced to gas phase Pt and Pd.

Structure: Pt (core), Pd (shell)	Relative energy, DFT, eV	Cohesive energy, DFT, eV
mix-1	0.00	-3.1962
mix-2	-0.19	-3.1975
mix-3	-1.47	-3.2062
mix-4	-0.14	-3.1972
mix-5	-1.02	-3.2032
mix-6	-0.41	-3.1990
mix-7	-0.85	-3.2020
mix-8	-0.01	-3.1963
mix-9	-0.49	-3.1996
mix-10	-1.86	-3.2089
mix-11	-1.77	-3.2082
mix-12	-2.92	-3.2161
mix-13	-1.83	-3.2086
mix-14	-2.44	-3.2128
mix-15	-3.97	-3.2232
mix-16	-3.61	-3.2207
mix-17	-2.95	-3.2163
mix-18	-2.48	-3.2131

Table S18: Relative energies and cohesive energies of 147 atom cuboctahedral Pt-Pd core-shell random alloys calculated using α_i^Z parameters. All relative energies are referenced to structure mix-1. Cohesive energies per atom are referenced to gas phase Pt and Pd. Residuals between model predictions and DFT calculations are also reported.

Structure: Pt (core), Pd (shell)	Relative energy, α_i^Z parameters, eV	Cohesive energy, α_i^Z parameters, eV	Residuals, Relative energy, eV	Residuals Cohesive energy, eV
mix-1	0.00	-3.3450	0.00	0.1488
mix-2	-0.39	-3.3476	0.20	0.1501
mix-3	-1.07	-3.3523	0.40	0.1461
mix-4	-0.38	-3.3476	0.24	0.1504
mix-5	-1.10	-3.3524	0.07	0.1493
mix-6	-0.65	-3.3494	0.24	0.1504
mix-7	-0.66	-3.3495	0.19	0.1475
mix-8	-0.05	-3.3453	0.04	0.1491
mix-9	-0.55	-3.3487	0.06	0.1492
mix-10	-1.88	-3.3577	0.01	0.1489
mix-11	-1.69	-3.3565	0.08	0.1482
mix-12	-2.69	-3.3633	0.23	0.1472
mix-13	-1.86	-3.3576	0.04	0.1490
mix-14	-2.32	-3.3608	0.11	0.1480
mix-15	-3.63	-3.3697	0.34	0.1465
mix-16	-3.34	-3.3677	0.27	0.1470
mix-17	-2.99	-3.3653	0.03	0.1490
mix-18	-2.45	-3.3616	0.03	0.1486

Table S19: Relative energies and cohesive energies of 147 atom cuboctahedral Pt-Pd core-shell random alloys calculated using the effective medium theory (EMT). All relative energies are referenced to structure mix-1. Cohesive energies per atom are referenced to gas phase Pt and Pd. Residuals between model predictions and DFT calculations are also reported.

Structure: Pt (core), Pd (shell)	Relative energy, EMT, eV	Cohesive energy, EMT, eV	Residuals, Relative energy, eV	Residuals Cohesive energy, eV
mix-1	0.00	0.00		
mix-2	0.31	-0.52	0.00	0.5158
mix-3	1.10	-1.32	0.34	0.4805
mix-4	0.54	-0.68	0.14	0.5415
mix-5	0.81	-0.96	0.54	0.5150
mix-6	0.29	-0.33	0.06	0.5205
mix-7	0.33	-0.48	0.08	0.5534
mix-8	0.38	-0.45	0.37	0.5536
mix-9	0.73	-0.76	0.44	0.5233
mix-10	1.39	-1.69	0.26	0.5288
mix-11	1.13	-1.44	0.18	0.7864
mix-12	1.89	-2.23	0.33	0.7669
mix-13	1.10	-1.34	0.69	0.8533
mix-14	1.36	-1.60	0.49	0.7758
mix-15	2.64	-3.07	0.83	0.7790
mix-16	2.19	-2.72	0.90	0.8487
mix-17	1.85	-2.07	0.89	0.8472
mix-18	1.71	-1.94	0.88	0.8577

Table S20: Cohesive energies of monometallic 147 atom cuboctahedral nanoparticles are calculated using DFT, α_i^Z parameters, EMT, and BCM. Cohesive energies per atom are referenced to corresponding gas phase atoms. Residuals between model predictions and DFT calculations are also reported.

Monometallic nanoparticles (147 atoms, cuboctahedral)	Cohesive energy, DFT, eV	Cohesive energy, α_i^Z parameters, eV	Cohesive energy, EMT, eV	Cohesive energy, Bond centric model, eV	Residual, α_i^Z parameters, eV	Residual, EMT, eV	Residual, Bond centric model, eV
Ag	-1.7263	-1.7212	-2.7133	-2.3592	0.0050	0.9871	0.6329
Au	-2.1778	-2.3017	-3.5641	-3.2639	0.1239	1.3863	1.0861
Cu	-2.5934	-2.5252	-3.1598	-2.9898	0.0682	0.5664	0.3964
Ir	-5.6620	-5.5467		-5.9453	0.1153		0.2833
Pd	-2.6150	-2.6473	-3.6212	-3.3325	0.0323	1.0062	0.7175
Pt	-4.1376	-4.3673	-5.5272	-5.0030	0.2297	1.3896	0.8654
Rh	-4.3688	-4.2826		-4.9259	0.0862		0.5570

Table S21: Cohesive energies of 147 atom cuboctahedral Pd-Pt core-shell random alloys calculated using the bond centric model (BCM). Cohesive energies per atom are referenced to gas phase Pt and Pd. Residuals between model predictions and DFT calculations are also reported.

Structure: Pd (core), Pt (shell)	Cohesive energy, Bond centric model, eV	Residuals, cohesive energy, eV
mix-1	-4.4100	0.8222
mix-2	-4.4059	0.8148
mix-3	-4.3905	0.8087
mix-4	-4.3964	0.8097
mix-5	-4.3676	0.7864
mix-6	-4.4023	0.8141
mix-7	-4.4079	0.8221
mix-8	-4.3909	0.8015
mix-9	-4.4332	0.8453
mix-10	-4.3899	0.8104
mix-11	-4.3766	0.7991
mix-12	-4.4532	0.8830
mix-13	-4.4014	0.8239
mix-14	-4.3819	0.8060
mix-15	-4.4039	0.8387
mix-16	-4.3520	0.7866
mix-17	-4.3585	0.7911
mix-18	-4.4066	0.8343

Table S22: Cohesive energies of 147 atom cuboctahedral Pt-Pd core-shell random alloys calculated using the bond centric model (BCM). Cohesive energies per atom are referenced to gas phase Pt and Pd. Residuals between model predictions and DFT calculations are also reported.

Structure: Pt (core), Pd (shell)	Cohesive energy, Bond centric model, eV	Residuals, cohesive energy, eV
mix-1	-3.7120	0.5158
mix-2	-3.6779	0.4805
mix-3	-3.7477	0.5415
mix-4	-3.7122	0.5150
mix-5	-3.7236	0.5205
mix-6	-3.7524	0.5534
mix-7	-3.7556	0.5536
mix-8	-3.7196	0.5233
mix-9	-3.7284	0.5288
mix-10	-3.9953	0.7864
mix-11	-3.9752	0.7669
mix-12	-4.0694	0.8533
mix-13	-3.9844	0.7758
mix-14	-3.9918	0.7790
mix-15	-4.0718	0.8487
mix-16	-4.0679	0.8472
mix-17	-4.0740	0.8577
mix-18	-4.0129	0.7998

Table S23: Comparing our approach (α_i^Z parameters) with effective medium theory[1], bond centric model[2], Bayesian linear regression[3,4] and cluster expansions[5]. Stated are the number of parameters, computational cost of parameter fitting, and accuracy in determining cohesive energies.

Chatracteristic	α_i^Z parameters,	Effective medium theory	Bond centric model	Bayesian linear regression	Cluster expansion
Number of parameters (AB alloy)	20 for each binary pair	7	2	800	35
Computational cost per bimetallic pairing (AB alloy)	~ 70 DFT calculations on surface slabs (24 -36 atoms each)	Can be fitted using handbook data	3 gas phase dimers (AB, A_2, and B_2), Bulk cohesive energies for A and B. Obtained using either DFT or handbook data	1106 DFT calculations on nanoparticles and surfaces	107 DFT calculations on nanoparticles (145-147 atoms)
Accuracy in determining cohesive energies	0.15 eV (PtPd random alloys)	1.18 eV (PtPd random alloys)	0.74 eV (PtPd random alloys)	0.02 eV (RhAu random alloys)	0.01 eV (FeNi random alloys) *Test set is structurally similar to training set*

Table S24: DFT derived and model predicted binding energies of Pt and Pd atoms having different coordination number (5, 7, 8, and 9) in CUB nanoparticles (147 atom). The nanoparticle

composition ranges from Pt rich to Pd rich. The corresponding parity plot is shown in Figure S12.

Coordination number of metal atom, composition	Nanoparticle compostion	Binding energy, DFT, eV	Binding energy, alpha parameters, eV
9, Pd	$Pt_{137}Pd_{10}$	-3.68	-4.42
8, Pt	$Pt_{82}Pd_{65}$	-5.25	-5.27
7, Pt	$Pt_{65}Pd_{82}$	-4.69	-4.85
5, Pd	$Pt_{10}Pd_{137}$	-2.97	-3.05
7, Pd	$Pt_{107}Pd_{40}$	-3.39	-3.73
9, Pt	$Pt_{107}Pd_{40}$	-5.25	-5.87
7, Pt	$Pt_{120}Pd_{27}$	-4.82	-5.18
9, Pd	$Pt_{120}Pd_{27}$	-3.65	-4.42
5, Pd	$Pt_{27}Pd_{120}$	-2.82	-2.90
8, Pd	$Pt_{27}Pd_{120}$	-3.52	-3.53
5,Pd	$Pt_{40}Pd_{107}$	-3.02	-3.16
8, Pt	$Pt_{40}Pd_{107}$	-4.98	-5.15
7, Pt	$Pt_{92}Pd_{55}$	-4.88	-5.23
9, Pd	$Pt_{92}Pd_{55}$	-3.79	-4.51
5, Pd	$Pt_{55}Pd_{92}$	-2.85	-2.90
8, Pt	$Pt_{55}Pd_{92}$	-4.96	-4.96

Table S25: DFT derived and model predicted cohesive energies of CUB nanoparticles (147 atoms) having compositions ranging from Pt rich to Pd rich. The corresponding parity plot is in Figure S13.

Fraction of Pd in the system (%)	Composition	Cohesive energy, DFT, eV	Cohesive energy, alpha parameters, eV	Relative energy, DFT, eV	Relative energy, alpha parameters, eV	dE, relative energy (DFT – alpha parameters), eV
0	$Pt_{147}Pd_{0}$	-4.14	-4.29	0.00	0.00	
7	$Pt_{137}Pd_{10}$	-4.04	-4.19	0.10	0.10	0.001
18	$Pt_{120}Pd_{27}$	-3.86	-4.01	0.28	0.28	0.003
27	$Pt_{107}Pd_{40}$	-3.75	-3.89	0.39	0.39	0.003
37	$Pt_{92}Pd_{55}$	-3.55	-3.71	0.59	0.58	0.014
44	$Pt_{82}Pd_{65}$	-3.48	-3.63	0.66	0.66	0.000
56	$Pt_{65}Pd_{82}$	-3.31	-3.45	0.83	0.83	0.002
63	$Pt_{55}Pd_{92}$	-3.24	-3.39	0.90	0.90	0.004
73	$Pt_{40}Pd_{107}$	-3.04	-3.19	1.10	1.10	0.002
82	$Pt_{27}Pd_{120}$	-2.92	-3.07	1.22	1.21	0.006
93	$Pt_{10}Pd_{137}$	-2.72	-2.88	1.42	1.41	0.010
100	$Pt_{0}Pd_{147}$	-2.61	-2.77	1.52	1.51	0.011

Table S26: DFT and model predicted binding energies of metal atoms in monometallic Pt and Pd nanoparticles having different morphologies (OCT, DEC, and ICO). The conrresponding parity plot is shown in Figure S14.

Nanoparticle morphology	Coordination number of metal atom	Binding energy, DFT, eV	Binding energy, alpha parameters, eV
Pt_{146}, Octahedron (OCT)	4	-4.49	-4.40
	7	-5.48	-5.45
	9	-5.70	-5.89
	12 (2nd)	-4.78	-4.51
	core	-5.27	-4.75
Pd_{146}, Octahedron (OCT)	4	-2.59	-2.74
	7	-3.43	-3.49
	9	-3.89	-3.97
	12 (2nd)	-4.06	-3.78
	core	-4.19	-3.99
Pt_{147}, Decahedron (DEC)	5	-4.34	-4.56
	6	-4.91	-4.68
	7	-4.80	-5.15
	8.1	-5.42	-5.37
	8.2	-4.77	-5.14
	9	-5.41	-5.56
	12 (2nd)	-4.57	-4.79
	core	-4.90	-4.75
Pd_{147}, Decahedron (DEC)	5	-2.78	-2.88
	6	-2.97	-3.10
	7	-3.34	-3.36
	8.1	-3.54	-3.66
	8.2	-3.58	-3.60
	9	-3.75	-3.96
	12 (2nd)	-3.93	-4.04
	core	-3.92	-3.99
Pt_{147}, Icosahedron (ICO)	12 (2nd)	-4.57	-4.79
	core	-4.90	-4.75
Pd_{147}, Icosahedron (ICO)	6	-2.96	-3.10
	8	-3.48	-3.66
	9	-3.72	-3.89
	12 (2nd)	-3.81	-3.89
	core	-3.61	-3.99

Table S27: DFT and model predicted cohesive energies of PtPd nanoparticles having wide ranging compositions (Pt to Pd rich), morphologies (CUB, OCT, DEC, ICO) and sizes (CUB – 147 atoms, CUB – Half-309 (175 atoms)). Representiative structures are depicted in Figure S15 while the partiy plot is shown in Figure S16(a).

Nanoparticle morphology	Nanoparticle composition	Cohesive energy, DFT, eV	Cohesive energy, alpha parameters, eV
Octahedron (OCT)	$Pt_{44}Pd_{102}$	-3.12	-3.28
	$Pt_{102}Pd_{44}$	-3.74	-3.86
	$Pt_{44}Pd_{102}$	-3.12	-3.28
	$Pt_{44}Pd_{102}$	-3.12	-3.28
	$Pt_{102}Pd_{44}$	-3.74	-3.86
	$Pt_{102}Pd_{44}$	-3.73	-3.86
	$Pt_{44}Pd_{102}$	-3.11	-3.26
	$Pt_{102}Pd_{44}$	-3.74	-3.87
Decahedron (DEC)	$Pt_{55}Pd_{92}$	-3.24	-3.40
	$Pt_{92}Pd_{55}$	-3.56	-3.72
	$Pt_{55}Pd_{92}$	-3.23	-3.40
	$Pt_{55}Pd_{92}$	-3.23	-3.40
	$Pt_{92}Pd_{55}$	-3.56	-3.72
	$Pt_{92}Pd_{55}$	-3.56	-3.72
	$Pt_{55}Pd_{92}$	-3.20	-3.36
	$Pt_{92}Pd_{55}$	-3.59	-3.74
Icosahedron (ICO)	$Pt_{55}Pd_{92}$	-3.24	-3.45
	$Pt_{92}Pd_{55}$	-3.57	-3.79
	$Pt_{55}Pd_{92}$	-3.24	-3.45
	$Pt_{55}Pd_{92}$	-3.24	-3.45
	$Pt_{92}Pd_{55}$	-3.57	-3.79
	$Pt_{92}Pd_{55}$	-3.57	-3.79
	$Pt_{55}Pd_{92}$	-3.22	-3.42
	$Pt_{92}Pd_{55}$	-3.59	-3.80
Cuboctahedron (CUB) – 147 atoms	$Pt_{147}Pd_{0}$	-4.14	-4.29
	$Pt_{137}Pd_{10}$	-4.04	-4.19
	$Pt_{120}Pd_{27}$	-3.86	-4.01
	$Pt_{107}Pd_{40}$	-3.75	-3.89
	$Pt_{92}Pd_{55}$	-3.55	-3.71
	$Pt_{82}Pd_{65}$	-3.48	-3.63
	$Pt_{65}Pd_{82}$	-3.31	-3.45
	$Pt_{55}Pd_{92}$	-3.24	-3.39
	$Pt_{40}Pd_{107}$	-3.04	-3.19
	$Pt_{27}Pd_{120}$	-2.92	-3.07
	$Pt_{10}Pd_{137}$	-2.72	-2.88
	$Pt_{0}Pd_{147}$	-2.61	-2.77
Cuboctahedron (CUB) – Truncated 309 atom nanoparticle, (175	$Pt_{73}Pd_{102}$	-3.22	-3.39
	$Pt_{73}Pd_{102}$	-3.23	-3.39
	$Pt_{73}Pd_{102}$	-3.22	-3.39
	$Pt_{73}Pd_{102}$	-3.23	-3.39

atom)	$Pt_{73}Pd_{102}$	-3.22	-3.39
	$Pt_{73}Pd_{102}$	-3.23	-3.39
	$Pt_{73}Pd_{102}$	-3.23	-3.39
	$Pt_{73}Pd_{102}$	-3.23	-3.39
	$Pt_{73}Pd_{102}$	-3.23	-3.39
	$Pt_{73}Pd_{102}$	-3.24	-3.40
	$Pt_{73}Pd_{102}$	-3.23	-3.39
	$Pt_{73}Pd_{102}$	-3.23	-3.40
	$Pt_{73}Pd_{102}$	-3.22	-3.39
	$Pt_{73}Pd_{102}$	-3.23	-3.40
	$Pt_{102}Pd_{73}$	-3.49	-3.65
	$Pt_{102}Pd_{73}$	-3.49	-3.65
	$Pt_{102}Pd_{73}$	-3.49	-3.65
	$Pt_{102}Pd_{73}$	-3.49	-3.65
	$Pt_{102}Pd_{73}$	-3.49	-3.65
	$Pt_{102}Pd_{73}$	-3.49	-3.65
	$Pt_{102}Pd_{73}$	-3.49	-3.65
	$Pt_{102}Pd_{73}$	-3.49	-3.65
	$Pt_{102}Pd_{73}$	-3.49	-3.65
	$Pt_{102}Pd_{73}$	-3.49	-3.65
	$Pt_{102}Pd_{73}$	-3.47	-3.63
	$Pt_{102}Pd_{73}$	-3.48	-3.65
	$Pt_{102}Pd_{73}$	-3.49	-3.65
	$Pt_{102}Pd_{73}$	-3.50	-3.65

Table S28: DFT and model predicted energy changes for single atom movements (ΔE_{swap}). Pt and Pd exchanges are carried out across nanoparticles having different compositions (Pt rich to Pd rich), morphologies (CUB, OCT, ICO, and DEC), and sizes (CUB – 147 atoms and CUB – Half-309 (175 atoms)). Representiative structures are depicted in Figure S15 while the partiy plot is shown in Figure S16(b).

Nanoparticle morphology	Nanoparticle composition	ΔE_{swap}, DFT, eV	ΔE_{swap}, alpha parameters, eV
Cuboctahedron (CUB) – 147 atoms	$Pt_{137}Pd_{10}$	0.08	0.07
	$Pt_{82}Pd_{65}$	0.04	0.05
	$Pt_{65}Pd_{82}$	-0.06	-0.02
	$Pt_{10}Pd_{137}$	-0.07	-0.03
Octahedron (OCT)	$Pt_{44}Pd_{102}$	-0.29	-0.38
	$Pt_{44}Pd_{102}$	0.03	0.14
	$Pt_{102}Pd_{44}$	-0.15	-0.23
	$Pt_{102}Pd_{44}$	0.10	-0.06
Icosahedron (ICO)	$Pt_{55}Pd_{92}$	-0.23	-0.24
	$Pt_{55}Pd_{92}$	-0.19	-0.11
	$Pt_{92}Pd_{55}$	-0.18	-0.11
	$Pt_{92}Pd_{55}$	0.04	0.14
Decahedron (DEC)	$Pt_{55}Pd_{92}$	-0.32	-0.30
	$Pt_{55}Pd_{92}$	0.11	0.10
	$Pt_{92}Pd_{55}$	-0.16	-0.23
	$Pt_{92}Pd_{55}$	-0.10	-0.13
Cuboctahedron (CUB) – Truncated	$Pt_{73}Pd_{102}$	-0.19	-0.16
	$Pt_{73}Pd_{102}$	-0.01	-0.01

309 atom nanoparticle, (175 atom)	$Pt_{73}Pd_{102}$	0.15	0.14
	$Pt_{73}Pd_{102}$	-0.38	-0.30
	$Pt_{102}Pd_{73}$	0.10	0.11
	$Pt_{102}Pd_{73}$	-0.03	0.00
	$Pt_{102}Pd_{73}$	-0.12	-0.12
	$Pt_{102}Pd_{73}$	0.27	0.26

8. References

1 K. W. Jacobsen, P. Stoltze and J. K. Nørskov, *Surf. Sci.*, 1996, **366**, 394–402.

2 Z. Yan, M. G. Taylor, A. Mascareno and G. Mpourmpakis, *Nano Lett.*, 2018, **18**, 2696–2704.

3 R. Jinnouchi, H. Hirata and R. Asahi, *J. Phys. Chem. C*, 2017, **121**, 26397–26405.

4 R. Jinnouchi and R. Asahi, *J. Phys. Chem. Lett.*, 2017, **8**, 4279–4283.

5 J. Teeriniemi, M. Melander, S. Lipasti, R. Hatz and K. Laasonen, *J. Phys. Chem. C*, 2017, **121**, 1667–1674.

6 L. T. Roling and F. Abild-Pedersen, *ChemCatChem*, 2018, **10**, 1643–1650.

7 J. K. Nørskov, T. Bligaard, B. Hvolbæk, F. Abild-Pedersen, I. Chorkendorff and C. H. Christensen, *Chem. Soc. Rev.*, 2008, **37**, 2163–2171.

8 J. Kleis, J. Greeley, N. A. Romero, V. A. Morozov, H. Falsig, A. H. Larsen, J. Lu, J. J. Mortensen, M. Dułak, K. S. Thygesen, J. K. Nørskov and K. W. Jacobsen, *Catal. Letters*, 2011, **141**, 1067–1071.

9 L. Li, A. H. Larsen, N. A. Romero, V. A. Morozov, C. Glinsvad, F. Abild-Pedersen, J. Greeley, K. W. Jacobsen and J. K. Nørskov, *J. Phys. Chem. Lett.*, 2013, **4**, 222–226.

10 L. Li, F. Abild-Pedersen, J. Greeley and J. K. Nørskov, *J. Phys. Chem. Lett.*, 2015, **6**, 3797–3801.

11 L. T. Roling, L. Li and F. Abild-Pedersen, *J. Phys. Chem. C*, 2017, **121**, 23002–23010.